

MECHANICAL AND OPTICAL CHARACTERIZATION
OF FORCE INDUCED CHEMICAL REACTIONS
IN SOLID STATE LINEAR POLYMERS

BY

BRETT A. BEIERMANN

DISSERTATION

Submitted in partial fulfillment of the requirements
for the degree of Doctor of Philosophy in Materials Science and Engineering
in the Graduate College of the
University of Illinois at Urbana-Champaign, 2013

Urbana, Illinois

Doctoral Committee:

Professor Nancy Sottos, Chair and Director of Research
Professor Paul Braun
Professor Scott White
Professor Jeffrey Moore
Professor Jianjun Cheng

UMI Number: 3603497

All rights reserved

INFORMATION TO ALL USERS

The quality of this reproduction is dependent upon the quality of the copy submitted.

In the unlikely event that the author did not send a complete manuscript and there are missing pages, these will be noted. Also, if material had to be removed, a note will indicate the deletion.



UMI 3603497

Published by ProQuest LLC (2013). Copyright in the Dissertation held by the Author.

Microform Edition © ProQuest LLC.

All rights reserved. This work is protected against unauthorized copying under Title 17, United States Code



ProQuest LLC.
789 East Eisenhower Parkway
P.O. Box 1346
Ann Arbor, MI 48106 - 1346

ABSTRACT

Traditionally, chemical reactions are driven by thermal, chemical, or electrical potential. By linking force-sensitive chemical species (mechanophores) into polymer backbones, mechanical force can drive chemical reactions. Mechanophores have been developed with potential as damage sensing, self-healing, and self-reinforcing materials. This research investigates the conditions for promoting mechanophore activation in bulk, linear polymers.

An optically active mechanophore is studied. The mechanophore, spiropyran (SP), reacts to a merocyanine (MC) form under tensile force when linked into a polymer backbone. This reaction is reversible and can be driven toward either SP or MC photochemically. Reaction of SP to MC (activation) is accompanied by the emergence of a strong color change and fluorescence signal. SP is incorporated into a polymer backbone by using the mechanophore as an initiator for a living radical polymerization and growing polymer chains at two sites across the SP molecule, thereby covalently bonding the mechanophore in the center of a polymer chain.

Polymer mechanics and mechanophore activation are characterized in both glassy and elastomeric polymers. An experimental set-up is designed and implemented to simultaneously measure stress, strain, fluorescence, and birefringence during tensile deformation of SP-linked polymer samples. By varying the loading conditions and polymer mechanical properties, mechanophore activation is examined as a function of the stress, polymer mobility, structure and orientation of polymer chains.

In an elastomeric polymer, poly(methyl acrylate) (PMA), higher macroscopic stress leads to higher degrees of SP activation at lower levels of deformation. By changing the polymer architecture - increasing the number of polymer chains attached to the mechanophore - increased

activation is demonstrated at relatively slow deformation rates. Activation energy for the SP \leftrightarrow MC conversion is quantified for an elastomeric polymer based on the kinetics of the reaction. The effect of varying stress on reaction rates and energy barriers is determined using a combined experimental and theoretical approach.

Tensile deformation of SP-linked glassy polymers at room temperature (RT) does not lead to detectable mechanophore activation. Increasing polymer chain mobility, either using a plasticizing solvent or varying test temperature, leads to a range of thermomechanical properties in which glassy SP-linked polymers can be activated by tensile deformation. Within this favorable activation window, the strain to activation varies based on the stiffness of the polymer. The minimum observed strain to activation is approximately 5%, coincident with the onset of polymer yield.

The role of polymer chain alignment and mechanophore orientation are studied using optical techniques. Polymer chain alignment is determined by measurement of birefringence. Activation of mechanophores occurred when polymer chains reached a maximum alignment implying that energy is most efficiently transferred to SP when the polymer chains are aligned in the direction of force. Additionally, mechanophore orientation within the polymer backbone is measured by polarized fluorescence measurements. Mechanophores oriented in the direction of force activate preferentially when compared to those unaligned with the loading direction. Polarized fluorescence measurements also provide insight on polymer mechanics and force on polymer chains.

The force driven reaction of spiropyran mechanophores investigated in this dissertation provides useful guidelines for development and characterization of future mechanochemically

active material systems. Polymer architecture, mobility and molecular force transfer are critical variables that control mechanophore activity in bulk polymers.

ACKNOWLEDGEMENTS

I want to acknowledge the mentors who have taken the time to support my curiosity and interests, starting with my parents, who raised me to ask questions, and all of the other teachers who have played a part in my life. Dr. Michael Keller introduced me to academic research and was an outstanding mentor during my undergraduate studies. My thesis committee, specifically Professors Scott White, Jeffrey Moore, Paul Braun, and Jianjun Cheng have provided guidance which has allowed me to succeed in graduate school. Most of all I would like to acknowledge the time, effort and interest my research advisor, Professor Nancy Sottos, has provided.

I'd like to thank all of the friends and colleagues within the AMS group who have helped me with research and served as positive examples for growth and success. Douglas Davis and Preston May provided materials and knowledge in the chemistry field, and without their help I would not be where I am today. Charlotte Kramer was an outstanding mentor who taught me optical techniques and helped drive my research forward. Meredith Silberstein, Cassandra Kingsbury and Corissa Lee were a consistent resource for intelligent conversation within my field.

Finally I would like to acknowledge funding from the Army Research Office, and the resources of the Beckman Institute and University of Illinois. I want to thank Greg Milner at the Aerospace Engineering machine shop, and Scott Robinson at Beckman's Imaging Technology Group for their assistance over the years.

TABLE OF CONTENTS

CHAPTER 1: INTRODUCTION	1
1.1 Mechanically Responsive Polymeric Materials	1
1.2 Force-Induced Reaction of Spiropyran-Linked Polymers	5
1.3 Thermomechanical Behavior of Mechanochemically Active Polymers	6
1.4 Polymer Orientation Measurement	8
1.5 Overview of Thesis Research	9
CHAPTER 2: SYNTHESIS AND FUNDAMENTAL CHARACTERIZATION OF SPIROPYRAN-LINKED POLYMERS	11
2.1 Introduction	11
2.2 Results	13
2.2.1 Synthesis of Linear Polymers by Living Radical Polymerizations ..	13
2.2.2 Thermomechanical Properties of SP-Linked Polymers	17
2.2.3 SP Cleavage Experiments	19
2.2.4 Fluorescence Spectra of SP-Linked Polymers	20
2.3 Conclusions	23
CHAPTER 3: MECHANICAL AND OPTICAL CHARACTERIZATION OF AN SP-LINKED ELASTOMER	25
3.1 Introduction	25
3.2 Experimental	26
3.2.1 Materials	26
3.2.2 Tensile Testing Protocol	28
3.2.3 Combined Mechanical and Optical Experimental Setup	28
3.2.4 Birefringence and Fluorescence Measurement	32
3.3 Results and Discussion	34
3.3.1 Simultaneous Measurement of Stress, Birefringence and Fluorescence	34
3.3.2 Deformation Rate Dependence in Linear Active SP-Linked PMA ..	37
3.3.3 Deformation Rate Dependence in Difunctional Control SP-Linked PMA	39
3.3.4 Stress Relaxation Behavior of Active SP-Linked PMA	43
3.3.5 Stress Relaxation Behavior of Difunctional Control SP-Linked PMA	45
3.3.6 Effect of Mechanophore Architecture: SP Activation in Linear, 4-Arm, and 8-Arm SP	46
3.4 Conclusions	50
CHAPTER 4: EFFECT OF STRESS ON SP-MC REACTION KINETICS AND ACTIVATION ENERGY	52
4.1 Introduction and Theory	52
4.2 Experimental Methods	55
4.2.1 SP-Linked PMA Samples and Treatment	55

<i>4.2.2 Combined Fluorescence Kinetics and Mechanical Testing</i>	56
4.3 Results and Discussion	57
<i>4.3.1 SP Reaction Kinetics with No Applied Load</i>	57
<i>4.3.2 Effect of Applied Mechanical Load on SP Reaction Kinetics</i>	60
4.4 Conclusions.....	66
 CHAPTER 5: SP ACTIVATION IN A GLASSY POLYMER: EFFECT OF THERMOMECHANICAL BEHAVIOR	
5.1 Introduction.....	67
5.2 Experimental Methods	68
<i>5.2.1 Synthesis and Characterization</i>	68
<i>5.2.2 Sample Molding</i>	68
<i>5.2.3 Mechanical Testing</i>	69
5.3 Results and Discussion	71
<i>5.3.1 Effect of Temperature on Mechanical Activation</i>	71
<i>5.3.2 SP Activation in MeOH Plasticized PMMA</i>	73
<i>5.3.3 SP Activation in DBP Plasticized PMMA</i>	75
<i>5.3.4 Creep Loading of SP-Linked PMMA</i>	77
5.4 Conclusions.....	78
 CHAPTER 6: FLUORESCENCE POLARIZATION MEASUREMENTS OF MECHANOPHORE ORIENTATION	
6.1 Introduction.....	80
6.2 Experimental Methods	81
<i>6.2.1 SP-Linked Polymer Samples</i>	81
<i>6.2.2 Mechanical Testing</i>	83
6.3 Results and Discussion	84
<i>6.3.1 Alignment of Mechanophores with the Tensile Direction</i>	84
<i>6.3.2 Role of Mechanophore Orientation in a SP-Linked Elastomer</i>	85
<i>6.3.3 Orientation in a Mechanically-Activated Glassy Polymer</i>	86
6.4 Summary and Conclusions	87
 CHAPTER 7: MECHANOPHORE ACTIVATION IN POLYSTYRENE THIN FILMS.....	
7.1 Introduction.....	89
7.2 Experimental Methods	90
<i>7.2.1 SP-Linked Polystyrene</i>	90
<i>7.2.2 Nd:YAG Shockwave Sample Preparation</i>	90
<i>7.2.3 Mechanical Loading and Analysis</i>	91
7.3 Results and Discussion	94
<i>7.3.1 Shockwave Loading of Thin Films</i>	94
7.4 Conclusions.....	98

CHAPTER 8: SUMMARY AND FUTURE WORK	100
8.1 Summary of Thesis Research.....	100
8.2 Future Work	101
<i>8.2.1 Solid State Activation of New Mechanophores</i>	101
<i>8.2.2 A Bio-Inspired Mechanochemical System: Synthetic Mechanotransductive Channels</i>	105
REFERENCES	110
APPENDIX A: BULK SAMPLE DIMENSIONS	116
APPENDIX B: EMPIRICALLY DERIVED SP-LINKED PMA FLUORESCENCE KINETICS	117

CHAPTER 1

INTRODUCTION

1.1 Mechanically Responsive Polymeric Materials

Traditionally, chemical reactions are driven by thermal, chemical, or electrical potential. Applications of mechanical force can also cleave chemical bonds and form new chemical species. In nature, mechanochemical processes are abundant, affecting processes such as bone growth, wound healing [1], maintaining cell pressure [2] and transduction of sound waves for hearing [3, 4]. Mechanochemistry in ceramics and metals has been studied throughout the 1900s. These processes typically involve milling, shearing or abrasion to achieve bond breakage and re-formation. Similarly in polymer chains mechanical force *via* milling in the solid state or sonication in solution state can cleave carbon-carbon bonds in polymer backbones [5-9]. These methods are typically destructive and the chemical changes are not particularly selective [10-12]. In recent years, a novel method of mechanochemistry has been developed incorporating site-specific force-responsive chemical moieties, or mechanophores, into polymer backbones [13-25]. The mechanophore approach promotes energy transfer, *via* mechanical force, to specific weak bonds along the polymer backbone. A variety of advantageous chemical responses can be achieved in response to applied force, such as color change, cross-linking and catalyst release. The research presented in this dissertation investigates parameters influencing mechanochemical response in bulk mechanophore-linked polymers.

Deformation of bulk polymeric materials requires the input of relatively large amounts of energy. The polymer must overcome both the intermolecular resistance of individual chains flowing past each other, and the configurational entropy change due to alignment of the polymer

chains [5, 26, 27]. Eventually, the energy input is sufficient to drive cleavage of a polymer backbone, and polymer failure results [28]. By incorporating mechanophores into the polymer backbone, this energy can facilitate an advantageous chemical change in the polymer system prior to cleavage of the polymer backbone and bulk failure.

A number of approaches have previously been taken to mechanically stimulate an advantageous response in solid state polymers, such as change in optical properties, cross-linking, or change in pH. Color change is one desirable mechanically-stimulated response, to act as visual sensors for stress, strain or damage in structural materials. To this end, Rubner *et al.* demonstrated that strain-induced conformational changes and alignment of poly(acetylene) affect the absorbance and therefore color of the bulk polymer [29]. Christoph Weder's research group similarly used conformational changes to vary the photoluminescent emission of eximers in response to applied deformation of a host polymer [30, 31]. Other relevant functionalities of force-stimulated response in polymer systems have been geared toward initiating a further reaction, such as cross-linking of the polymer. Huck *et al.* have demonstrated the ability to alter the pH state of polymer brushes based on applied deformation [32]. This change in pH – particularly acid generation – has potential to initiate cross-linking reactions.

In 2008, Hickenboth *et al.* published seminal work indicating site-specific force-induced chemical reaction of benzocyclobutene 4-member rings, covalently bonded into the center of polymer backbones [13]. Force was applied to polymer chains in a dilute solution *via* sonication. Sonication is known to cleave polymers of sufficient molecular weight along C-C bonds of the polymer backbone. Benzocyclobutene units (mechanophores) were incorporated into a polymer backbone, and under force the 4-member butane ring was selectively cleaved, and not the polymer chains [13]. Subsequently a number of mechanophore chemistries have been covalently

bonded into polymer chains and activated by sonication [14, 17, 19, 22-25]. Table 1.1 provides an overview of mechanophore chemistries and functionalities developed since 2007.

The mechanophore functionalities demonstrated in solution have a broad range of applicability. For example, a number of mechanophores are geared toward driving reactions with mechanical force that are difficult or impossible to achieve by other methods. Examples include cycloreversion of azide and alkyne moieties (“unclicking a click reaction”) [21] and force-driven retro-Diels-Alder reactions [20]. Bielawski *et al.* as well as Sijbesma *et al.* have demonstrated release of organometallic catalysts by mechanical force [22, 23, 25]. Catalyst-releasing mechanophores have been used to stimulate additional reactions to alter mechanical, optical or electronic properties of the material system.

Perhaps the most prominent method for achieving mechanophore reactivity is ring-opening reactions. Ring-opening of 3, 4, 5, and 6 member cyclic structures have been driven by an applied force [13, 14, 17, 18]. Ring-opening chemistries have been designed such that activation is accompanied by favorable material changes, such as color change [14], radical formation [17], and acid release [18]. Ring-opening chemistries are as yet the only mechanophores which have shown mechanochemical activity in solid state polymers [15, 16, 18].

Solid state mechanochemical activation, as opposed to solution state, is a major step toward applicability of mechanophores in commercial and/or structural polymeric materials. The predominant goals for solid state mechanochemical functionality include color change for visual stress or damage sensors, or cross-linking for adaptive mechanical properties (particularly stiffness) with applied load. Research presented in this dissertation utilizes a spiropyran- (SP-)

Table 1.1. Overview of mechanophores developed since 2007. Force-sensitive bonds are labeled in red.

Reaction Type	Chemical Structure	Functionality	Year, Reference
Ring Opening		Ring-opening to E,E isomeric product only	2007, 13
		Colored, fluorescent merocyanine product	2007, 14
		Rearrangement product, free radical intermediate	2009, 16
		Acid generation (HCl)	2012, 18
Ring Cleavage & Reactant Forming		Yields cyanoacrylate	2010, 19;
		Retro-Diels-Alder, yields Diene and dieneophile	2011, 20
		Reverse "click" reaction, yields triazole and alkyne	2011, 21
Organometallic Cleavage & Catalyst Releasing		Chain transfer, reduction in molecular weight	2008, 22
		Metathesis catalyst for ring opening polymerization, ring closing reactions	2009, 23
		Anionic polymerization initiator	2010, 24

based mechanophore devised by Potisek *et al.*[14] Spiropyrans undergo a reversible electrocyclic ring opening reaction (Fig 1.1), which is accompanied by a strong color change and the emergence of a fluorescence signal. Ease of detection and reversibility make SP an ideal

probe for determining factors which influence mechanochemical reactions in bulk polymer systems.

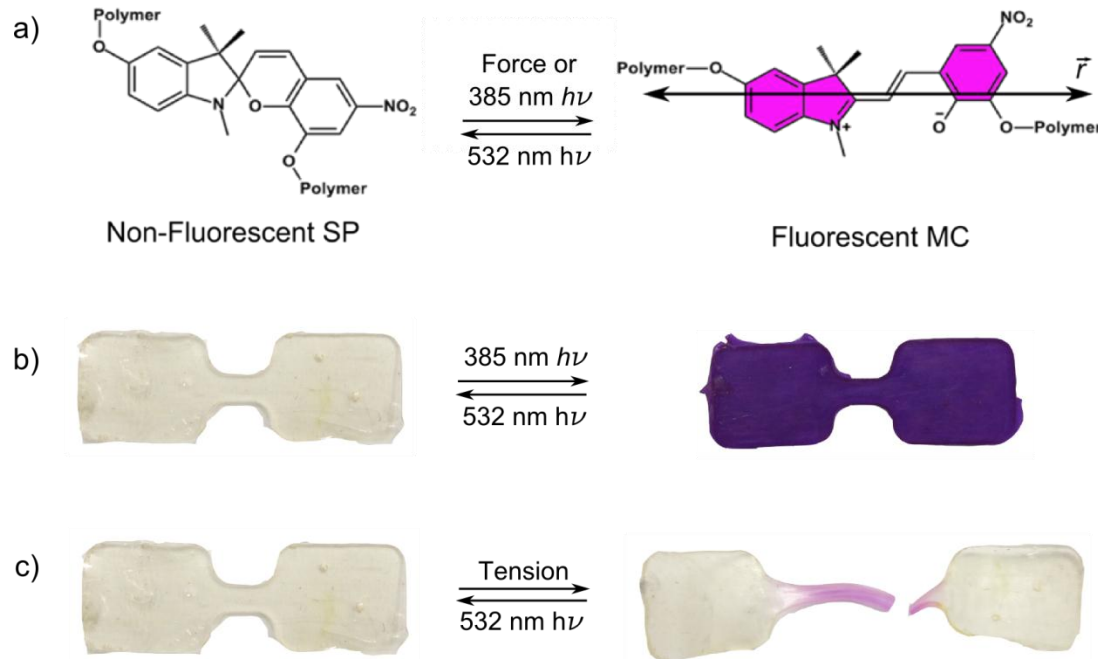


Figure 1.1. Mechanochemically active SP linked into a polymer backbone. a) Chemical structures of SP (left) and MC (right). b) SP-linked poly(methyl acrylate) (PMA) driven toward the SP form with 532 nm light (left) and toward the MC form with 385 nm light (right). c) SP-linked PMA driven toward the SP form with 532 nm light (left) and mechanically activated to the MC form in the gauge section (right).

1.2 Force-Induced Reaction of Spiropyran-Linked Polymers

Spiropyrans are a class of molecules known since the 1950s to undergo a 6- π electrocyclic ring-opening reaction to a vibrantly colored merocyanine (MC) form [33, 34]. Chemical structures for SP and expected MC form investigated in this dissertation are included in Fig 1.1a. A fluorescence signal in the visible range accompanies the absorbance (i.e. color change) of the MC form [35]. The particular absorption and fluorescence emission spectra of MC depend on any attached side groups on the SP/MC molecule (for example, the attached polymer chains are side groups) as well as the polarity of the surrounding environment [36, 37].

At room temperature with no external stimuli, both the SP and MC forms are effectively stable. The transition between the two forms is reversibly photochromic: UV light (ca. 385 nm) drives equilibrium toward the MC form, while visible (typically green) light promotes the SP species. Images of a SP-linked polymer sample, driven toward the SP form and MC form with appropriate light sources, are included in Fig 1.1b. The purple color of the UV-irradiated sample indicates presence of the MC form.

Potisek *et al.* first devised a method to functionalize the SP molecule such that it can be covalently bonded into a polymer backbone [14]. A number of publications have subsequently achieved solid state mechanically-induced activation of SP in a variety of bulk polymers [15, 38-40]. Fig 1.1c is a representative image of force-induced mechanochemical activation of a SP-linked polymer (discussed in Chapter 3). However, many of the fundamental parameters affecting mechanophore activation, such as stress, strain and polymer chain orientation have not been fully explored. The thesis research presented in this dissertation combines mechanical and optical measurements of SP-linked polymers to define the parameters promoting mechanochemical activation of SP, which can be applied to emerging mechanophore chemistries.

1.3 Thermomechanical Behavior of Mechanochemically Active Polymers

A fundamental topic of research for solid state mechanophore-linked polymers is the interplay between stress, strain and activation. Although SP activation has been shown in a number of different polymers [15, 38, 39], the relationship between polymer mechanics and activation is not yet fully understood. In this dissertation, the mechanochemical response of SP-linked polymers was monitored while varying parameters such as mechanical test protocol,

polymer chemistry, mechanophore structure, and thermomechanical response of a specific polymer chemistry.

Polymer mechanical behavior is strongly time and temperature dependent, with viscous response typically corresponding to high temperatures and long time frames, and elastic behavior at cold temperatures and short time scales [41, 42]. Typical polymer viscoelastic response in terms of the elastic modulus as a function of temperature is shown in Fig 1.2a, reproduced from Ward [43]. Ideally the solid state mechanical behavior of an amorphous polymer is viscoelastic, and can be divided into glassy and rubbery (or elastomeric) regimes, separated by a glass transition temperature, T_g , marked with a dashed line in Fig 1.2a. The corresponding mechanical behavior of a typical polymer under tensile deformation at different temperatures is included in Fig 1.2b. At temperatures well below T_g brittle failure (curve A) occurs. For temperatures close to T_g the mechanical behavior ranges from ductile (curve B) to cold drawing (curve C). At temperatures well above T_g polymers exhibit an elastomeric response (curve D) [43].

The relevant parameter when considering thermomechanical properties of polymers is the difference between the test temperature and T_g . This temperature difference can be affected by controlling test temperature in an environmental chamber, or introducing a plasticizing solvent to reduce the glass transition temperature of a polymer in its glassy state [44, 45]. Thermomechanical response of SP-linked poly(methyl methacrylate) (PMMA) – a glassy polymer at room temeprature - is described in Chapter 4. The effects of both temperature and plasticizing agent on SP activation are investigated.

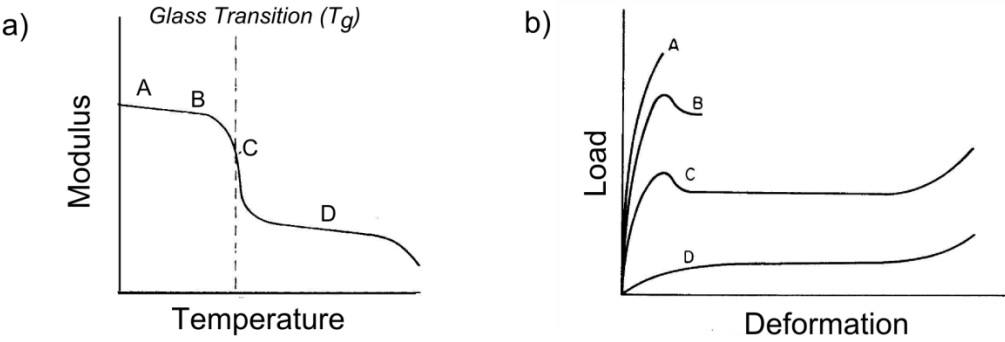


Figure 1.2. Thermomechanical behavior of polymers revised from [43]. a) Representative stiffness (elastic modulus) as a function of temperature, with glass transition temperature denoted. b) Load vs. deformation for polymer with varied viscoelastic response, corresponding to the moduli labeled in a). Mechanical behavior A is brittle, B is ductile, C corresponds to cold drawing and D is elastomeric.

1.4 Polymer Orientation Measurement

Previous publications have alluded to the importance of polymer chain alignment and orientation in the direction of applied force for achieving mechanochemical reactions [38, 39]. The hypothesis for mechanical activation in bulk polymers is that linearly oriented polymer chains, aligned in the direction of macroscopic stress, transfer force to the mechanophore more efficiently than a randomly oriented chain.

A variety of methods can be used to monitor the alignment of polymer chains, including x-ray diffraction, NMR, and birefringence [46, 47]. Of these methods, birefringence provides an appealing optical method to be combined with mechanical testing, as it is non-destructive and can be measured *in situ*. Birefringence in polymers is due to a difference in polarizability of the bonds along the polymer backbone compared to perpendicular to the backbone [48]. As the polymer chains orient in the draw direction, the anisotropic polarizability causes differing index of refraction between principle axes, i.e. birefringence, which can be quantified optically. In this dissertation, phase stepped photoelasticity was adopted for quantification of birefringence [49]. The change in birefringence is linearly proportional to the degree of polymer chain alignment [47, 50].

The orientation of the MC form of the mechanophore, distinct from the rest of the polymer chain, can also be monitored based on the transition dipole of MC. Transition dipoles indicate directional dependence of absorbance [51] and/or fluorescence emission [52] depending on the chemical structure and shape of the molecule. Experimental and computational measurements indicate that the transition dipole (\vec{r}) of the MC species lies across the long axis of the molecule (see Fig 1.1a) for both absorbance and fluorescence emission [53, 54]. As a result, fluorescence emitted from MC will be polarized roughly in the direction of the transition dipole. We can then analyze the average orientation of MC based on the polarization of its fluorescence emission [47, 55].

Chapters 3 and 5 of this dissertation report optical measurements of birefringence and fluorescence polarization, respectively, of SP-linked polymers. Correlation of these optical measurements with mechanophore activation provides insight about the role of orientation on mechanochemical reactions.

1.5 Overview of Thesis Research

The work presented in this dissertation has two overarching objectives:

- 1) Demonstrate the conditions which promote force-induced chemical reactions in linear polymers.
- 2) Use the mechanochemical reaction of SP to MC to gain knowledge about polymer mechanics.

The approach to these objectives is to incorporate SP into a variety of polymer backbones and correlate solid state SP to MC conversion with the mechanical response of the polymer. Glassy

and elastomeric polymers were tested in tension with a range of loading conditions (varied strain rate, stress relaxation, creep, etc.) in order to probe the mechanical response. Polymer structure (polymer chemistry, molecular weight and mechanophore linkage) was also controlled and SP activity was monitored.

A combined mechanical and optical experimental set-up has been developed to monitor the mechanochemical response of SP-linked polymers *in situ* during tensile loading. SP activation was quantified based on the fluorescence signal of the reacted MC form of the mechanophore. Additional optical measurements, combined with fluorescence, correlated the mechanochemical activation with alignment of the mechanophore and polymer.

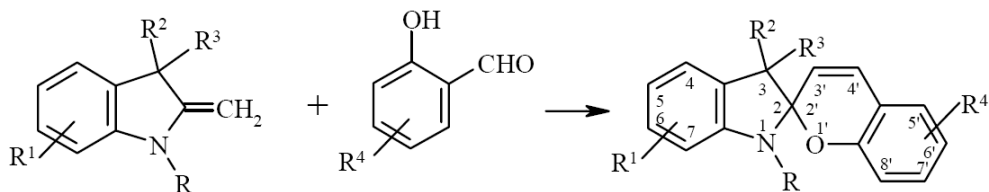
The result of this research provides fundamental guidelines for promoting force-induced chemical reactions of SP-linked polymers. The activation trends for SP-linked polymers provide a reference for achieving bulk activation of emerging mechanophore chemistries. Moreover, SP activation improves our understanding of polymer mechanics, specifically force on a polymer chain subjected to tensile deformation.

CHAPTER 2

SYNTHESIS AND FUNDAMENTAL CHARACTERIZATION OF SPIROPYRAN-LINKED POLYMERS

2.1 Introduction

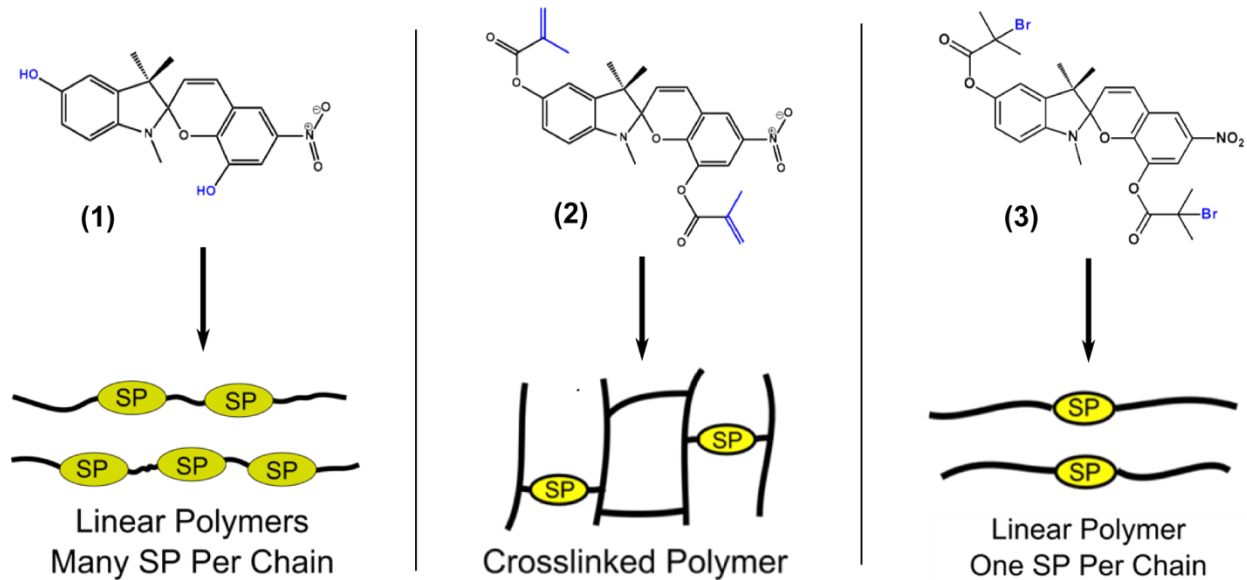
Electrocyclic ring-opening of spiropyrans has been studied extensively since the 1950s [33, 34, 56]. The spiropyran (SP) species contains a weak carbon-oxygen spiro bond which can cleave to form a zwitterionic merocyanine (MC) form. Typically this reaction has been driven photochemically or thermally. In 2001 Tipkin demonstrated mechanochemical conversion of spiropyran (SP) molecules by grinding the small molecule with a mortar and pestle [57]. Potisek *et al.* [14] later presented a chemical route for covalently bonding the molecule into a polymer backbone such that force was transferred across the SP species, and SP to MC conversion was driven with an applied tensile force. This chapter presents synthesis and characterization of SP-linked polymers following the precedence of Potisek [14] and Davis *et al.* [15], as well as additional SP-linked polymer chemistries.



Scheme 2.1. Typical synthesis of SPs by reaction of a methylene base with an *ortho*-hydroxy aromatic aldehyde, reproduced from Lukyanov et al [56].

SP is typically synthesized by condensation of a methylene base with an *ortho*-hydroxy aromatic aldehyde in the presence of piperidene, shown in Scheme 2.1 [56]. By adding functional groups on the 5 and 8' positions of this spiropyran structure, SP can be covalently

bonded into a polymer backbone [14, 15]. Three moieties shown in Scheme 2.2 have been devised for incorporation of SP into polymers. With hydroxyl functionality (Scheme 2.2, species **1**), SP acts as a monomer for a condensation polymerization [38]. The hydroxyl groups can be further functionalized to methacrylate [15] (Scheme 2.2, species **2**) or α -bromo ester [14, 15] (Scheme 2.2, species **3**) moieties. Species **2** incorporates SP as a cross-linker in a vinyl polymer. Species **3** acts as a living radical initiator off of which polymer chains can be grown. In all incorporation methods presented in Scheme 2.2, SP is covalently bonded into the polymer backbone and serves as a mechanochemically active species, or mechanophore.



Scheme 2.2. Chemical structures of bis-functionalized SP and method of incorporation into mechanochemically active polymer backbones. Species **1**: Hydroxide functionality to serve as a monomer for condensation polymers. Species **2**: Methacrylate functionality as a cross-linking unit in vinyl polymers. Species **3**: α -bromo ester functionality to act as an initiator for living radical polymerizations.

The predominant functionality explored in this work is the α -bromo ester moieties of species **3**, which acts as an initiator for synthesis of a variety of vinyl polymers by living radical polymerizations. Living radical polymerizations are characterized by a fast initiation step and relatively slow propagation of the polymer chain, resulting in low polydispersity indices

(PDIs) [58]. For the bis-functionalized SP (**3**) depicted in Scheme 2.2, low PDIs imply that polymer chains grown on each side of the SP species will reach similar degrees of polymerization, and SP will be centrally located in the polymer backbone. Single electron transfer living radical polymerization (SET-LRP) yields low PDIs [58], and is effective for synthesis of SP-linked poly(methyl acrylate) (PMA) [14, 15]. This chapter also explores SP as an initiator for atom transfer radical polymerizations, pioneered by Matyjaszewski *et al.* [59]. ATRP is initiated by the same functional moieties in species **3**, with a slight difference in the catalytic mechanism distinguishing ATRP from SET-LRP [60]. ATRP provides a synthesis route for additional SP-linked polymer systems, such as polystyrene (PS) and poly(methyl methacrylate) (PMMA).

2.2 Results

2.2.1 Synthesis of Linear Polymers by Living Radical Polymerizations

Three types of polymers were synthesized by living radical polymerizations: active SP-linked polymer, difunctional control SP-linked polymer, and plain polymer (without SP). Chemical structures of each are shown in Scheme 2.3. SP-linked polymers were synthesized using SP as a bis-functionalized initiator for the polymerization, i.e. polymer was grown at two sites on the mechanophore and one SP unit was centrally located in each polymer chain. Active SP structure **3a*** was linked into the polymer (at the 5 and 8' positions from scheme 2.1) to synthesize active SP-linked polymer species **3b**. This configuration promoted force transfer across the weak carbon-oxygen spiro bond bridging the 2' and 1' positions in Scheme 2.1. Species **3c** is the desired force-driven (activated) MC product. Species **4a** represents a control

* SP small molecules were synthesized by Douglas Davis and Preston May, UIUC Department of Chemistry

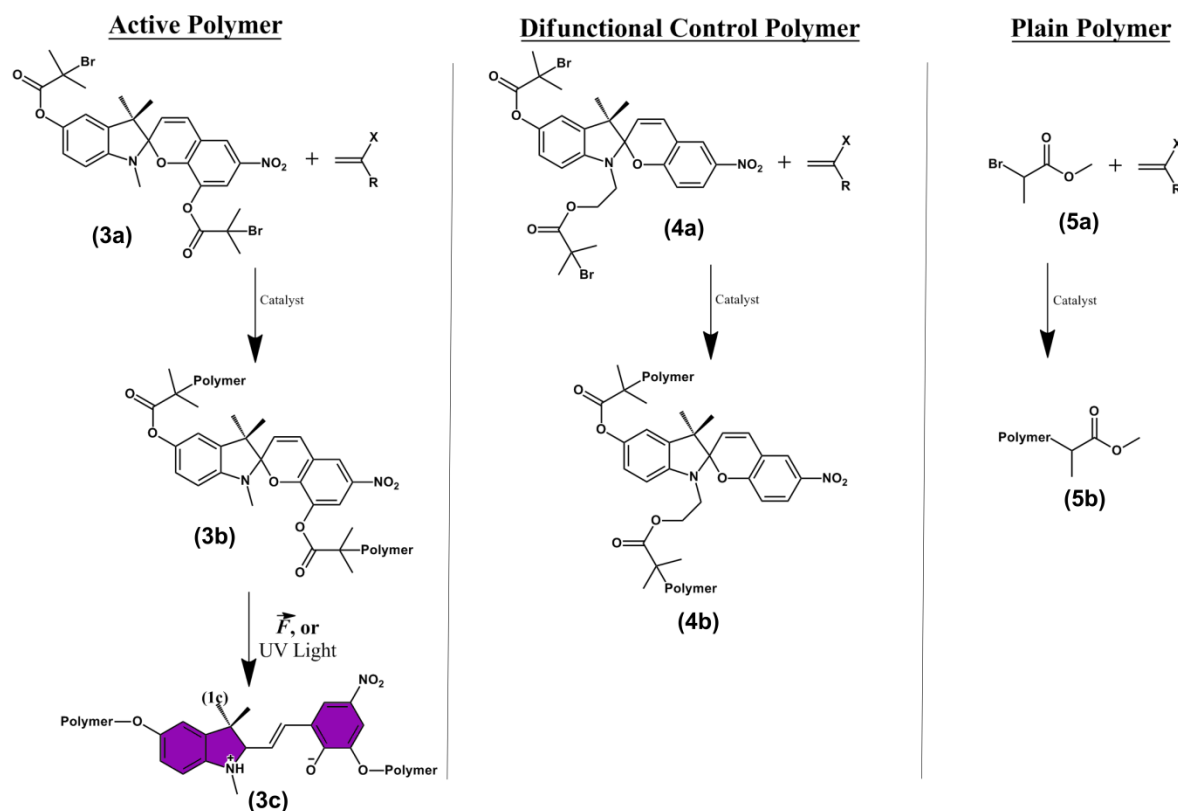
molecule containing SP, referred to as the difunctional control SP. Polymer chains were attached to the 1 and 5 positions of the SP species (scheme 2.1) such that load is not transferred across the force-sensitive spiro bond. Plain polymer without SP was synthesized using methyl-2-bromopropionate (M2BP) (species **5a**) as the initiator for polymerization. Relevant information for polymer syntheses is shown in Table 2.1 and described in detail below.

Table 2.1. Details for synthesis of vinyl polymers studied.

Polymer Type	Catalyst	Solvent	Reaction Temp. (°C)	Reaction Time (hrs)	Typical PDI
PMA	Cu Metal, Me-6-TREN	DMSO	22	4	1.1
PMMA	Cu Metal, CuCl, BPY	Acetonitrile	70	24	2.0
PS	Cu Metal, CuCl, BPY	None	100	24	2.0

PMA was synthesized *via* a SET-LRP reaction described in prior publications [14, 15]. Methyl acrylate monomer was purchased from Sigma-Aldrich and inhibitor was removed by filtration through basic alumina. Monomer and dimethyl sulfoxide (DMSO), a solvent for the polymerization, were sparged with Argon for 30 minutes. The catalyst system for this polymerization was metallic copper and tris[2-(dimethylamino)ethyl]amine, referred to as Me-6-TREN. Monomer, initiator, catalyst and solvent were mixed in a Pyrex flask with a Teflon-coated stir bar. Monomer amount was based on the amount of polymer desired, and was typically on the order of 5 g. The volume of solvent was the same as the volume of monomer. SP or M2BP concentration was calculated based on the desired molecular weight, ranging from 80-350 kDa in this study. The molar concentration of each catalyst component unit was 4x the concentration of the initiator. Once all materials were added, the flask was submerged in liquid nitrogen until frozen, at which time a vacuum was applied for 30 minutes. The flask was then sealed and the mixture was thawed. After thawing, the mixture was frozen again and the freeze-

pump-thaw cycle was repeated 3x in order to minimize any dissolved gasses (oxygen and water vapor) in the monomer which would inhibit radical polymerization. After the third freeze-pump thaw cycle, the flask was placed under an argon atmosphere. A Schlenk line was used so that no air was introduced into the system between pulling vacuum and adding argon. The mixture was then submerged in a water bath at room temperature (approximately 22 °C) for 4 hours. The product was a reddish brown viscous liquid or gel.



Scheme 2.3. Chemical structures and living radical polymerizations for mechanochemically active SP-linked polymer (**3a-c**), difunctional control SP-linked polymer (**4a-b**), and plain polymer (**5b**) without SP, initiated by methyl-2-bromopropionate (**5a**).

The product was dissolved into ca. 200 mL tetrahydrofuran (THF) and filtered three times through silica powder and a coarse Buchner funnel to remove catalyst. Roto-Vap equipment was used to evaporate off the majority of the remaining solvent. The solution was

reduced to approximately 20 mL volume using the Roto-Vap, and then dripped into methanol (MeOH). Approximately 200 mL MeOH was used for every 5 mL polymer solution. Methanol provided a solvent for THF but not for PMA, and the polymer crashed out of solution as a solid. Solid PMA was collected in a flask and vacuum was applied to dry the polymer.

PMA was initially dried at room temperature, but the resulting polymer properties were inconsistent between batches. $^1\text{H-NMR}$ indicated the presence of residual THF accounting for plasticizing and variability in properties. Plasticized difunctional control PMA described in Chapter 3, dried at room temperature, contained approximately 3 wt% THF by NMR analysis. All other polymers presented in this thesis were dried for 24 hours at 60 °C – above the boiling point of THF. NMR analysis of the resulting polymer did not show traces of THF.

Poly(methyl methacrylate) and polystyrene were synthesized via atom transfer radical polymerization (ATRP) described by Matyjaszewski [59, 61] and further studied by Wang *et al.* [62]. The experimental procedure for the ATRP reaction was fundamentally the same as SET-LRP, with different catalyst, solvent, reaction time and reaction temperatures, outlined in Table 2.1. The ATRP catalyst system was copper powder (99%), CuCl (\geq 99%), and 2,2'-bipyridine (BPY) (\geq 99%), purchased from Sigma-Aldrich and used as received. All catalyst components had concentration equal to 4x the molar concentration of initiator. Monomer (with inhibitor removed by basic alumina), solvent (if applicable) and catalysts were mixed and subjected to the same freeze-pump-thaw cycles described above. The polymerization was allowed to run at elevated temperature for 24 hours. The resulting solid polymers were dissolved into THF, filtered through silica powder, and dried for 24 hours at 60 °C.

Polymers were synthesized with near theoretical yield. The process of filtering and drying led to some material loss, and approximately 60-70% of the monomer mass was

recovered as a dry polymer. Number average molecular weights of polymers typically agreed to within 15% of theoretically predicted values assuming full consumption of the monomer. PDIs were consistent from batch to batch for each polymer type. The PDI of SP-linked PMA synthesized by a SET-LRP method was approximately 1.1, implying a centrally located mechanophore. The PDIs of SP-linked PMMA and PS were approximately 2.0.

2.2.2 Thermomechanical Properties of SP-Linked Polymers

The glass transition temperatures (T_g) of the polymers studied were determined by differential scanning calorimetry (DSC) using Mettler-Toledo model DSC821 equipment. Sample temperature was ramped at 3 °C/min and a shoulder on the curve of heat flow *vs.* temperature was taken as the T_g . Representative DSC curves are provided in Fig 2.1 for PMMA polymer of the three structures shown in Scheme 2.3. The T_g values for each initiator type agree to within *ca.* 2 °C. Glass transition temperatures from DSC analysis of each polymer type studied in this thesis are presented in Table 2.2. Dynamic mechanical analysis (DMA) was used to confirm the glass transition temperature of active SP-linked polymers using TA Instruments RSA3 equipment, also at a ramp rate of 3 °C/min. A representative $\tan(\delta)$ curve for active SP-linked PMMA is also plotted in Fig 2.1. The T_g determined from the peak of the $\tan(\delta)$ temperature sweep is in close agreement with the DSC results.

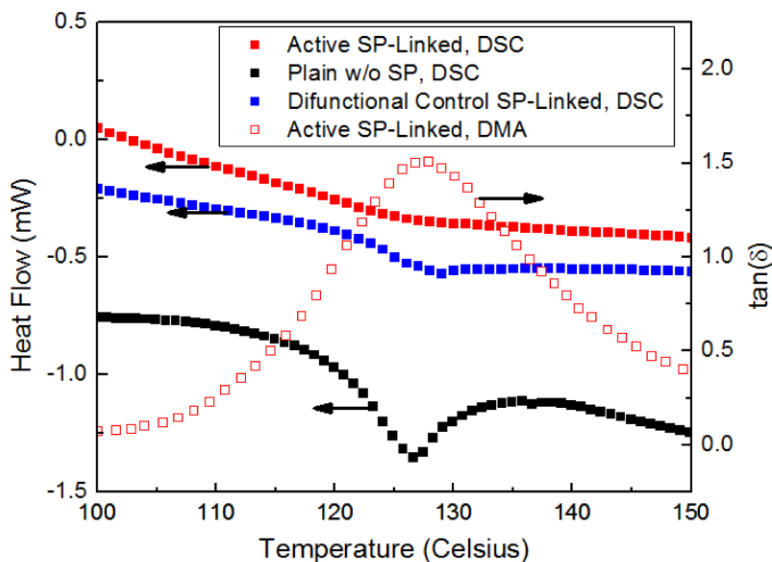


Figure 2.1. Representative DSC curves of active SP-linked PMMA, difunctional control SP-linked PMMA and plain PMMA. DMA analysis has been included for active SP-linked PMMA.

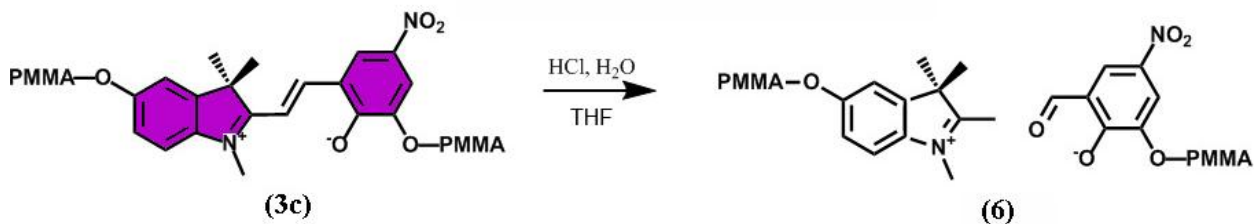
The glass transition of PMA occurred at a temperature of approximately 12 °C, and the resulting polymer is elastomeric at room temperature. T_g of PMMA and PS were 127 °C and 105 °C, respectively, corresponding to glassy polymers. The T_g of each polymer was unchanged by incorporation of SP. Thus the effect of SP incorporation on the thermomechanical properties of the polymers studied was considered negligible. Polymers studied had molecular weights greater than 80 kDa, and T_g for each polymer type was not affected by the molecular weight.

Table 2.2. Glass transition temperatures of polymers studied, as determined by DSC analysis.

Polymer	SP Incorporation	T_g (°C)
PMA	No SP (Plain)	12
	Active SP-Linked	13
	Difunctional Control SP-Linked	12
PMMA	No SP (Plain)	126
	Active SP-Linked	127
	Difunctional Control SP-Linked	129
PS	No SP (Plain)	104
	Active SP-Linked	105
	Difunctional Control SP-Linked	105

2.2.3 SP Cleavage Experiments

The mechanophore in its MC form, linked into linear PMMA, was cleaved in order to provide insight on the location of the SP within the polymer backbone. Cleavage of SP subspecies was performed via the method introduced by Stafforst [63] and outlined in Scheme 2.4. 100 mg polymer was dissolved in 2 mL THF, and 0.5 mL 1 M HCl was added and the solution was irradiated with UV light to drive the active mechanophore species toward the open MC form **3c**, which was hydrolyzed to species **6**. The solution was then re-filtered by the method described in section 2.2.1 and GPC was run on the resulting polymer to measure molecular weights after cleavage. Difunctional control SP-linked PMMA and plain PMMA were subjected to the same treatment.



Scheme 2.4. Cleavage of the mechanophore in its MC form by a strong acid.

Molecular weights before and after acid treatment are summarized in Table 2.3. Cleavage of SP reduced the molecular weight of active material roughly in half, while the PDI was not substantially increased, implying that SP was centrally located in the PMMA chains. Plain PMMA and difunctional SP-linked control PMMA showed no reduction in molecular weight under SP cleavage conditions, thus the polymer itself was unaffected by SP cleavage conditions.

Table 2.3. Molecular weight characterization of as-synthesized and SP-cleaved PMMA.

PMMA Type	Synthesized M_N (kDa)	SP Cleaved M_N (kDa)	Synthesized PDI	SP Cleaved PDI
Plain	78	82	1.5	1.5
Active	260	123	2.0	2.1
Difunctional Control	185	181	2.0	2.0

2.2.4 *Fluorescence Spectra of SP-Linked Polymers*

The equilibrium of SP and MC can be driven toward either form by the appropriate wavelength of light. Visible light - particularly green light with maximum absorbance near $\lambda = 550$ nm - drives the molecule to its SP form, which is typically uncolored or slightly yellow. Irradiation with UV light at ca. 385 nm (UV-activation) promotes the MC form, which is accompanied by a vibrant purple or red color from visible-range absorbance of the MC species. In addition to a color change of the MC form, the MC form is known to fluoresce with broad excitation and emission in the visible spectrum [35]. The locations of excitation and emission peaks vary with the polarity of the environment [36], which in this case is solid polymer. The research presented in this dissertation makes use of the fluorescence signal of the MC form as a relative indicator of mechanophore activation.

SP-linked PMA was driven toward the MC form by UV light, and excitation and emission peaks in the visible spectrum were taken by a Fluoromax Model 4 Spectrophotometer. Fluorescence spectra are plotted in Fig 2.2. Excitation and emission peaks for UV-activated SP-linked PMA were located at approximately 550 nm and 650 nm, respectively. The fluorescence emission of samples driven toward the SP form using visible light was orders of magnitude smaller than the UV activated case and was considered negligible. Fluorescence spectra of UV-

activated SP-linked PMA provided the basis for an experimental set-up combining mechanical and fluorescence measurement described thoroughly in Chapter 3.

A 532 nm excitation source was selected for the combined mechanical and optical testing set-up. This wavelength lies near the excitation peak for SP-linked PMA. MC fluorescence emission was filtered to wavelengths greater than 575 nm and collected *in situ* (during mechanical testing) on a hand-held Ocean Optics spectrometer, model HR2000+. Fluorescence emission spectra under these excitation conditions are shown in Fig 2.3 for active SP-linked PMA. A UV-activated case and a mechanically activated case are plotted for comparison. In the mechanically activated case, mechanophore-linked polymer was first driven toward the SP form using visible light, then a tensile force was applied to mechanically drive the SP to the fluorescent MC form, and a spectrum was taken. The emission peak shifts to lower wavelengths for mechanically activated SP-linked PMA (ca. 600 nm) when compared with the UV activated case (650 nm). A possible explanation for the spectral shift is different isomeric configuration of the MC species in the mechanically activated case compared to the UV activated case [37]. In both cases, a strong fluorescence signal was detectable only after the application of a driving force toward the MC form (mechanical or photochemical).

Excitation and emission spectra for mechanically activated SP-linked PMMA are included in Fig 2.4. Irradiation with UV light was not sufficient to drive the mechanophore to the MC form in glassy polymer systems, so the UV activated case was not analyzed. An emission peak was located at *ca.* 620 nm for 532 nm excitation, thus the 532 nm light source effectively excited MC fluorescence in this polymer system. Bulk SP-linked polystyrene was not activated by either UV light or mechanical force, therefore spectra are not included. However, mechanical deformation of SP-linked polystyrene thin films described in Chapter 6 led to the

emergence of a fluorescence signal when excited with 532 nm light. A similar fluorescence signal was assumed for MC in a PS environment to that of MC in PMA and PMMA.

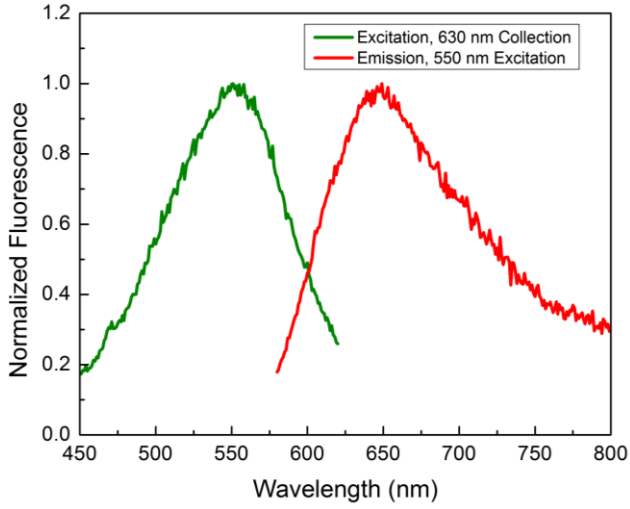


Figure 2.2. Excitation and emission spectra for UV-activated SP-linked PMA. Fluorescence intensity has been normalized by the maximum fluorescence value for each spectrum.

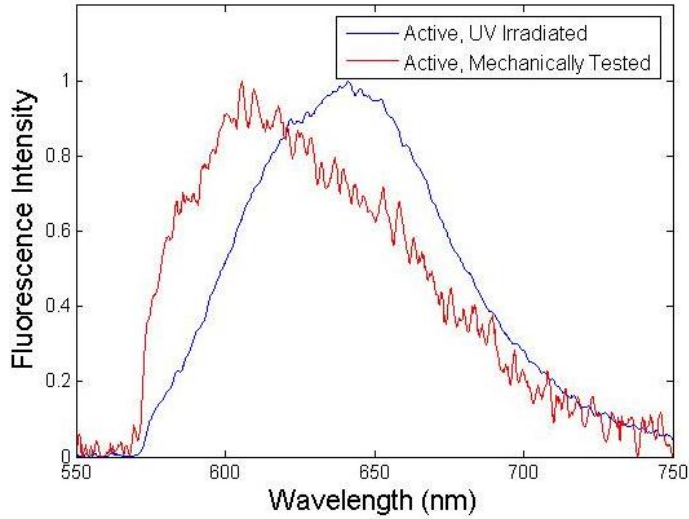


Figure 2.3. Active SP-linked PMA fluorescence emission after UV irradiation and mechanical activation. Fluorescence was excited with a 532 nm laser and collected at wavelengths greater than 575 nm *in situ* using a hand-held spectrometer. Noise in the mechanically tested case was due to low signal relative to the UV irradiated case. Fluorescence intensity has been normalized by the maximum fluorescence value for each spectrum.

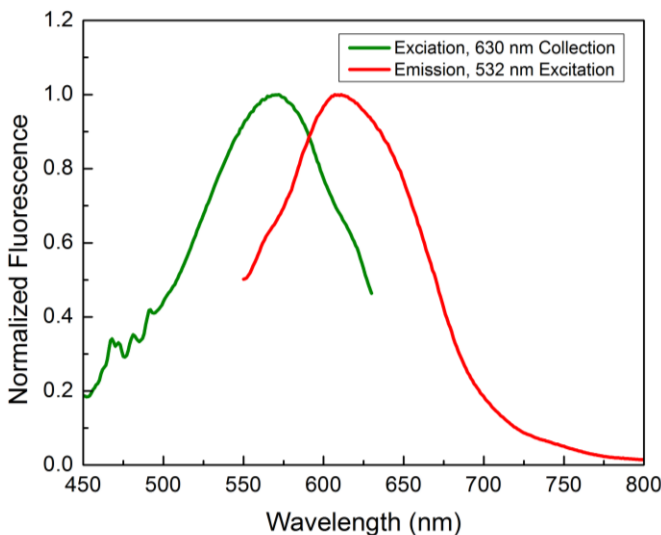


Figure 2.4. Excitation and emission spectra for mechanically activated SP-linked PMMA. The sample was strained to failure at 90 °C and quenched at room temperature prior to fluorescence measurement. Fluorescence intensity has been normalized by the maximum fluorescence value for each spectrum.

2.3 Conclusions

Spiropyran has been covalently bonded into the center of a several different polymer backbones using SP as an initiator for living radical polymerizations. Mechanochemically active SP-linked linear PMA was synthesized with low PDIs by the SET-LRP method previously described by Potisek [14] and Davis *et al.* [15]. Glassy SP-linked polymers (polystyrene and PMMA) were synthesized *via* ATRP polymerizations. Controls containing SP and plain polymer controls (without SP incorporated) have been synthesized for each polymer type. Incorporation of SP had a negligible effect on thermomechanical behavior of polymers.

Fluorescence spectra were recorded for SP-linked PMA. After irradiation with visible light such that the mechanophore was predominantly in its SP form, very little fluorescence was detectable. When the mechanophore was driven to its MC form by UV irradiation ($\lambda = 385$ nm), strong excitation and emission peaks were located at 550 nm and 650 nm, respectively. These studies establish that a green light source is effective at exciting MC fluorescence, which can be

collected and quantified as a relative measure of mechanically-driven SP to MC conversion. Fluorescence detection is shown to be feasible for a glassy mechanophore-linked polymer system (SP-linked PMMA) as well.

CHAPTER 3

MECHANICAL AND OPTICAL CHARACTERIZATION OF AN SP-LINKED ELASTOMER

3.1 Introduction

In a seminal publication by Davis *et al.*[15] force-induced chemical conversion of spiropyran (SP) was demonstrated when the mechanophore was bonded into the backbone of poly(methyl acrylate) (PMA), a linear elastomer. SP was activated to its merocyanine (MC) form (chemical structures shown in Chapter 2) with applied tensile deformation. Activation was detectable at strains on the order of hundreds of percent, i.e. stretch ratios greater than two times the un-deformed sample length. SP activation was indicated visually by the emergence of purple color in the gauge section of tensile specimens.

While SP activation has been demonstrated qualitatively in elastomeric PMA and other polymers [38-40], many of the fundamental parameters influencing mechanophore activation, such as stress, deformation and polymer chain orientation have not been fully explored. The following chapter utilizes SP-linked PMA in its linear form as a model system to study parameters which affect mechanochemical reactions.

In addition to a color change, the activation of SP to MC is accompanied by the emergence of a fluorescence signal of the MC form described in Chapter 2. The fluorescence signature can be utilized in order to quantify the activation of the mechanophore. In this chapter, fluorescence detection is combined with tensile loading. The influence of key and controlling parameters such as deformation rate, load times, and polymer architecture are investigated to

provide insight on the interplay between stress, deformation, and time in mechanochemical reactions.

Recent publications have proposed that alignment of polymer chains in the direction of macroscopic force promotes mechanochemical reactions [38, 39], but as yet polymer orientation and activation have not been quantitatively correlated. This chapter combines mechanical and fluorescence measurement with a third technique, birefringence, which provides a relative measure of polymer chain alignment [50]. Photoelasticity was selected as an optical method for calculation of birefringence, and this method could be added using the same light source as the fluorescence excitation.

The trends established in this chapter serve as guides for development of new mechanophore-linked polymers, particularly elastomeric systems. Optimal parameters for SP activation in an elastomeric polymer are discussed.

3.2 Experimental

3.2.1 Materials

Linear mechanochemically active SP-linked PMA was synthesized using SP as an initiator for a single electron transfer living radical polymerization (SET-LRP) described in Chapter 2. Control PMA was synthesized with SP linked into the backbone such that force was not transferred across the sensitive C-O spiro bond. This linkage will be referred to as difunctional control SP-linked polymer throughout this dissertation. Active and difunctional control SP chemical structures are included in the Scheme 2.3. Linear polymers synthesized had polydispersity indices (PDIs) of below 1.2. Glass transition temperatures measured by differential scanning calorimetry and confirmed by dynamic mechanical analysis (both at

temperature ramp rates of 3°C) were approximately 12 °C for active, SP-linked control, and plain PMA without SP linked into the polymer backbone. The effect of SP incorporation on polymer thermomechanical properties was considered negligible. Over the range of polymer molecular weights considered in this study ($M_n > 80$ kDa) the thermomechanical properties were essentially constant as well.

SP was also synthesized with a dendrimeric structure such that multiple α -bromo ester functionalities were present at both attachment points of the mechanophore, as described by May *et al.* [64]. Synthesis of the dendrimeric mechanophore structures was based off work by Ihre *et al.* [65]. Multiple polymer chains (Fig 3.1) were then added to the SP molecule via the same SET-LRP reaction described in Chapter 2. The aim of multiple polymer arms at each attachment point was to magnify the force across the mechanophore. The three structures will be referred to as linear, 4-arm and 8-arm SP-linked PMA. If not otherwise specified, active SP-linked PMA refers to the linear configuration.

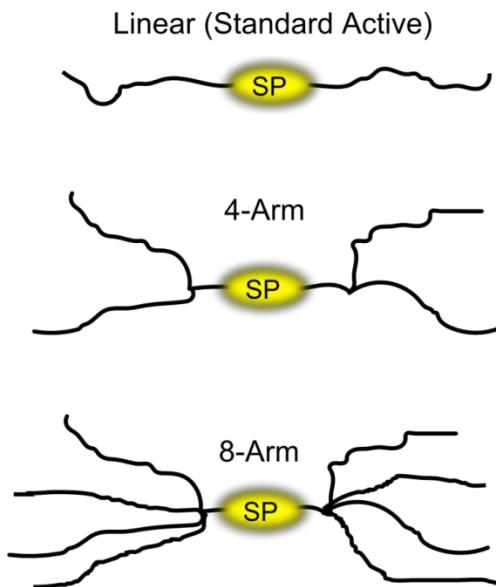


Figure 3.1. Representative structures of linear, 4-arm and 8-arm SP-linked PMA.

Active, difunctional control, and plain PMA samples were molded from dried pellets at PMA was molded at a pressure of 200 psi at 150 °F (66 °C) for 10 minutes in a closed mold. Approximate sample dimensions are shown in Appendix A.

3.2.2 Tensile Testing Protocol

All polymer samples in this study were tested in tension using a custom uniaxial load frame from IMAC Motion Control Corporation. Two opposing screw driven actuators applied an identical displacement to each side of polymer sample such that the center of the sample remained in the field of view for optical studies. Load in the polymer sample was detected using a 5-lb Honeywell Sensotec Load Cell (Model 31) attached to one of the actuators. Displacement of the actuators was controlled through NI LabVIEW. The load frame was oriented horizontally on an optical table.

Unless otherwise specified, samples were irradiated with green light ($\lambda = 532$ nm) for 10 minutes at RT prior to testing in order to drive the mechanophores predominantly to the SP form. For monotonic tensile testing, the load frame was displacement-controlled and applied stretch rates were 0.10 s^{-1} , 0.02 s^{-1} , or 0.004 s^{-1} . For stress relaxation testing, samples were loaded at a relatively high deformation rate (0.10 s^{-1}) then held at a constant amount of deformation, and the optical and mechanical response was monitored over time.

3.2.3 Combined Mechanical and Optical Experimental Setup

A novel mechanical and optical experimental set-up was developed to monitor *in situ* activation of the mechanophore during tensile testing. Fluorescence was captured as a full field image via a CCD camera and defined as average pixel intensity over the gauge section of the

sample. Birefringence was simultaneously detected with mechanical and fluorescence measurements.

A schematic and photo of the full optical and mechanical setup are shown in Figs 3.2a and 3.2b, respectively. A collimated circularly polarized incident light source was incident on a polymer sample, which acted both as a monochromatic light source for photoelasticity (birefringence measurement) and a excitation source for fluorescence of the activated MC form of the mechanophore. After passing through the sample, the incident wavelength ($\lambda = 532$ nm) was reflected at 90° for the photoelastic beam, while higher wavelengths ($\lambda > 575$) were passed for collection of the fluorescence signal on a color CCD camera (AVT Stingray F504c). The photoelastic beam was then separated into four identical beams using a two-dimensional diffraction grating, and the resulting images were passed through polarization optics such that the photoelastic state could be fully characterized. The birefringence signal was then captured as four images in a single CCD (AVT Stingray F145b) and values for birefringence, Δn , were calculated by phase stepping [49, 66]. Birefringence detection and polarization optics used in these experiments are explained more thoroughly by Kramer *et al.* [67]. Full field fluorescence and birefringence signals were simultaneously captured with the same field of view during tensile testing of dog-bone shaped specimens (Fig 3.3).

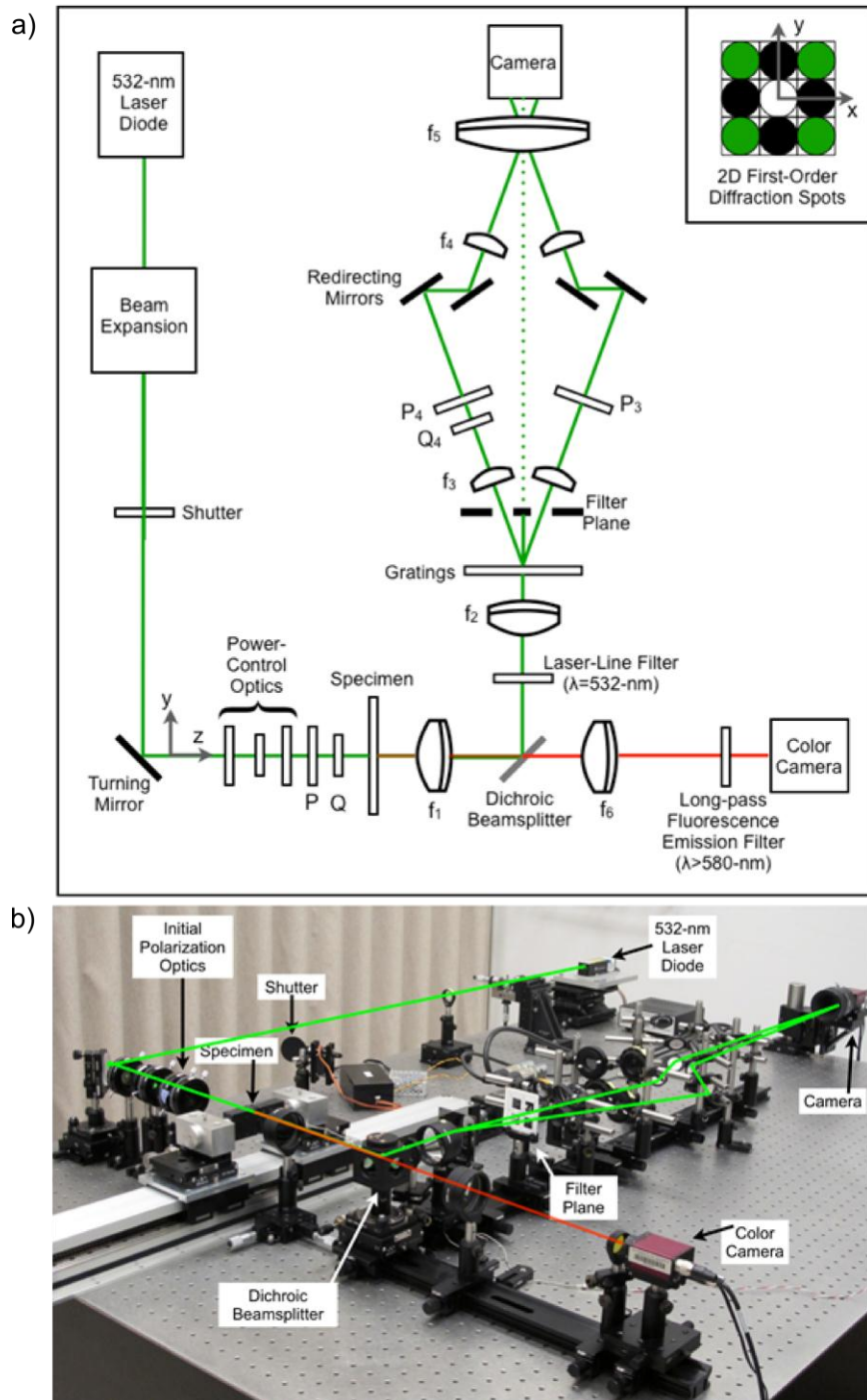


Figure 3.2. Combined optical and mechanical setup shown as a) a schematic, and b) a photographic image. The illustrated green beam represents the incident laser wavelength (532 nm) while the red beam represents fluorescence signal from MC present in the polymer. Only two of the four diffracted beams for birefringence detection are indicated for image clarity.

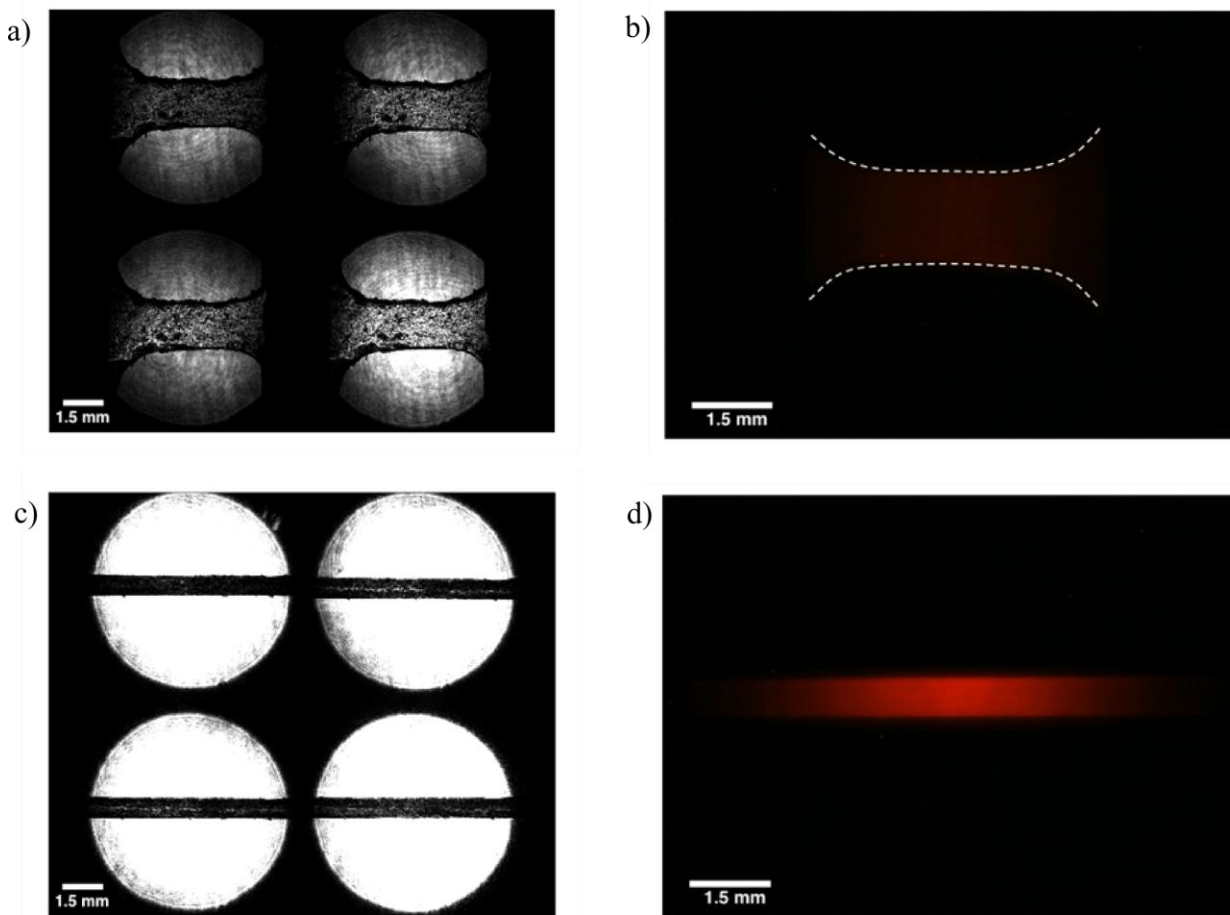


Figure 3.3 Typical images for simultaneous capture of fluorescence and photoelasticity: a) Four photoelastic beams (I_1 upper left; I_2 upper right; I_3 lower left; and I_4 lower right) for $\lambda = 1.0$; b) fluorescence image for $\lambda = 1.0$ with the edges of the sample outlined in dashed white lines; c) four photoelastic beams for $\lambda = 9.0$; and d) fluorescence image for $\lambda = 9.0$.

Birefringence and fluorescence images were taken at intervals of 1 s, 5 s, and 25 s corresponding to deformation rates of 0.10 s^{-1} , 0.02 s^{-1} , or 0.004 s^{-1} , respectively. Constant fluorescence imaging conditions (180 μW laser power, 800 ms exposure) were maintained unless otherwise stated. Although 532 nm light drives the mechanophore equilibrium toward the SP form, the laser power was selected so that photochemical conversion was considered negligible when compared with the mechanical activation. A mechanical shutter between the laser and

sample blocked the laser between fluorescence images to further minimize conversion of MC species to the SP form.

3.2.4 Birefringence and Fluorescence Measurement

The optical birefringence, Δn , of a polymer gives a relative measure of polymer chain alignment with respect to a reference direction [50]. Here, the optical birefringence is determined using phase-stepped photoelasticity. In a standard phase-stepped photoelastic setup, two quantities, the isoclinic angle, θ , (the angle of principal optical axis) and the isochromatic phase, δ , (the relative retardation of the polarized light through the polymer) can be extracted from four different interference patterns [49, 66, 67]. The isochromatic phase is related to the birefringence by following equation:

$$\delta = \frac{\Delta n \lambda}{2\pi h} \quad 3.1$$

where λ is the wavelength of incident light (532 nm) and h is the thickness of the sample. Using polarization optics oriented as described by Kramer *et al.* [67], the intensities of the four images in Fig 3.3a and 3.3c are, from top left to bottom right,

$$I_1 = I_0[1 - \sin(\delta)\cos(2\theta)] \quad 3.2a$$

$$I_2 = I_0[1 + \sin(\delta)\sin(2\theta)] \quad 3.2b$$

$$I_3 = I_0[1 - \sin(\delta)\sin(2\theta)] \quad 3.2c$$

$$I_4 = I_0[1 + \cos(\delta)] \quad 3.2d.$$

From these equations the isoclinic angle and isochromatic phase can be derived:

$$\theta = \frac{1}{2}\arctan\left(\frac{I_2 - I_3}{I_2 + I_3 - 2I_1}\right) \quad 3.3$$

and

$$\delta = \arctan\left(\frac{I_2 + I_3 - 2I_1}{\cos(2\theta)[2I_4 - (I_2 + I_3)]}\right) \quad 3.4.$$

The pixel intensities were averaged over the gauge section of each image to determine $I_1 - I_4$. The resulting isochromatic phase, δ , is “wrapped” with bounds of $(-\pi/2, \pi/2]$, and had to be “unwrapped” by adding the absolute value of the change in the phase whenever the phase reaches its upper bound. The “unwrapped” phase could then be converted to a birefringence value using Eq. 3.1.

Fluorescence was defined as the red channel intensity of the color images (representative images are included in Fig 3.3b and 3.3d), averaged over pixels in the gauge section of the sample. The field of view was kept constant for each fluorescence measurement. The thickness corrected fluorescence was obtained by correcting for (i) the change in the number of SP in the field of view of the camera due to the large thickness change during the course of each test, and (ii) the variation in initial thickness between specimens. The stretch ratio in the thickness direction, λ^T , was assumed to be the same as the stretch ratio in the width direction, λ^W , since both of those directions were unconstrained during the uniaxial loading. The material did not exhibit incompressible behavior. The width stretch ratio was determined by optically measuring the gauge section width in each image. Length stretch ratio was determined from crosshead displacement. The thickness correction was applied by dividing the raw fluorescence intensity by thickness stretch ratio, assuming $\lambda^W = \lambda^T$. Thickness corrected fluorescence was also normalized by the initial intensity at $\lambda = 1$.

3.3 Results and Discussion

3.3.1 Simultaneous Measurement of Stress, Birefringence and Fluorescence

Active PMA samples were deformed at a constant deformation rate until failure and the mechanical and optical response was measured. Images of a representative active SP-linked PMA sample before and after testing are provided in Fig 1.1c. Stretch ratio (λ , defined as instantaneous sample gauge length divided by un-deformed gauge length) and true stress (σ_{true} , calculated based on optically measured sample width and assuming the width stretch ratio was the same as the thickness stretch ratio) were determined from the sample thickness and measured load. Representative data for a mechanochemically active sample tested at a stretch rate ($d\lambda/dt$) of 0.02 s^{-1} are plotted in Fig 3.4. Stress increased consistently as a function of increasing stretch ratio until failure, which typically occurred at a stretch ratio between 10 and 12. An increase in slope of the stress *vs.* stretch ratio plot, i.e. hardening, occurred with increasing deformation. Birefringence (Δn) had a negative value with respect to the tensile direction, agreeing with previously published data by Saiz *et al.* [68]. This effect was likely due to bulky pendant methacrylate groups on the PMA backbone. In figure 3.4, the birefringence was plotted in terms of its relative magnitude (the Δn value multiplied by -10^3). The magnitude of Δn increased with increasing stretch ratio, indicating alignment of the polymer backbone in the direction of loading, and then leveled out at large stretch ratios as the polymer chains reached maximum alignment. The intensity of the fluorescence signal (I_{fl}) was assumed proportional to the amount of activated SP, i.e. MC, in the beam path. At room temperature ($RT = 22 \text{ }^\circ\text{C}$), a small amount of MC was present in the specimen, which led to some fluorescence at a stretch ratio of 1.0 ($\lambda = 1$). During the initial loading, the fluorescence signal decreased due to sample thinning (i.e. lower mechanophore concentration in the fluorescence image field of view.) With increasing stretch

ratio, the fluorescence intensity began to increase indicating activation of SP to the fluorescent MC form. The onset of activation was defined at the stretch ratio, λ^* , at which the increase in SP activation was significant enough that the slope of the raw fluorescence intensity *vs.* stretch ratio having a positive value, as is marked by an arrow in Fig 3.4.

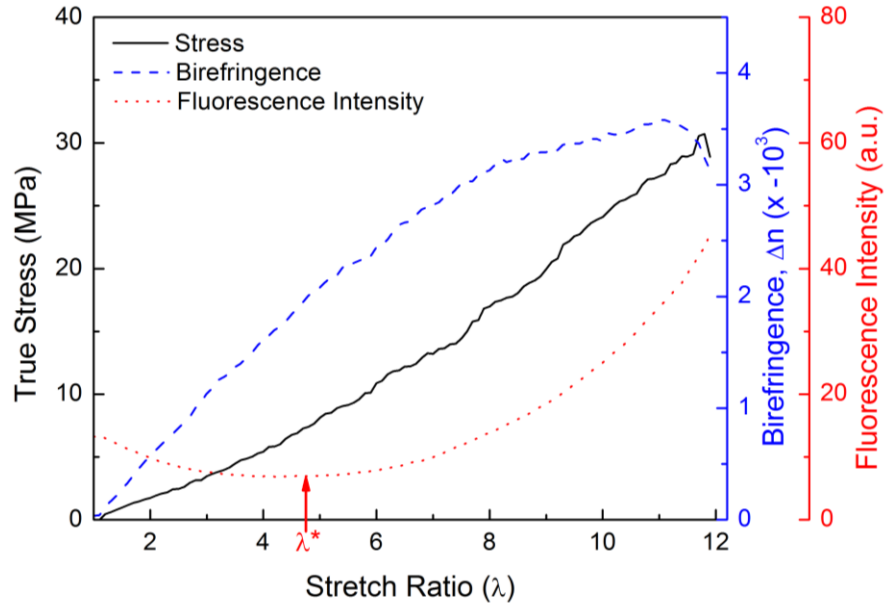


Figure 3.4. Simultaneously obtained stress, birefringence and raw fluorescence intensity *vs.* stretch ratio for active SP-linked PMA under tensile deformation at a rate of 0.02 s^{-1} . The stretch ratio at activation, λ^* , is indicated by an arrow.

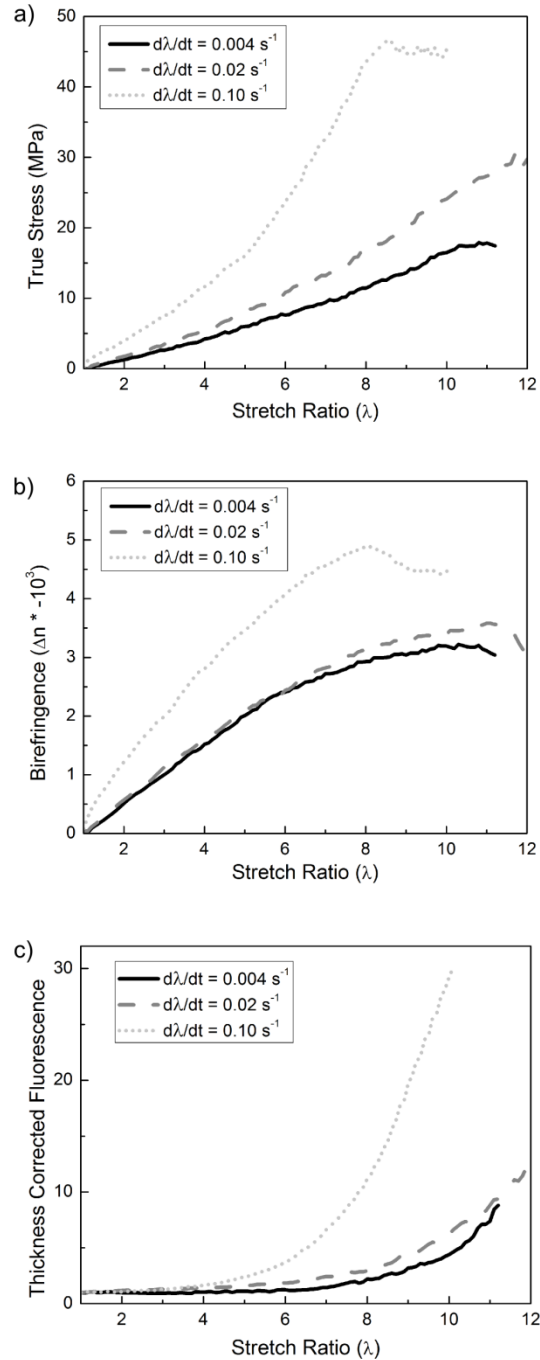


Figure 3.5. Representative properties of active SP-linked PMA at stretch rate ($d\lambda/dt$) of 0.004 s^{-1} , 0.02 s^{-1} and 0.10 s^{-1} . a) True stress vs. stretch ratio, b) birefringence vs. stretch ratio, and c) thickness-corrected, normalized fluorescence intensity vs. stretch ratio.

3.3.2 Deformation Rate Dependence in Linear Active SP-Linked PMA

Active PMA samples were tested at stretch rates of 0.004 s^{-1} , 0.02 s^{-1} and 0.10 s^{-1} . The resulting polymer behavior – stress, birefringence, and thickness corrected fluorescence – are plotted in Fig 3.5 for representative samples at each stretch rate. The stress (Fig 3.5a) in the polymer samples increased with increasing stretch rate as expected for an elastomeric material. In virtually all samples hardening was observed with increasing stretch ratio. Birefringence (Fig 3.5b) also increased with increasing stretch rate. Birefringence values began to plateau at high stretch ratios as the chains became maximally aligned in the direction of force. The fluorescence intensity (Fig 3.5c) was adjusted for the number of mechanophores in the field of view and normalized by the fluorescence value at ambient equilibrium ($\lambda = 1$) fluorescence intensity, as described in section 3.2.4. For all stretch rates, rapid activation of SP at large stretch ratios coincided with a plateau in the birefringence, during which polymer chains approached maximum alignment and hardening. Increased birefringence and fluorescence were considerably more apparent in the fastest testing rate (0.10 s^{-1}) when compared with middle and slowest stretch rates (0.004 s^{-1} and 0.02 s^{-1}). The marked increase in fluorescence at higher stretch rates coincided with an increase in load on the polymer samples. This finding implies that larger macroscopic stress at higher stretch rate leads to greater force across the mechanophore and more extensive ring opening of SP.

Figs 3.6a-c reveal the trend in stretch ratio, stress, and birefringence at the activation point, as defined in section 3.3.1, averaged over three samples at each deformation rate. The stretch value at activation, λ^* , shows a marked decrease at the fastest deformation rate. The true stress, σ^* , shows an increasing trend, indicating that although macroscopic stress is positively correlated to SP activation, the same macroscopic stress does not necessarily translate to the

same force and activation of SP at the molecular scale. Activation birefringence values, Δn^* , were similar between stretch rates, indicating that a similar degree of chain alignment was present at the onset of SP activation, regardless of the stretch rate. Finally, the rate of change of fluorescence intensity with respect to stretch ratio was averaged between stretch ratios of 8 and 9, where all samples showed an increasing fluorescence signal, but none had failed. The results plotted in Fig 3.6d show a clear trend of greater rate of fluorescence change (i.e. SP activation) with increasing deformation rates.

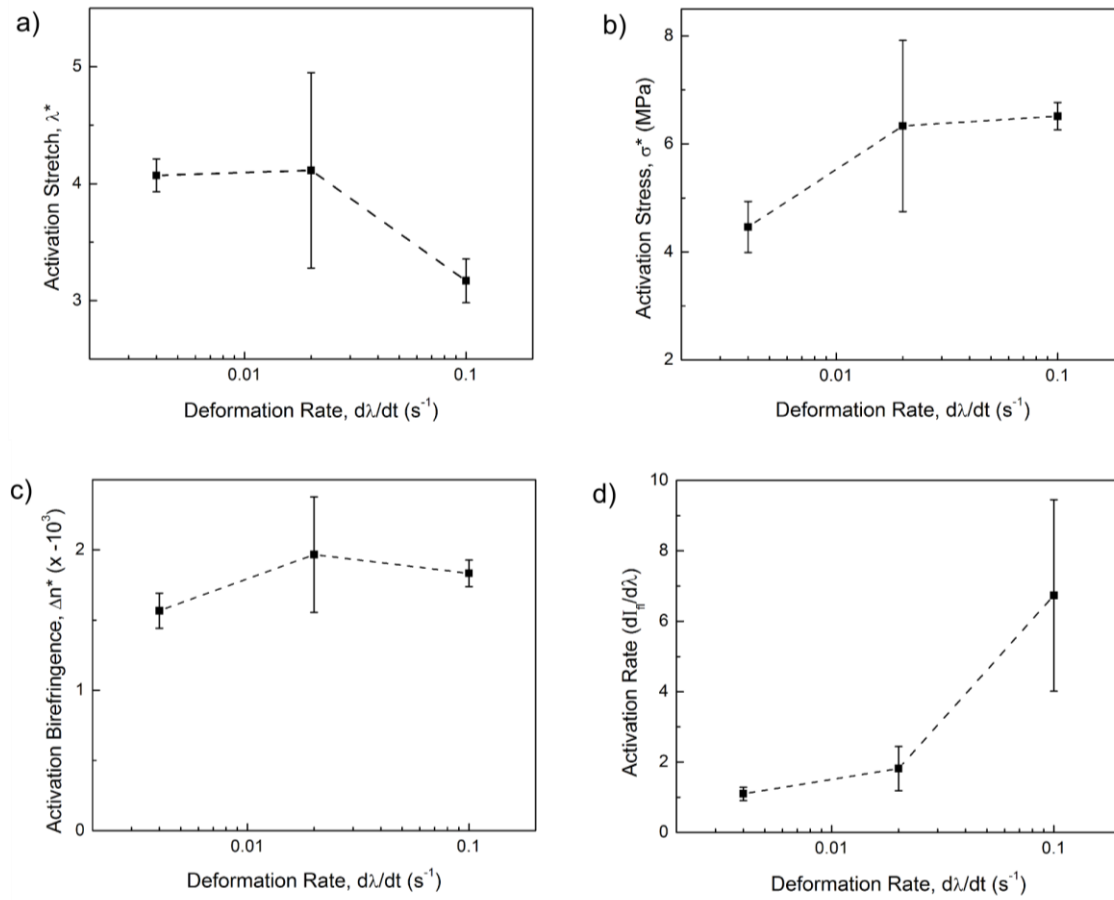


Figure 3.6. Activation points, defined at λ^* , for active SP-linked PMA as a function of stretch rate. a) Activation stretch, b) activation stress, c) activation birefringence, and d) average activation rate ($dI_{fl}/d\lambda$) between $\lambda = 8$ and $\lambda = 9$.

Polymers of various molecular weights (80 kDa – 360 kDa) were tested in tension at the same stretch rates as described above to determine the effect of polymer chain length. Molecular weights under 50 kDa were not tested because the samples lacked mechanical integrity for tensile testing. The behavior of the fluorescence intensity with increasing stress was effectively the same for all molecular weights. The activation stretch ratio, λ^* , for varied molecular weight (min. 3 samples per data point) is plotted in Fig 3.7. A linear fit is laid over the data for each deformation rate, and shows essentially constant stretch to activation, indicated by the horizontal slope of the fit lines, thus molecular weight (above ca. 80 kDa) did not have a detectable effect on SP activation.

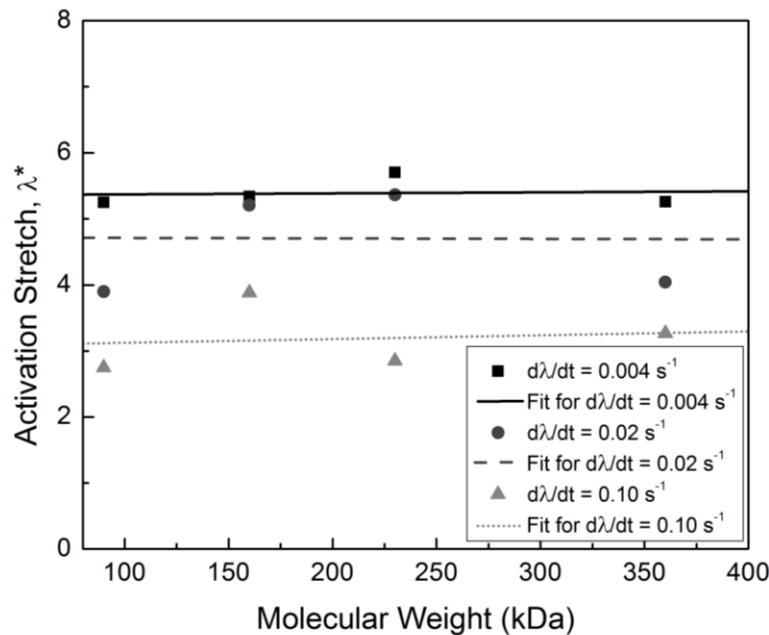


Figure 3.7. Activation stretch ratio, λ^* , for active SP-linked PMA at various molecular weights tested at deformation rates of 0.004 s^{-1} , 0.02 s^{-1} and 0.10 s^{-1} .

3.3.3 Deformation Rate Dependence in Difunctional Control SP-Linked PMA

Difunctional control SP-linked PMA was tested in tension at the same stretch rates as mechanochemically active polymer. Stress, birefringence and fluorescence data are shown in

Fig 3.8. The mechanical and birefringence behavior were similar to the mechanochemically active case. Despite being linked in a manner that should not transmit force across the mechanophore, an increase in fluorescence signal (activation) was evident with increasing stretch ratio. The extent of fluorescence increase was lower than the active case, but still showed deformation rate dependence – higher deformation rate led to greater fluorescence.

The fluorescence increase in difunctional control PMA had a virtually identical spectroscopic fluorescence peak as the active sample, and no fluorescence signal was present in polymer without SP incorporated, providing evidence that fluorescence increase in the difunctional control was due to SP ring opening.

To further investigate the stress- and stretch-dependence of the fluorescence signal in the control, a batch of difunctional control SP-linked PMA was (accidentally) plasticized with a solvent (~3% tetrahydrofuran, THF) as described in section 2.2.1, such that the mechanical stress was significantly lower in plasticized polymer. The stress, birefringence and fluorescence of plasticized difunctional control samples are included in Fig 3.9. At the lower applied stresses in the plasticized polymer, the control typically exhibited no fluorescence. For the highest deformation rate, i.e. greatest stress, plasticized difunctional control SP-linked PMA showed a slight amount of fluorescence increase. This finding indicated that fluorescence increase (and presumably activation of the difunctional control SP) was a stress-induced process and not an optical effect induced by deformation of the material. The control fluorescence and apparent SP activation is discussed further in section 3.3.5.

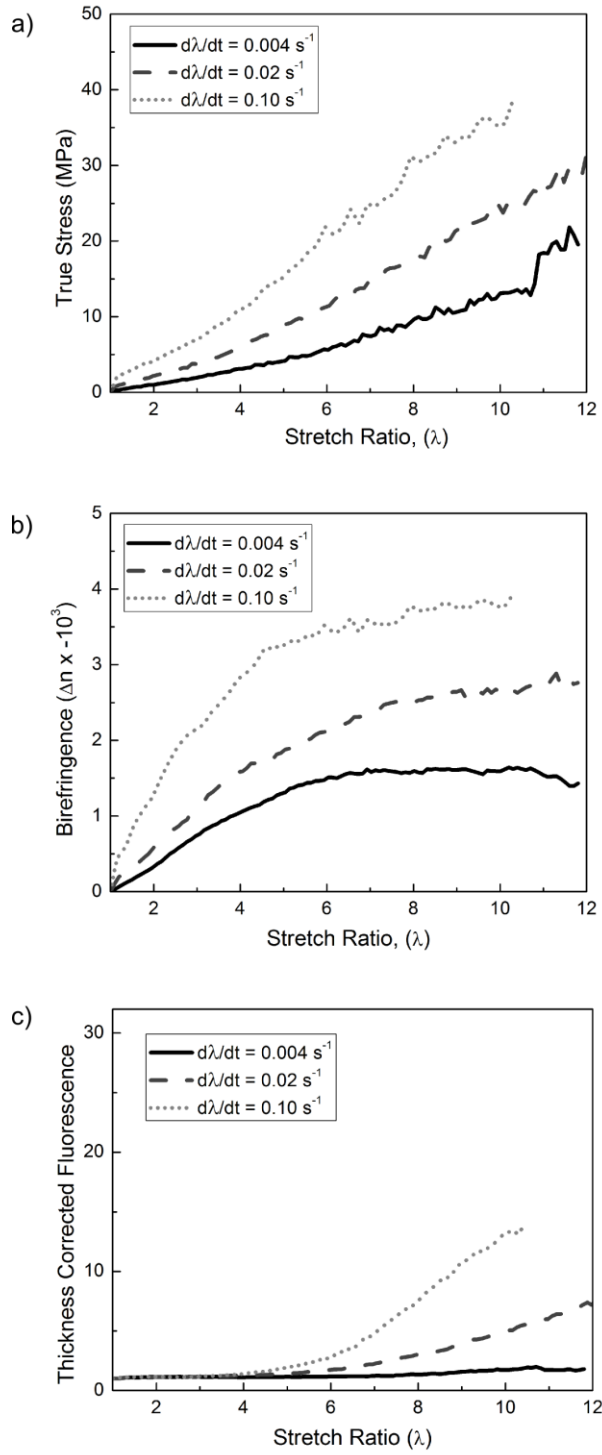


Figure 3.8. Difunctional control SP-linked PMA loaded in tension at deformation rates of 0.004 s^{-1} , 0.02 s^{-1} and 0.10 s^{-1} . a) Stress vs. stretch ratio, and b) birefringence vs. stretch ratio, and c) thickness-corrected, normalized fluorescence intensity vs. stretch ratio.

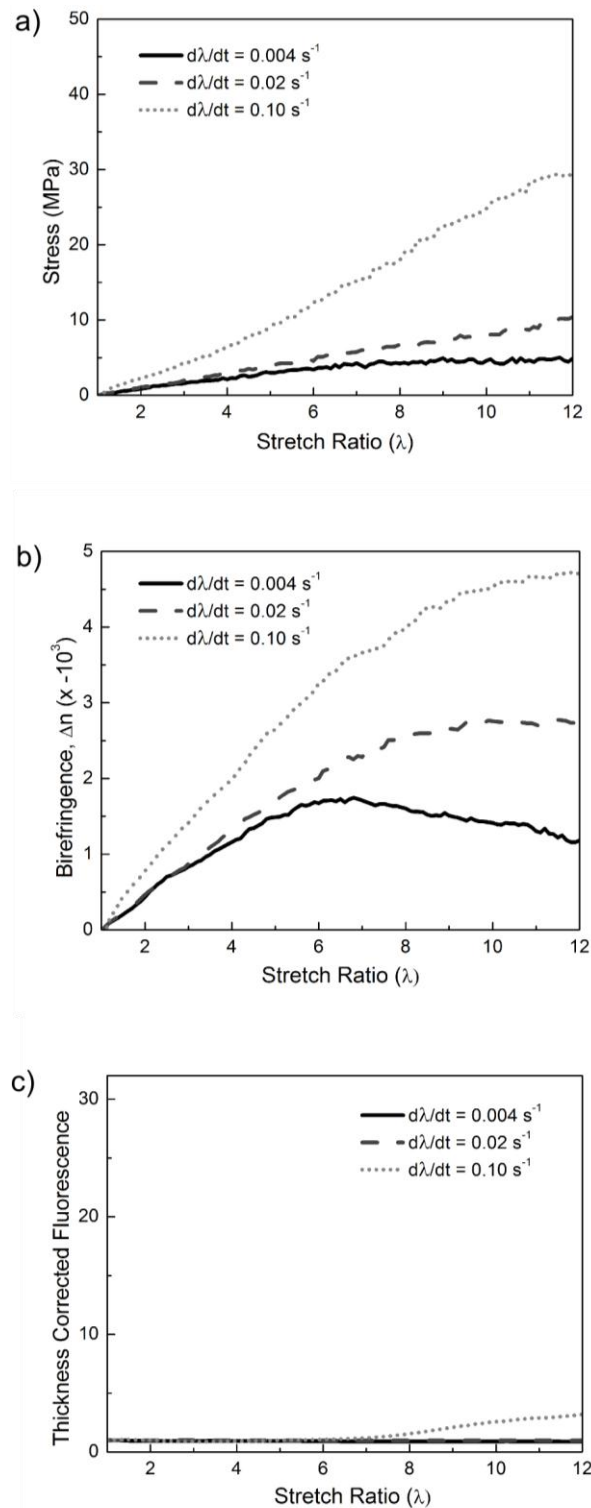


Figure 3.9. Difunctional control SP-linked PMA plasticized with ca. 3 wt% THF. a) Stress vs. stretch ratio, and b) birefringence vs. stretch ratio, and c) thickness-corrected, normalized fluorescence intensity vs. stretch ratio.

3.3.4 Stress Relaxation Behavior of Active SP-Linked PMA

Active SP-linked PMA samples were drawn to $\lambda = 9$, and the relaxation response of stress, birefringence and activation were measured as a function of time. A representative case deformed at a stretch rate of 0.10 s^{-1} is shown in Fig 3.10. The stress and birefringence during the constant stretch ratio stage were fitted to exponential decay curves with effective time constants (τ_{eff}) of 54 s and 83 s, respectively.

During stress relaxation, the fluorescence intensity in the polymer continued to increase, indicating time dependence of the force-induced chemical reactions. Although macroscopic deformation had stopped, stress in the system was sufficient to drive the reaction forward without further deformation. The fluorescence reached a maximum as the stress decayed and eventually decreased slightly over time due to the incident light source ($\lambda = 532\text{ nm}$) driving MC to SP. The stress relaxation region in which fluorescence intensity was also increasing was fit to an exponential curve. The effective time constant of the fluorescence increase was 53 s – virtually the same as the effective stress relaxation time constant, $\tau_{\text{eff},\sigma}$ – indicating a possible link between the decay in activation rate and the decay in stress.

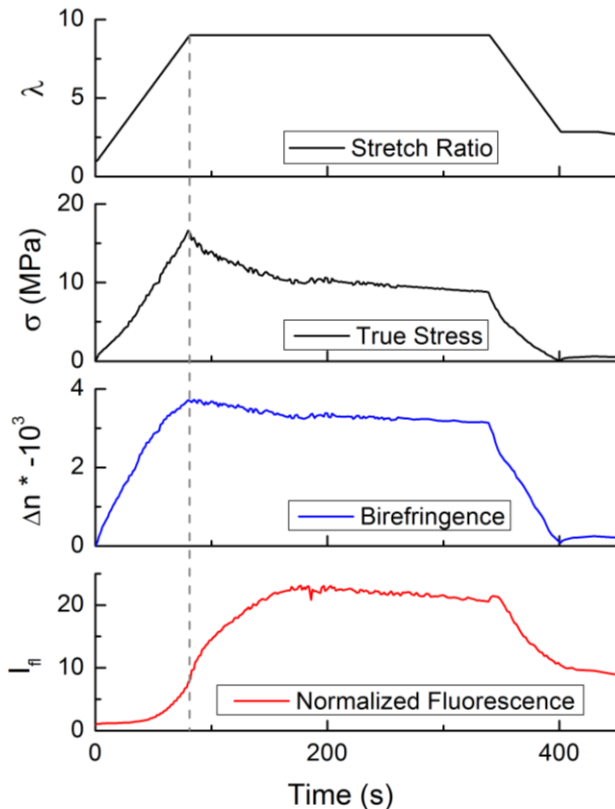


Figure 3.10. Stress relaxation, birefringence relaxation and thickness corrected fluorescence intensity (activation) of active SP-linked PMA loaded and unloaded at a stretch rate of 0.10 s^{-1} .

The sample was unloaded at the same stretch rate as the loading segment by moving the load frame crossheads together until the load was reduced to zero. During unloading the fluorescence intensity decreased, showing some reversion of the MC to SP. After returning to zero load, some fluorescence increase remained in the sample.

Effective time constants (τ_{eff}) measured from stress and birefringence relaxation conditions (fitted to exponential decay for 400 s after the onset of relaxation) were between 50-100 s at all loading rates. These relaxation time scales were similar to the test time for the fastest deformation rate ($d\lambda/dt = 0.10 \text{ s}^{-1}$). Slower deformation rates ($d\lambda/dt = 0.004 \text{ s}^{-1}$ and $d\lambda/dt = 0.02 \text{ s}^{-1}$) correspond to test times substantially longer than relaxation times ($t_{\text{test}} \sim 5-25 \times \tau_{\text{eff}}$), and presumably polymer relaxation had a more pronounced effect. The

increase in stress, birefringence, and ultimately activation at the highest deformation rate (Fig 3.5) is attributed to less prominent effect of polymer chain relaxation for short test durations.

3.3.5 Stress Relaxation Behavior of Difunctional Control SP-Linked PMA

Difunctional control SP-linked PMA was subjected to stress relaxation loading conditions similar to the active case presented in the previous section. The sample in Fig 3.11 was loaded at a stretch rate of $d\lambda/dt = 0.10 \text{ s}^{-1}$ to a stretch ratio greater than 9, and then the deformation was held constant. Load and fluorescence were monitored as a function of time. The fluorescence signal increased during deformation, indicating activation of SP. In contrast to active samples, the fluorescence signal did not continue to increase during the stress relaxation stage. The fluorescence signal in the control decreased during relaxation, indicating that SP to MC conversion had stopped proceeding forward, and was slowly reverted by the incident light source.

Stress relaxation behavior indicates a differing mechanism for fluorescence increase (i.e. activation) of difunctional control SP-linked PMA when compared to active polymer. Activation of control SP during stretching may be due to a drag force in the polymer from solvent friction. Polymer dynamics theory, based on of Rouse [69] and Zimm [70] models, typically assumes an effect of solvent friction, ξ , which applies drag force on a flowing polymer chain [71, 72]. The drag force is the product of a drag coefficient from polymer interaction with the solvent (in this case other polymer chains), and the rate of polymer flow. Experimental data exhibits the expected trends for drag force-induced activation of the control, with activation (fluorescence increase) proportional to the deformation rate, and no activation during stress relaxation when

the rate of polymer flow (and therefore drag force) is negligibly small. THF-plasticized polymer (refer to Fig 3.9) presumably had a smaller coefficient of solvent friction ($\xi_{\text{PMA+THF}} < \xi_{\text{PMA}}$) and therefore the drag force was not sufficient to drive SP-MC conversion in the plasticized control SP-linked polymer.

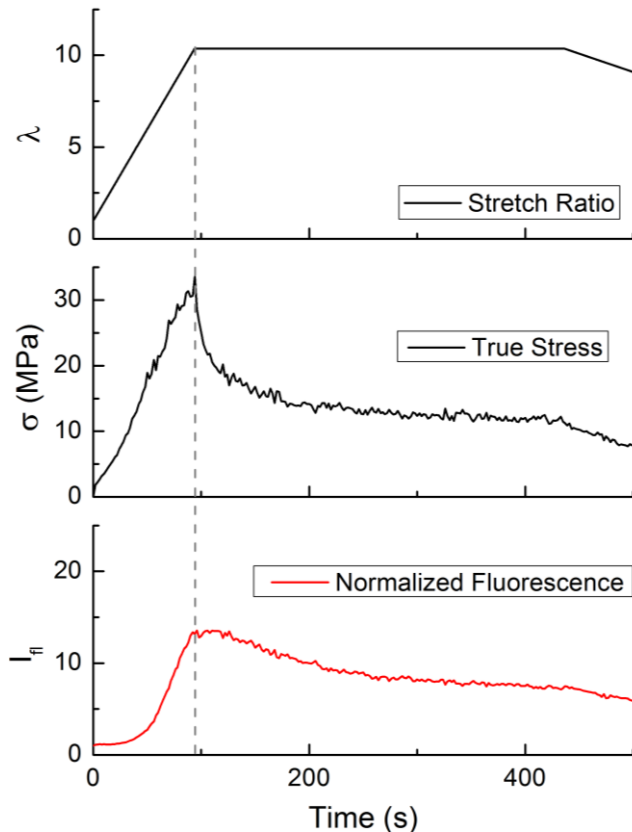


Figure 3.11. Stress relaxation and thickness corrected fluorescence of difunctional control SP-linked PMA loaded at a stretch rate of 0.10 s^{-1} .

3.3.6 Effect of Mechanophore Architecture: SP Activation in Linear, 4-Arm, and 8-Arm SP

Multiple polymer arms were bonded to the mechanophore in the configurations shown schematically in Fig 3.1. Each polymer in this section was synthesized with a total molecular

weight of approximately 250 kDa. Samples of 4- and 8-arm SP-linked PMA were tested at stretch rates of 0.004 s^{-1} , 0.02 s^{-1} , and 0.10 s^{-1} and the fluorescence intensities as a function of stretch ratio were compared to the behavior of linear PMA. Macroscopic stress at each deformation rate was virtually the same for the different polymer architectures. Representative plots of normalized fluorescence (the normalization calculation is described earlier in this chapter) at each deformation rate are included in Fig 3.12. The fluorescence intensity of 4-arm and 8-arm architectures increased at lower stretch ratios and reached greater magnitudes. The increased activation was more pronounced at slow deformation rates ($d\lambda/dt = 0.004\text{ s}^{-1}$ and 0.02 s^{-1}) than at the fastest deformation rate ($d\lambda/dt = 0.10\text{ s}^{-1}$).

Activation stretch ratios, λ^* , were averaged for each mechanophore architecture and deformation rate (minimum 3 samples per data point) and plotted in Fig 3.13. For linear SP-linked PMA, λ^* decreased with increasing deformation rate (described in section 3.3.3). In contrast the 4- and 8-arm mechanophore structures were effectively unaffected by deformation rate. The earlier onset of activation in the 4- and 8-arm structures was pronounced at slow deformation rates. At the fastest deformation rate, the dendrimeric SP-linked structures showed no statistically significant difference in activation behavior.

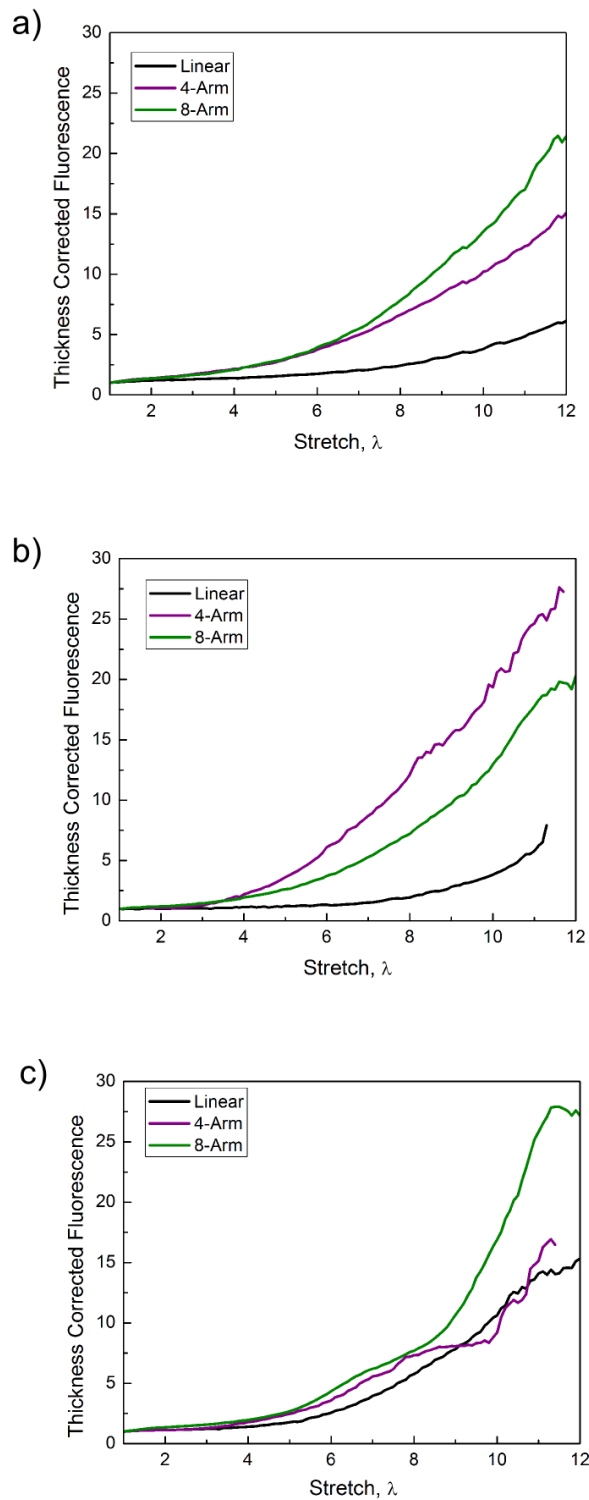


Figure 3.12. Representative normalized fluorescence curves for linear, 4-arm and 8-arm SP-linked PMA tested in tension at deformation rates ($d\lambda/dt$) of a) 0.004 s^{-1} , b) 0.02 s^{-1} and c) 0.10 s^{-1} .

In linear polymer, the stress effective relaxation time ($\tau \approx 70$ s) was similar to the time scale for tensile testing at the fastest deformation rate (approximately 100s). At fast deformation rates, higher forces were applied across each polymer chain with little effect of relaxation, and activation was far more prominent. In the dendrimeric (4-arm and 8-arm) SP architectures, the relaxation effect was not evident in the data at the slower deformation rates, possibly due to the mechanophore being pinned by multiple polymer chains on each side. In such dendrimeric mechanophore structures, all of the polymer chains would have to move in concert in order to relieve the stress on the mechanophore subunit. Because of polymer chains attached at multiple sites on the mechanophore, relaxation was not prominent in 4-arm and 8-arm SP structures, and a higher degree of activation was evident in the solid state at low deformation rates.

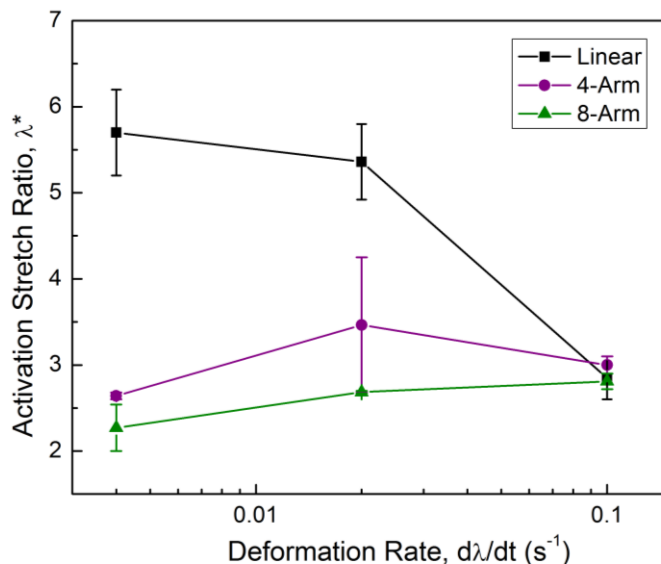


Figure 3.13. Stretch ratio at the activation point, λ^* , for linear and multi-arm SP-linked PMA plotted as a function of deformation rate.

3.4. Conclusions

SP-linked poly(methyl acrylate) provided a model system for measuring the mechanochemical response in an elastomeric polymer. Previous work by Davis *et al.* [15] demonstrated mechanophore activation when linked into a PMA backbone under tensile deformation *via* a color change. The work presented in this chapter provides a thorough quantitative study of a SP-linked elastomer subjected to a tensile load, and the parameters which affect mechanophore activation in an elastomeric polymer.

A novel experimental set-up was designed to simultaneously apply a mechanical load to polymer samples and collect *in situ* optical measurements of fluorescence and polymer chain alignment. The SP-to-MC conversion was quantified *via* the fluorescence signal of the MC form, excited by a 532 nm laser and collected at $\lambda > 575$ nm. Birefringence provided a relative measure of the polymer chain alignment, which was correlated to the mechanophore activation. The findings indicate that rapid activation of SP occurred when birefringence began to plateau and reach a maximum, thus when polymer chains were most aligned in the direction of macroscopic force.

The effect of tensile deformation rate was studied and indicated that for increasing deformation rate, the macroscopic stress in the polymer increased and a corresponding increase in the rate and degree of activation ensued. Stress relaxation behavior of SP-linked PMA indicated that SP activation is a time dependent process, and mechanochemical conversion will continue at a constant deformation, provided that the stress remains sufficiently high (above *ca.* 10 MPa).

A difunctional SP-linked control was incorporated into the PMA backbone such that force was not transferred across the sensitive C-O spiro bond of the mechanophore. In this

configuration, some amount of fluorescence increase, i.e. SP activation was detected in the control under tension. The fluorescence increase was of smaller magnitude and did not continue under stress relaxation conditions, indicating a different mechanism for activation in the control case. Experimental evidence supports a theory of molecular friction acting to open the control SP species to its MC form.

The SP molecule was designed with dendrimeric functionality, such that multiple polymer arms could be attached to each side of the SP unit. The aim was to magnify the force across the mechanophore. The result obtained from fluorescence measurement during tensile deformation was improved activation of the dendrimeric structures when compared to a linear structure at low deformation rates, when polymer relaxation effects dominated.

CHAPTER 4

EFFECT OF STRESS ON SP-MC REACTION KINETICS AND ACTIVATION ENERGY

4.1 Introduction and Theory

Hickenboth [13] and Davis [15] proposed that force alters the chemical pathway for a mechanophore reaction by decreasing the activation energy, ΔE_a , of mechanophore conversion. First principles molecular dynamic models of mechanophore bond cleavage supported this hypothesis [15, 19, 73], and Lee *et al.* [38] reported experimental evidence for a decreased energy barrier for SP-to-MC conversion. In this chapter, an experimental approach is taken to calculate the effect of stress on activation energies for the forward reaction of SP to MC, $\Delta E_{a,f}$, and the reverse reaction of MC to SP, $\Delta E_{a,r}$. A schematic of the proposed energy landscape for $\text{SP} \leftrightarrow \text{MC}$ conversion with the effect of mechanical loading is included in Fig 4.1. Stress-dependent reaction kinetics and activation energies were determined by applying tensile loads to polymer samples and monitoring SP-MC conversion *via* the fluorescence signal of MC.

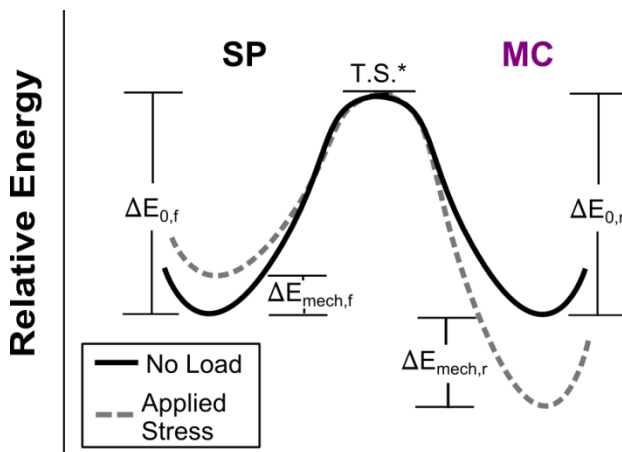


Figure 4.1. Energy barriers for SP-to-MC conversion relative to the transition state, T.S.*. $\Delta E_{0,f}$ and $\Delta E_{0,r}$ are the activation energies in the absence of a load. $\Delta E_{\text{mech},f}$ and $\Delta E_{\text{mech},r}$ represent the effect of an applied stress.

The effect of stress on reaction kinetics and activation energy can be incorporated into transition state theory [74]. According to the Eyring-Polanyi equation, a reaction rate constant, k , is dependent on the activation energy ΔE_a of the species following an Arrhenius agreement [75, 76]:

$$k \approx \frac{k_b T}{h} \exp\left(-\frac{\Delta E_a}{k_b T}\right) \quad 4.1$$

Variables k_b and h are the Boltzman constant and Planck's constant, respectively, and T is temperature. Because SP-MC conversion is reversible, there is a forward rate constant, k_f for SP→MC conversion, and a reverse rate constant, k_r for MC→SP conversion. These rate constants correspond to activation energies, $\Delta E_{a,f}$ and $\Delta E_{a,r}$, respectively.

Both $\Delta E_{a,f}$ and $\Delta E_{a,r}$ of SP/MC are assumed to be a linear combination of the inherent thermal activation energy, ΔE_0 , the effect of the applied mechanical load, ΔE_{mech} , and a photochemical term, ΔE_λ :

$$\Delta E_{a,f} = \Delta E_{0,f} + \Delta E_{\lambda,f}(P) + \Delta E_{mech,f}(\sigma) \quad 4.2a$$

$$\Delta E_{a,r} = \Delta E_{0,r} + \Delta E_{\lambda,r}(P) + \Delta E_{mech,r}(\sigma) \quad 4.2b$$

The photochemical effect is a function of the wavelength, λ , and power, P , of light incident on the sample, and the mechanical effect is described in terms of the applied stress, σ .

Following from Ward [43], the dependence of activation energy on an applied stress is assumed linear, thus

$$\Delta E_{mech} = v^* \sigma \quad 4.3$$

where v^* is the activation volume, with units of m^3 . The activation volume can be intuitively be described as the product of the volume of the species and the strain required for a mechanically-

induced transformation [77]. Combining Eqs. 4.1-4.3, the effect of stress on the forward and reverse reaction rates follows [5, 26, 43, 78]:

$$k_f \approx \frac{k_b T}{h} \exp\left(-\frac{\Delta E_{a,f}}{k_b T}\right) = k_{\sigma=0,f} \exp\left(-\frac{\nu^*_f \sigma}{k_b T}\right) \quad 4.4a$$

$$k_r \approx \frac{k_b T}{h} \exp\left(-\frac{\Delta E_{a,r}}{k_b T}\right) = k_{\sigma=0,r} \exp\left(-\frac{\nu^*_r \sigma}{k_b T}\right) \quad 4.4b,$$

where $k_{\sigma=0,f}$ and $k_{\sigma=0,r}$ represent the rate constants in the absence of an applied load.

Transition state theory effectively describes molecular-level mechanically induced processes such as dislocation motion and polymer yielding, wherein the stress reduces the energy barrier for molecular motion and flow [5, 26, 77, 79]. In biological systems, proteins have been tethered to an atomic force microscope and deformed, and the rate of protein debonding [43, 80] and unfolding [81] has been similarly described with the exponential relationship of Eq 4.4. In this work, SP-linked polymers were subjected to various loading conditions and kinetics were monitored to empirically determine the relationship between stress and reaction kinetics in a bulk SP-linked polymer.

The conversion between SP and MC is first order and reversible. The reaction rate, in terms of MC concentration, $[MC]$, follows:

$$\frac{d[MC]}{dt} = k_f[SP] - k_r[MC] \quad 4.5.$$

The kinetics of the reaction were investigated based on the measured fluorescence intensity as described in Chapter 3. Fluorescence intensity, I_f , was assumed proportional to the relative concentration of MC:

$$\frac{[MC]}{[MC_{\max}]} = \frac{I_f}{I_{f,\max}} \quad 4.6$$

where $[MC_{\max}]$ represents 100% of the mechanophores in the MC form, I_{fl} , is the average measured fluorescence intensity, and $I_{fl,max}$ corresponds to the fluorescence intensity if all mechanophores were in the MC form. In this study $I_{fl,max}$ was assumed to be 10x the fluorescence intensity of polymer samples in equilibrium with the 385 UV light incident on the samples to drive equilibrium toward the MC form ($I_{fl,max} = 10I_{UV}$). At this value of $I_{fl,max}$, equilibrium slightly favors the SP form. A parametric study of the effect of $I_{fl,max}$ is included in Appendix B.

The relative proportion of mechanophores in the SP form is equal to:

$$\frac{[SP]}{[SP_{\max}]} = 1 - \frac{[MC]}{[MC_{\max}]} \quad 4.7.$$

Combining Equations 4.5-4.7, the reaction kinetics is expressed in terms of the fluorescence intensity:

$$\frac{d(I_{fl} / I_{fl,max})}{dt} = k_f(1 - \frac{I_{fl}}{I_{fl,max}}) - k_r \frac{I_{fl}}{I_{fl,max}} \quad 4.8.$$

The results presented in this chapter establish a framework for understanding the relationship between SP reaction kinetics and applied stress in a solid polymer, from which the change in the energy barriers due to loading, $\Delta E_{mech,f}$ and $\Delta E_{mech,r}$ were calculated.

4.2 Experimental Methods

4.2.1 SP-Linked PMA Samples and Treatment

Mechanochemically active SP-linked PMA was synthesized and molded into dog-bone shaped specimens as described in Chapter 3. The samples were subjected to lighting and mechanical testing conditions described in Table 4.1. Prior to testing, samples were irradiated for 30 minutes with either UV light ($\lambda_{UV} = 385$ nm) or green (G) light ($\lambda_{green} = 532$ nm) in order

to drive the mechanophore equilibrium toward either the MC form or SP form, respectively. Images of PMA samples driven toward SP and MC are included in Chapter 1.

After pre-treatment with light, the fluorescence signal was monitored using a green laser light source ($\lambda_{\text{green}} = 532$) with constant beam size (approximately 10 mm). This light source served both as an excitation source for the MC fluorescence and to drive equilibrium toward the SP form over reasonable experimental time scales. Samples of Type 1 were subjected to no load in order to characterize the thermal energy barriers, $\Delta E_{0,f}$ and $\Delta E_{0,r}$. The power of the light source used during fluorescence measurement was varied for Type 1UV samples using polarization optics to measure the effect of the light source ($\Delta E_{\lambda=532}$) on reaction kinetics. Type 2 samples were subjected to mechanical loading described in the following section to determine how activation energies vary as a function of applied load, $\Delta E_{\text{mech},f}$ and $\Delta E_{\text{mech},r}$.

Table 4.1. Treatment of sample types before and during fluorescence measurements.

Sample Type	Pre-Test Lighting	Laser Power During Testing	Mechanical Loading	Variables Determined
Type 1UV	30 min UV $\lambda_{\text{UV}} = 385 \text{ nm}$	50 μW - 2500 μW	None	$k_{0,r}$ $\Delta E_{0,r}$ $\Delta E_{\lambda=532,r}$
Type 1G	30 min Green $\lambda_{\text{green}} = 532 \text{ nm}$	2500 μW	None	$k_{0,f}$ $\Delta E_{0,f}$
Type 2UV	30 min UV $\lambda_{\text{UV}} = 385 \text{ nm}$	2500 μW	Stretch $\lambda = 4$ to $\lambda = 9$	C_f , C_r , $\sigma_{f,\text{lim}}$, $\sigma_{r,\text{lim}}$, $\Delta E_{\text{mech},f}$ $\Delta E_{\text{mech},r}$
Type 2G	30 min Green $\lambda_{\text{green}} = 532 \text{ nm}$	2500 μW	Stretch $\lambda = 4$ to $\lambda = 8$	C_f , C_r , $\sigma_{f,\text{lim}}$, $\sigma_{r,\text{lim}}$, $\Delta E_{\text{mech},f}$ $\Delta E_{\text{mech},r}$

4.2.2 Combined Fluorescence Kinetics and Mechanical Testing

All samples were monitored at room temperature ($RT \approx 22^\circ\text{C}$) in the mechanical set-up using full-field fluorescence described in Chapter 3. Load, displacement, and fluorescence

intensity were measured over time for each sample. Fluorescence images were taken at image periods between 5 s and 20 s. Laser power was controlled using polarization optics, and the light was circularly polarized prior to incidence on the sample. Exposure was constant for all samples except Type 1UV, in which the exposure was scaled inversely with laser power. Fluorescence intensity, I_{fl} , for each image was defined as the red channel intensity with a constant field of localized in the middle of the sample, corrected by a factor the thickness of the sample (see Chapter 3 for details of thickness correction). I_{fl} was then normalized by a constant $I_{fl,max}$.

A mechanical load was applied to sample Types 2UV and 2G using stress relaxation condition conditions (i.e. constant stretch ratio, λ) described in Chapter 3. Samples were loaded to pre-defined stretch ratios at a deformation rate of $d\lambda/dt = 0.1 \text{ s}^{-1}$, and the fluorescence intensity was measured as a function of time after the deformation stopped ($t = 0$), coinciding with the onset of relaxation. Stress relaxation was chosen because it allowed measurement of the fluorescence change over long periods of time with no change in the sample thickness or imaging conditions. The true stress, $\sigma(t)$, was calculated at the time of each fluorescence image based on the applied force and optically measured width of the sample as described in Chapter 3.

4.3 Results and Discussion

4.3.1 SP Reaction Kinetics with No Applied Load

The effect of incident 532 nm laser power on the $\text{SP} \leftrightarrow \text{MC}$ reaction kinetics was examined first using sample Type 1UV (see Table 4.1). After UV irradiation, MC form was evidenced by a strong purple color and fluorescence intensity (I_{UV}) in the samples. During fluorescence measurement, the 532 nm laser exposure drove equilibrium toward SP and also served as an excitation source for MC fluorescence excitation. Sample Type 1UV images are

included in Fig 4.2a. Evolution of fluorescence intensity (normalized by $I_{fl,max} = 10I_{UV}$) is shown in Fig 4.2b for various laser powers. At room temperature with no light incident on the sample, the fluorescence signal was virtually constant over a span of days, indicating a relatively stable MC form. With 532 nm light incident on the sample, the fluorescence intensity readily decayed over time. Increasing laser power led to more rapid decay in the fluorescence signal. A single exponential function was fit to the fluorescence data for each sample in Fig 4.2b and the corresponding time constants, τ , are listed in Table 4.2.

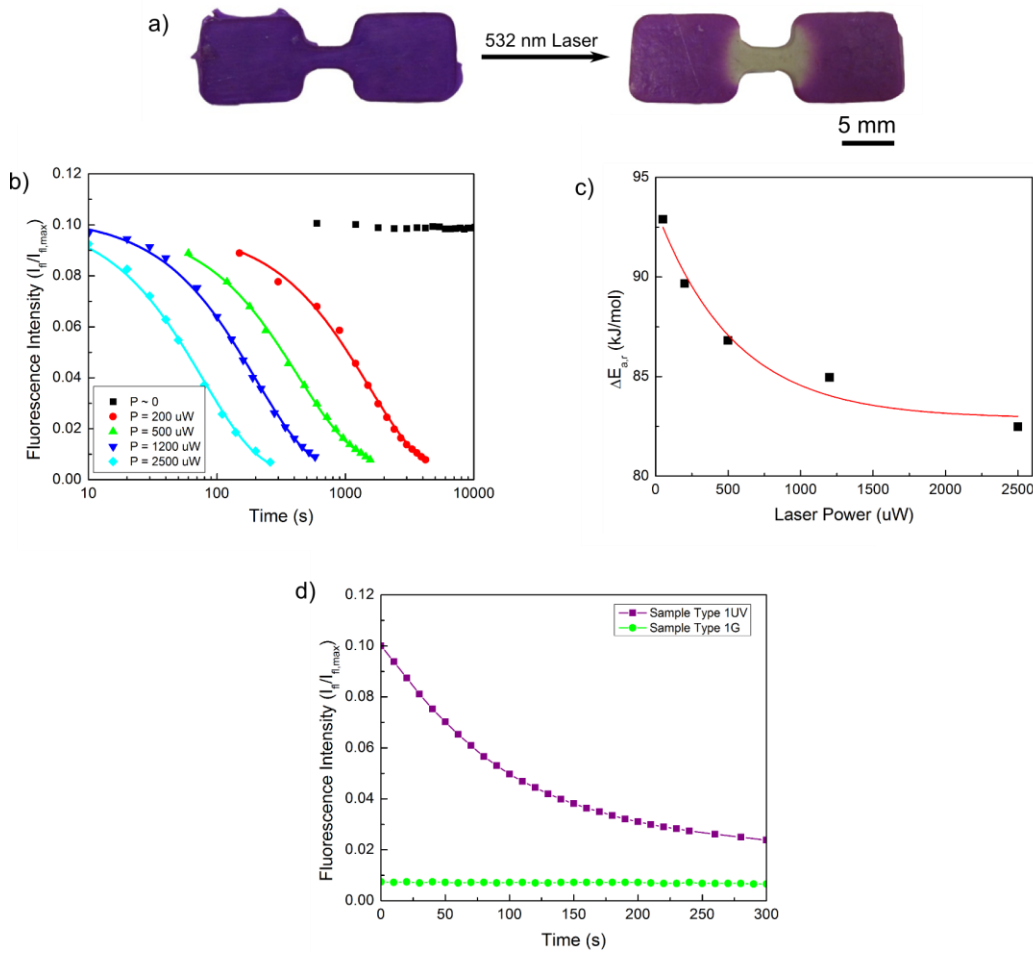


Figure 4.2. Effect of 532 nm laser power on fluorescence decay and reaction kinetics. a) Type 1UV sample before and after testing. b) Decay of sample Type 1UV fluorescence intensity vs. log of time at varied incident laser power. Exponential decay curves are fit to the experimental data. c) Activation energies for the reverse reaction ($\Delta E_{a,r}$) with an exponential curve fitted to the data. d) Fluorescence intensity of samples pre-treated with UV light (Type 1UV) and 532 nm light (Type 1G), exposed to 2500 μW laser exposure during fluorescence imaging.

Kinetic curves of UV-irradiated samples in Fig 4.2b fit closely to exponential decay curves until they reach low intensities, *i.e.* low MC concentrations. Under these conditions the forward rate constant is negligibly small, and only the reverse rate constant is considered. The MC \rightarrow SP (reverse) rate constant, k_r , was taken as the inverse of the fluorescence decay time constant, and the effective activation energy, $\Delta E_{a,r}$, was calculated using Eq. 4.1. Experimentally determined time constants, rate constants and activation energies for the reverse reaction with varied incident laser power are listed in Table 4.2.

Table 4.2. Rate kinetics and estimated activation energy for MC \rightarrow SP conversion with 532 nm incident light and no load, assuming negligible SP \rightarrow MC conversion.

Laser Power (μW)	Time Constant (s)	Rate Constant, k_r (s^{-1})	Activation Energy $\Delta E_{a,r}$ (kJ/mole)	Photochemical Effect $\Delta E_{\lambda=532,r}$ (kJ/mole)
0	$\sim\infty$	~ 0	93.1 [†]	0
50	5070	0.00020	92.9	-0.2
200	1370	0.00073	89.7	-3.4
500	427	0.0023	86.8	-6.3
1200	205	0.0049	85.0	-8.1
2500	95	0.011	82.5	-10.6

Activation energy for the MC \rightarrow SP reaction, $\Delta E_{a,r}$, as a function of incident laser power is plotted in Fig 4.2c. The data was fit to an exponential curve and the thermal energy barrier for the reverse reaction, $\Delta E_{0,r}$, was extrapolated at zero laser power as approximately 93 kJ/mole. The forward rate constant at no applied load, $k_{0,f}$, and corresponding thermal activation energy for the forward reaction, $\Delta E_{f,0}$, were calculated from the fluorescence intensity at equilibrium with the 532 nm laser ($P_{\lambda=532} = 2500 \mu\text{W}$) incident on the sample. Sample Type 1G provided the

[†] Value extrapolated from the curve in Fig 4.1b.

equilibrium fluorescence intensity, $I_{fl,eq}$, plotted in Fig 4.2d. Representative fluorescence of sample Type 1UV is included for comparison. Type 1G had constant fluorescence intensity, indicating equilibrium, and $dI_{fl}/dt = 0$. Substituting this value into Eq 4.8, the rate constant for the forward reaction, k_f , was calculated:

$$k_f = k_r \frac{I_{fl,eq}}{I_{fl,max} - I_{fl,eq}} = k_{0,f} \quad 4.9$$

where k_r corresponds to the reverse reaction rate at the test laser power. The SP form does not absorb light in the green range, and it was assumed that the laser light did not affect the forward reaction ($\Delta E_{\lambda=532,f} = 0$), therefore $k_f = k_{0,f}$. The calculated forward reaction rate with no applied load was approximately $6 \times 10^{-5} \text{ s}^{-1}$. The corresponding thermal activation energy for the forward reaction calculated from Eq. 4.1 was $\Delta E_{0,f} = 96 \text{ kJ/mole}$. These calculated thermal activation energies for the forward and reverse reactions indicate a small preference for the SP form.

Activation energies for SP and MC have been calculated by the Martinez group at Stanford University using molecular dynamics simulations. At no load, $\Delta E_{0,f}$ and $\Delta E_{0,r}$ are approximately 110 kJ/mole and 97 kJ/mole respectively [82]. The experimentally derived reverse activation energy is within approximately 3% of the molecular dynamics simulation, while the activation energy for the forward reaction is lower than expected. This difference may be due to the interaction of the mechanophore with the polymer matrix, which is not accounted for in the simulations.

4.3.2. Effect of Applied Mechanical Load on SP Reaction Kinetics

Sample Types 2UV and 2G were subjected to mechanical loading with stress relaxation conditions at various stretch ratios, λ . A 532 nm laser was applied incident on the sample at $t = 0$ coinciding with the onset of stress relaxation, again to drive the reaction toward the SP form and

simultaneously excite fluorescence. Incident laser power ($P_{\lambda=532 \text{ nm}}$) of 2,500 μW was chosen during mechanical testing such that the fluorescence decay ($\tau_{\text{fl}} \sim 95 \text{ s}$) and effective stress relaxation time ($\tau_{\text{eff}} \sim 70 \text{ s}$) were similar. At this laser intensity and with no applied stress, the rate constant of the reverse reaction (0.01 s^{-1}) was more than two orders of magnitude greater than the forward rate constant ($6 \times 10^{-5} \text{ s}^{-1}$).

Evolution of fluorescence intensity is shown in Fig 4.3a and 4.3b for sample Types 2UV and 2G, respectively. Deformed sample fluorescence intensity was normalized by the sample thickness in the manner described in Chapter 3. The fluorescence signal for all samples was then divided by the maximum value, $I_{\text{fl},\text{max}}$, and the fluorescence intensities in Fig 4.3 are presented in terms of the value $I_{\text{fl}} / I_{\text{fl},\text{max}}$.

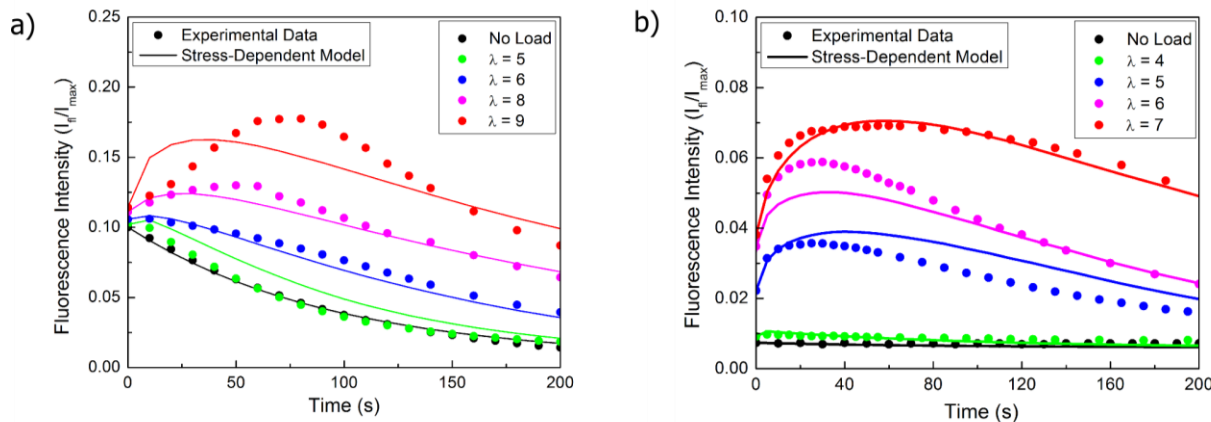


Figure 4.3. Normalized fluorescence intensity ($I_{\text{fl}} / I_{\text{fl},\text{max}}$) over time after the onset of stress relaxation at predefined stretch ratios, λ . a) Samples irradiated with UV light prior to testing. b) Sample irradiated with green light prior to testing. Individual data points represent experimental results, and curves correspond to calculated stress-dependent kinetics.

In Fig 4.3a the black data points corresponding to sample Type 1UV decayed exponentially, indicating that the reverse reaction occurred with little effect from the forward reaction. The fluorescence decay was detectably slower at applied stretch ratios of 5 and greater.

At stretch ratios of 8 and 9 the fluorescence intensity increased significantly above the intensity after UV irradiation, confirming that not all of the mechanophores were driven to the MC form by UV light and additional mechanically-induced SP-to-MC activation occurred.

As the applied stress relaxed, the decay rate of the fluorescence signal approached the fluorescence decay rate with no applied load. The nature of the relationship between the reaction rate and applied stress was investigated by plotting $\Delta I_f/\Delta t$ as a function of the stress, $\sigma(t)$, at the time of each fluorescence measurement for sample Types 2UV and 2G (Fig 4.4). The relationship was approximated as bi-linear. At low stresses there was no detectable effect of stress on the reaction rate, whereas above a threshold level near 10 MPa, the trend of $\Delta I_f/\Delta t$ was linearly proportional to the applied stress.

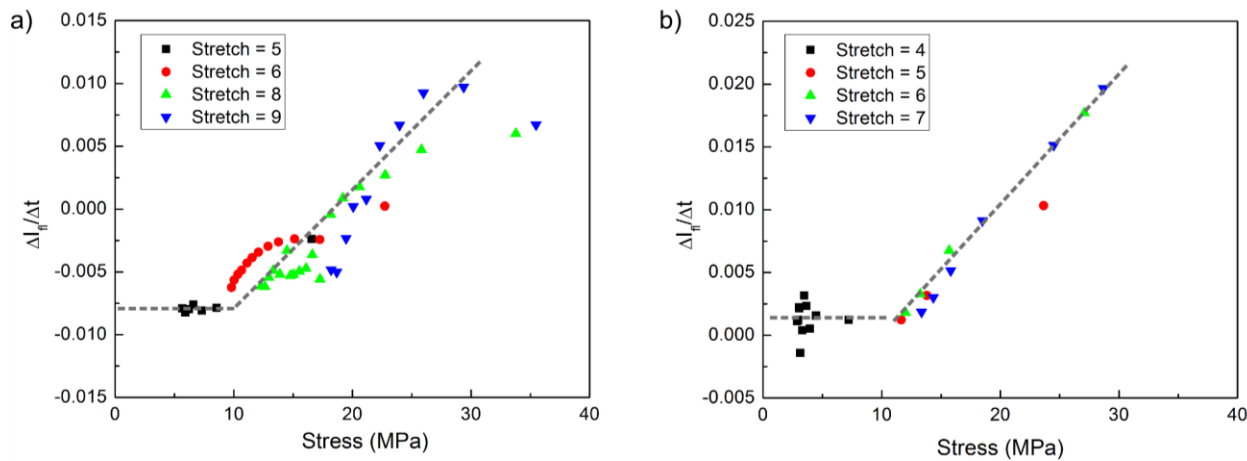


Figure 4.4. Fluorescence change in active SP-linked PMA at various applied loads with bi-linear fits overlaid. a) Sample Type 2UV. b) Sample Type 2G.

The reaction kinetics were empirically modeled based on trends shown in Fig 4.4, and calculated based only on the macroscopic stress in the polymer samples. A bi-linear relationship for both the forward and reverse rate constants was assumed:

$$\begin{aligned} k_f &= k_{f,\sigma=0} && \text{for } \sigma \leq \sigma_{f,\lim} \\ k_f &= k_{f,\sigma=0} + C_f(\sigma - \sigma_{f,\lim}) && \text{for } \sigma > \sigma_{f,\lim} \end{aligned} \quad 4.10\text{a}$$

and

$$\begin{aligned} k_r &= k_{r,\sigma=0} && \text{for } \sigma \leq \sigma_{r,\lim} \\ k_r &= k_{r,\sigma=0} - C_r(\sigma - \sigma_{r,\lim}) && \text{for } \sigma > \sigma_{r,\lim} \end{aligned} \quad 4.10\text{b.}$$

The forward and reverse rate constants, $k_{f,\sigma=0}$ and $k_{r,\sigma=0}$, at no applied load with test lighting conditions ($P_{\lambda=532 \text{ nm}} = 2500 \mu\text{W}$) were known following from section 4.3.1. Values for k_r were limited to only positive values, and assumed to be virtually zero when the calculated rate reaction decreased below zero. Variables to be optimized were critical stress, $\sigma_{f,\lim}$ and $\sigma_{r,\lim}$, above which an effect of mechanical loading on the rate constant could be detected, and C_f and C_r correlating applied stress and the change in reaction rate. Matlab software was used to iterate values for the unknown variables (C_f , C_r , $\sigma_{f,\lim}$ and $\sigma_{r,\lim}$) and calculate reaction kinetics using only the stress in the sample, σ , by substituting the stress-dependent rate constants from Eqs. 4.10a and 4.10b into Eq 4.8. For each iteration, the calculated fluorescence kinetics were compared to the data in Fig 4.3, and best fit values for the unknown variables were defined as those with the smallest standard error between calculated and experimental kinetics. A detailed description of the code to optimize $k_f(\sigma)$ and $k_r(\sigma)$ is included in Appendix B. Best fit curves for the predicted fluorescence are plotted with the experimental data in Fig 4.3a and Fig 4.3b. The average percent error between the experimental data and empirical predictions of all data points in the best fit activation rates was below 6%.

The best fit rate constants for the forward and reverse reaction, k_f and k_r , are plotted as a function of stress in Fig 4.5a. The forward reaction rate increased with applied stress, and the reverse reaction rate decreased with increasing stress. The onset of a detectable change in the kinetics of SP-MC conversion was at approximately $\sigma_{\lim} = 8 \text{ MPa}$, for both the forward and

reverse reactions. At stresses greater than 40 MPa the reverse rate constant was effectively zero. The correlation factors C_f (8×10^{-5} MPa $^{-1}$ s $^{-1}$) and C_r (3×10^{-4} MPa $^{-1}$ s $^{-1}$) had similar magnitudes. The effect of stress accelerating the forward reaction was comparable to the effect retarding the reverse reaction.

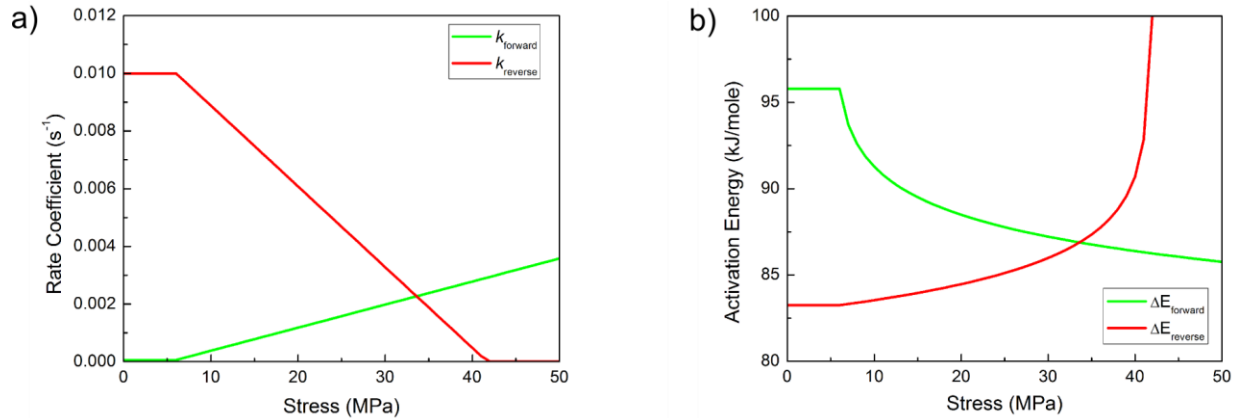


Figure 4.5. Empirically derived parameters for kinetics of SP-MC conversion as a function of applied stress. a) Reaction rates for the forward and reverse reactions, and b) activation energies for the forward and reverse reactions at laser power of 2500 μ W.

The bi-linear (Eq 4.10) trend describing the experimental data was determined empirically from experimental data. Compared with the Eyring model (Eq 4.4), two differences are apparent. In our model, a threshold of macroscopic stress (σ_{lim}) was required before a change in the reaction rates and activation energies was detectable. This may be due to initial deformation energy being applied to uncoiling and aligning polymer chains – an argument posed and supported in the previous chapter – before the macroscopic stress translated to a tensile force along the polymer chains. Additionally, an exponential agreement between reaction kinetics and applied stress did not effectively describe the kinetics, overestimating the change in reaction kinetics at large applied stress. If the exponential term of the Eyring model in Eq. 4.4 is approximated as linear for small values of ΔE_{mech} [43], e.g.:

$$k_f = k_{\sigma=0,f} \exp\left(\frac{\Delta E_{mech,f}}{k_b T}\right) \approx k_{\sigma=0,f} \left(1 + \frac{\Delta E_{mech,f}}{k_b T}\right) = k_{\sigma=0,f} \left(1 + \frac{\sigma v_f^*}{k_b T}\right) \quad 4.11$$

then the reaction rate from the Eyring model follows the same trend observed in the experimental data and simulated for $\sigma > \sigma_{lim}$. Equations 4.10a and 4.11 were combined and the activation volume for the forward reaction, v_f^* , is $3.5 \times 10^{-26} \text{ m}^3$, with a corresponding characteristic length ($d_f^* = v_f^{*1/3}$) of approximately 3 nm. The reverse reaction had an activation volume, v_r^* , of $9.5 \times 10^{-29} \text{ m}^3$, with a characteristic length scale, d_r^* , of 2 nm. The long axis of the SP and MC forms have lengths of approximately 0.7 nm and 1.3 nm based on molecular modeling. Thus activation volumes and characteristic length scales for both the forward and reverse direction are on the same size scale as the SP molecule, as is expected for a stress-activated process [77].

Activation energies for the forward and reverse reactions were calculated from the rate constants using Eq 4.1 and are plotted as a function of stress in Fig 4.5b. Even with a relatively strong photochemical driving force for the reverse reaction applied by a 532 nm laser at $2500 \mu\text{W}$, the forward reaction dominated at stresses over 35 MPa. If the photochemical effect from the laser $\Delta E_{\lambda=532,r}$ is subtracted, the activation energies, ΔE_a , of both SP and MC correspond to relatively stable species. Below a threshold stress of approximately 8 MPa, no change in activation energy was detected. At high levels of stress (50 MPa) the energy barrier for activation of SP to MC, $\Delta E_{mech,f}$, was decreased by approximately 12 kJ/mole. At stresses above 40 MPa, the reverse reaction (MC \rightarrow SP) was not detectable, and the activation energy, $\Delta E_{mech,r}$, was not measured and presumed large.

The effect of stress on reaction kinetics described in this chapter applies to an elastomeric polymer in which polymer chain mobility is relatively high and yield was virtually immediate. In a glassy polymer system (described in the following chapter) polymer yield and flow is an additional requirement for stress to affect reaction kinetics.

4.4 Conclusions

Kinetics of the SP-MC reaction equilibrium were measured at room temperature (22 °C) by the fluorescence signal of the MC form of the mechanophore. Applied stress causes an increase in the reaction rate of the forward reaction (SP→MC) and a decrease in the reverse reaction rate (MC→SP). The reaction rates as a function of stress were simulated based on the macroscopic stress and fitted to experimental data. A bi-linear agreement between reaction rate and applied stress provided the best fit to the experimental data. At stresses below 8 MPa, no change in reaction kinetics was detected. At higher stresses the relationship between reaction rate and stress increased linearly for the forward reaction and decreased linearly for the reverse reaction. Activation energies for the forward and reverse reactions were approximated based on the experimentally determined reaction rates. The calculated decrease in the forward reaction activation energy, $\Delta E_{mech,f}$, was on the order of 12 kJ/mol, corresponding to the difference between a reaction time constant of days and a time constant of seconds. The activation energy of the forward reaction without applied load ($\Delta E_{0,f} \approx 96$ kJ/mol), and effect of an applied stress ($\Delta E_{mech,f}(\sigma=50$ MPa) ≈ -12 kJ/mol), provide benchmarks for favorable chemical energetics of new mechanophore design.

CHAPTER 5

SP ACTIVATION IN A GLASSY POLYMER: EFFECT OF THERMOMECHANICAL BEHAVIOR[‡]

5.1 Introduction

SP has typically been incorporated into elastomeric or ductile polymers such as linear poly(methyl acrylate) (PMA) or polyurethane (PU). SP activation in elastomeric polymers occurs at relatively large deformations, on the order of hundreds of percent strain [38, 83]. In this chapter SP is incorporated into a linear engineering polymer, poly(methyl methacrylate) (PMMA), with the goal of imparting higher force to the mechanophore at low strains, and achieving low-strain SP activation. As opposed to the elastomeric system described in Chapter 3, PMMA fails at relatively small applied displacements. Therefore engineering strain is used as the metric to define deformation as opposed to stretch ratio. Linear PMMA has a relatively high glass transition temperature and exhibits brittle fracture at room temperature. At higher temperatures approaching T_g , the yield stress decreases and PMMA exhibits the ability to be drawn [5, 84]. The glass transition temperature of PMMA can also be reduced by plasticizing with a dilute concentration of solvent, allowing yielding at lower temperatures [44, 45, 85]. Ductile mechanical response was elicited by testing at elevated temperature or after plasticizing to achieve activation in SP-linked PMMA.

[‡] The results presented in this chapter are published in: Beiermann, B.A., et al., *Environmental effects on mechanochemical activation of spiropyran in linear PMMA*. Journal of Materials Chemistry, 2011.

5.2 Experimental Methods

5.2.1 Synthesis and Characterization

Linear PMMA was synthesized by an ATRP reaction described in Chapter 2. Active SP-linked PMMA and difunctional control SP-linked PMMA were synthesized using SP as the free radical initiator and linking the mechanophore into the polymer backbone. Plain SP-linked PMMA was synthesized with no SP incorporated into the polymer. All polymers were glassy at room temperature, with T_g of approximately 127 °C (refer to Table 2.2) regardless of SP incorporation.

5.2.2 Sample Molding

Polymer powder was molded into tensile dog-bone samples via compression molding in a closed mold. A pressure of 200 psi was applied to the mold at a temperature of 160 °C, for 10 minutes. The mold was then quenched in water. Samples were polished before testing, and SP-linked polymer, held at 100 °C, was irradiated with a 530 nm diode lamp for 24 hours to drive the active species toward the closed SP form. Sample dimensions are shown in Appendix A.

Thermal energy from molding at high temperature (160 °C) led to some ring opening. Molded samples exhibited a red or orange appearance, indicating a combination of the clear/yellow SP form and the purple MC form. Visible spectrum light, particular in the green region of the visible range, is known to drive the MC isomer to the SP form [34]. However, at room temperature, 532 nm light was not effective at reverting MC to SP. By irradiating with 532 nm light at 100 °C for 24 hours, the color faded to a clear or yellowish color indicating that most MC had been driven to SP.

5.2.3 Mechanical Testing

Specimens were tested in tension over a range of temperatures, using an environmental chamber to control temperature. The equipment used for temperature controlled mechanical testing was TA Instruments RSA3, typically used for dynamic mechanical analysis. Prior to testing, samples were equilibrated for 5 minutes at the desired test temperature under a small tensile preload (0.1 N). The samples were then loaded in displacement control at a rate of 5 $\mu\text{m/s}$. Initial gauge lengths varied between 5-7 mm.

Additional samples were plasticized solvents in order to reduce T_g . Dibutyl phthalate (DBP) and methanol (MeOH) are documented plasticizers for PMMA and were used in this research [44, 84, 85]. For methanol plasticizing, samples were soaked in methanol for approximately 48 hours. A corresponding solvent uptake of 15-20 wt% was observed. At this MeOH content, mechanical behavior was similar to unplasticized PMMA at 90 °C.

To plasticize PMMA with dibutyl phthalate (DBP), 2 g dried polymer powder was mixed with a defined amount of DBP and 100 mL MeOH for 24 hours. The methanol (boiling point = 65 °C) was then driven off by drying the polymer at 80 °C for 24 hours, leaving only the desired amount of DBP (boiling point = 344 °C). The glass transition temperature for each polymer batch was determined by the peak of a $\tan(\delta)$ curve from dynamic mechanical analysis, ramped at 3 °C per minute. Glass transition temperatures peaks are plotted as a function of DBP concentration in Fig 5.1. Polymer samples were molded into dog-bone shaped samples at approximately 30 °C above T_g for each batch.

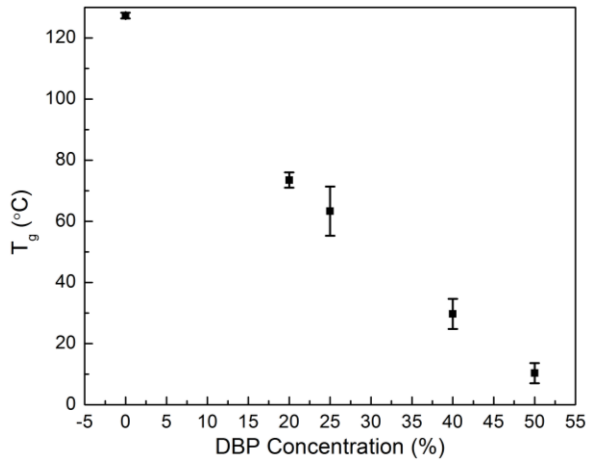


Figure 5.1. Polymer glass transition temperature as a function of dibutyl phthalate concentration as taken from the dynamic mechanical analysis $\tan(\delta)$ peak.

All plasticized samples were tested at room temperature ($T = 22^\circ\text{C}$) with a custom-built load frame described in Chapter 3. For PMMA mechanical testing a larger capacity load cell (220 N) was used. Strain rates were consistent (approximately 0.001 s^{-1}) with testing at elevated temperatures. The fluorescence signal was monitored on a color CCD camera (AVT Stingray model F-125C) using the experimental setup shown schematically in Fig 5.2. Fluorescence intensity was reported as the red pixel intensity averaged over the polymer sample, disregarding values less than 10 pixels from the edge of the sample to minimize edge effects. Laser power and CCD exposure settings were kept constant between all tests.

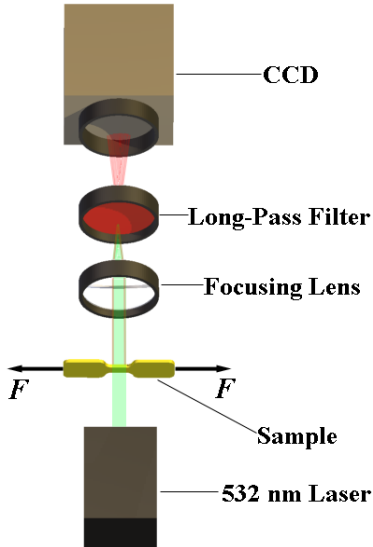


Figure 5.2. Experimental set-up for *in situ* fluorescence imaging of solvent-plasticized specimens.

5.3 Results and Discussion

5.3.1 Effect of Temperature on Mechanical Activation

The stress-strain response of the active PMMA is shown in Fig 5.3a over a range of test temperatures from 22 °C to 120 °C. Specimens tested in tension at 22 °C and 80 °C failed in a brittle manner ($\varepsilon_{\text{ult}} < 10\%$). No color change was detected in these specimens prior to failure, and fluorescence imaging indicated no measurable activation at the fracture surface. At higher temperatures of 90 °C and 105 °C, the yield stress dropped significantly and substantial plastic flow was observed. Evidence of the mechanochemical reaction was visible as a purple color in the sample at ca. 10% applied strain in samples tested at 90 °C. Color change appeared shortly after yielding of the polymer, and was localized in the gauge section, coinciding with necking and drawing. As strain increased, the color became more vibrant in the drawn section of specimens tested at 90 °C and 105 °C. Qualitatively, samples tested at 90 °C exhibited more

intense color change than at 105 °C, presumably due to higher stress in the sample during the drawing process. At a temperature of 120 °C, just below the glass transition, deformation was dominated by viscous flow. Samples deformed over 100% strain at low stress and no color change was observed. Representative images of samples tested at various temperatures are included in Fig 5.3b.

Control samples were mechanically tested at 90 °C. Both plain PMMA (without SP incorporated) and difunctional control SP-linked PMMA behaved mechanically similar to active polymer, with no significant variation in yield stress, yield strain, or strain at failure. Difunctional control samples tested at 90 °C did not exhibit a color change, indicating that the color change in active samples was due to mechanically induced opening of SP, and not thermal activation.

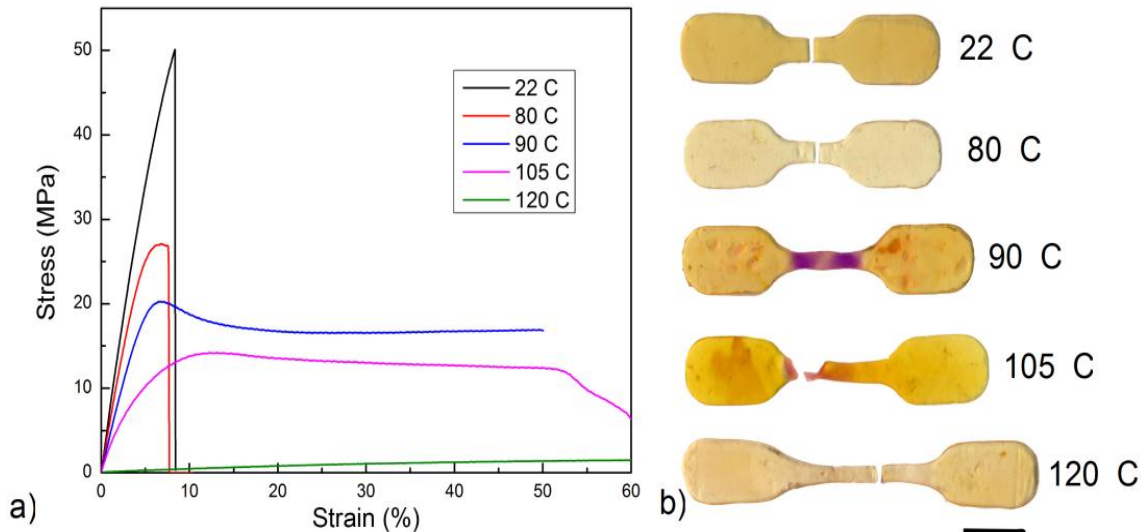


Figure 5.3. Effect of temperature on mechanochemical behavior of active SP-linked PMMA. a) Mechanical response at various testing temperatures. b) Optical images of samples after testing. Scale bar = 6 mm.

5.3.2 SP Activation in MeOH Plasticized PMMA

As molded PMMA specimens were plasticized with methanol by submerging samples in the solvent to increase polymer mobility at RT (22 °C). Samples with 15-20% MeOH uptake by mass exhibited similar mechanical behavior at RT compared to unplasticized samples at 90 °C. Samples with < 15 wt% MeOH uptake exhibited brittle failure and no activation at RT. Samples with > 20 wt% MeOH uptake showed significant nonuniformity and inconsistent mechanical behavior. RT testing of plasticized PMMA allowed for *in situ* fluorescence imaging; a capability which was prevented by the thermal control chamber used for high temperature testing of unplasticized polymer.

Fluorometry in the visible range (see Chapter 2 for spectra) showed little fluorescence signal for untested active samples, indicating that the mechanophore is predominantly in the SP form. However, mechanically activated samples exhibited strong fluorescence, with broad

excitation and emissions bands peaking at 560 nm and 620 nm, respectively. These peaks are presumed to correspond to the MC form of the mechanophore.

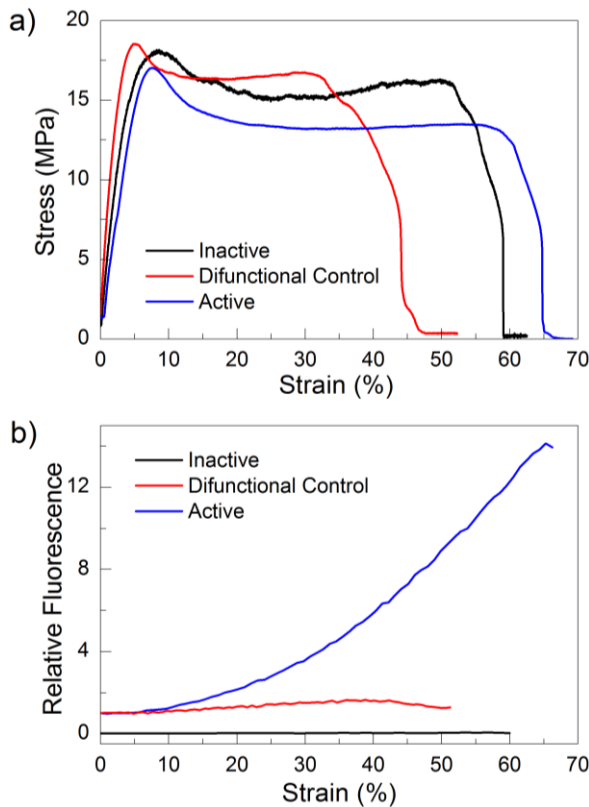


Figure 5.4. Mechanical and fluorescent response of MeOH plasticized (~15 wt%) PMMA. a) mechanical response at room temperature. b) Corresponding fluorescence intensity from full field fluorescence imaging during mechanical testing.

Representative stress-strain and fluorescence intensity data are plotted in Fig 5.4 for methanol soaked samples of plain PMMA, active SP-linked PMMA, and difunctional control SP-linked PMMA. All three samples had approximately 15% MeOH uptake prior to testing. Relative fluorescence was defined as the fluorescence signal divided by the fluorescence signal with no deformation. All three polymers had similar stress-strain responses, with a significant amount of drawing prior to failure. Only active PMMA exhibited a substantial increase in fluorescence with mechanical loading. Onset of activation at room temperature was observed below 10% strain in all plasticized active PMMA samples, occurring just after polymer yield.

The fluorescence intensity continued to increase during drawing until failure. Plain PMMA showed no measurable fluorescence intensity before or after loading, confirming that any fluorescence is due to the incorporation of SP. The fluorescence signal present in the active and difunctional control PMMA prior to testing was likely due trace remaining amounts of MC. A slight change in the difunctional control fluorescence intensity was observed during loading, but was considered negligible when compared with the active SP-linked polymer.

5.3.3 SP Activation in DBP Plasticized PMMA

Although plasticizing PMMA with MeOH effectively promoted ductile behavior of the polymer, MeOH solvent wasn't stable in the polymer and evaporated out of the sample in a time scale of hours in air at room temperature. DBP has a high boiling point of approximately 340 °C, thus very low vapor pressure at room temperature , and provided a stable plasticizing solvent. The polymer glass transition temperature of DBP plasticized PMMA could be measured by dynamic mechanical analysis (Fig 5.1). T_g measurements of PMMA with DBP plasticizer were consistent over a period of weeks.

Active SP-linked PMMA samples with varying DBP concentration were tested in tension and the load and fluorescence were monitored in the same manner as the MeOH-plasticized polymer. The true stress and fluorescence, normalized relative to the initial sample fluorescence, were plotted as a function of strain. Representative curves at varied polymer T_g are included in Fig 5.5a-d. At relatively high concentration of DBP corresponding to T_g near room temperature (Fig 5.5a), the stress in the polymer sample was low and little or no activation was observable in the fluorescence signal. For higher polymer T_g , the stresses were higher, and activation was evident via marked increase in the fluorescence signal (Figs 5.5b-c). Room temperature testing

of DBP-plasticized PMMA with T_g above 80 °C (Fig 5.5d) resulted in brittle failure at high stresses and no detectable activation.

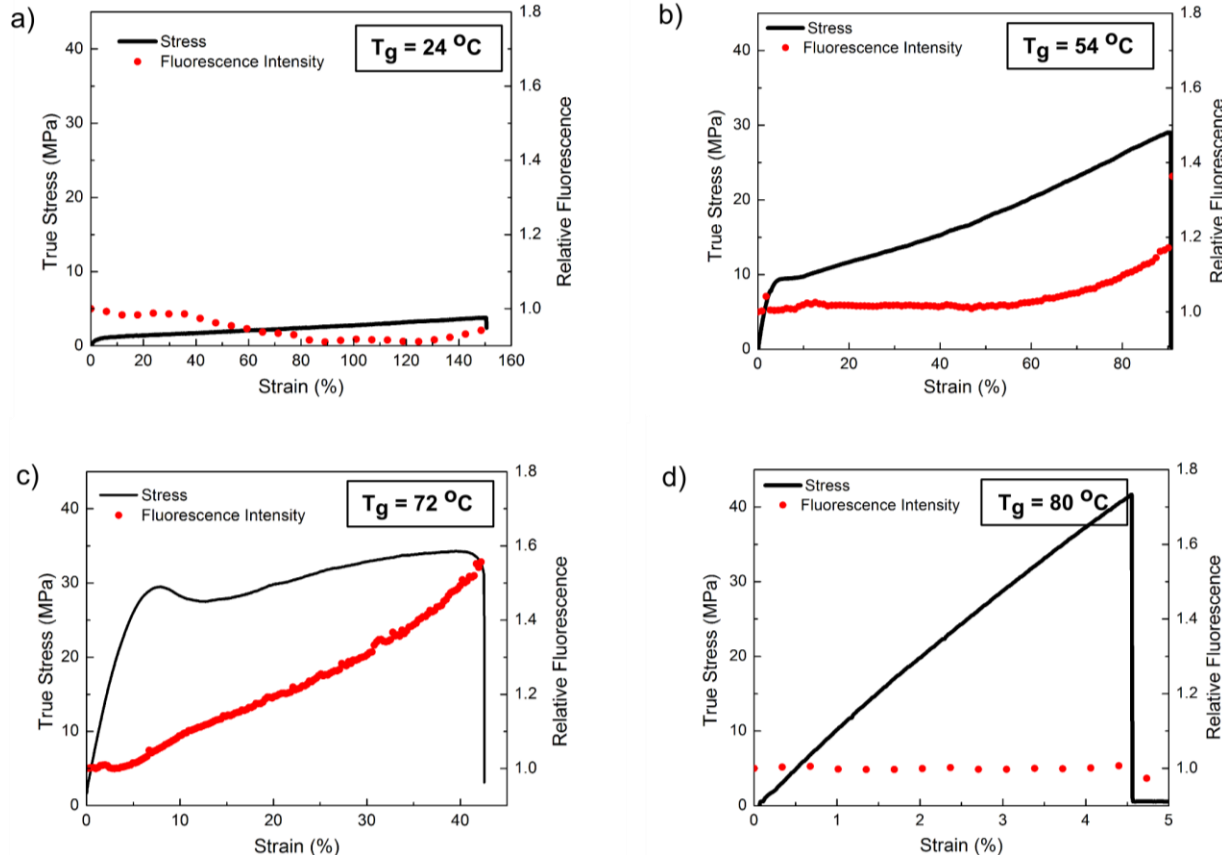


Figure 5.5. Mechanical and raw fluorescence (normalized by the un-deformed fluorescence signal) data for DBP-plasticized PMMA with T_g of a) 24 °C, b) 54 °C, c) 72 °C, and d) 80 °C.

Strain to activation was defined as when the slope of the fluorescence signal as a function of strain begins to increase, as described in Chapter 3. Over the range of mechanical behavior at which activation was detectable ($T_g \approx 30\text{ }^{\circ}\text{C}$ to $T_g \approx 80\text{ }^{\circ}\text{C}$), the strain to activation varied with polymer T_g . Strains to activation are plotted as a function of the glass transition temperature in Fig 5.6. With increasing T_g , polymer stiffness and macroscopic stress increased, and activation occurred at lower strains. The minimum strain to activation was approximately 5% at a T_g of

approximately 75 °C. In all cases yielding and plastic deformation were required before activation occurred, as well as a relatively high level of stress.

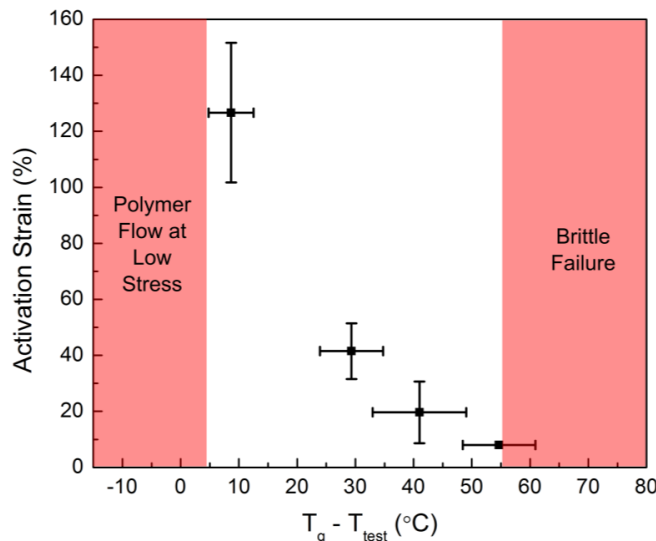


Figure 5.6. Strain at which the onset of activation was apparent *via* an increase in the fluorescence signal, plotted against varying polymer glass transition temperature.

5.3.4 Creep Loading of SP-Linked PMMA

Unplasticized active polymer was subjected to creep loading conditions, in which a load was applied and held constant over time. The strain and fluorescence response were monitored. The stress, strain, and fluorescence behavior of a representative sample held at approximately 52 MPa for 12 hours is demonstrated in Fig 5.7. A control program was devised using LabView software such that the sample was deformed in the same manner as tensile testing described previously in this chapter, until the stress was greater than a critical load (in this case 52 MPa) and the deformation was held constant. When the stress in the sample relaxed below 52 MPa, a stepwise motion of 1 μm was applied. The resulting stress was held at approximately the same level, with slight fluctuation giving the curve a saw-tooth appearance of the black curve in Fig 5.7. The strain increased gradually but to modest strains below 10%. At larger applied

loads, the sample failed at ca. 6% strain. The fluorescence signal was virtually constant as a function of time. A slight initial increase was present in the fluorescence signal, but a similar increase could be seen in the difunctional control SP-linked PMMA. Therefore no considerable activation was detectable over long times with a relatively large loads applied by a creep loading condition.

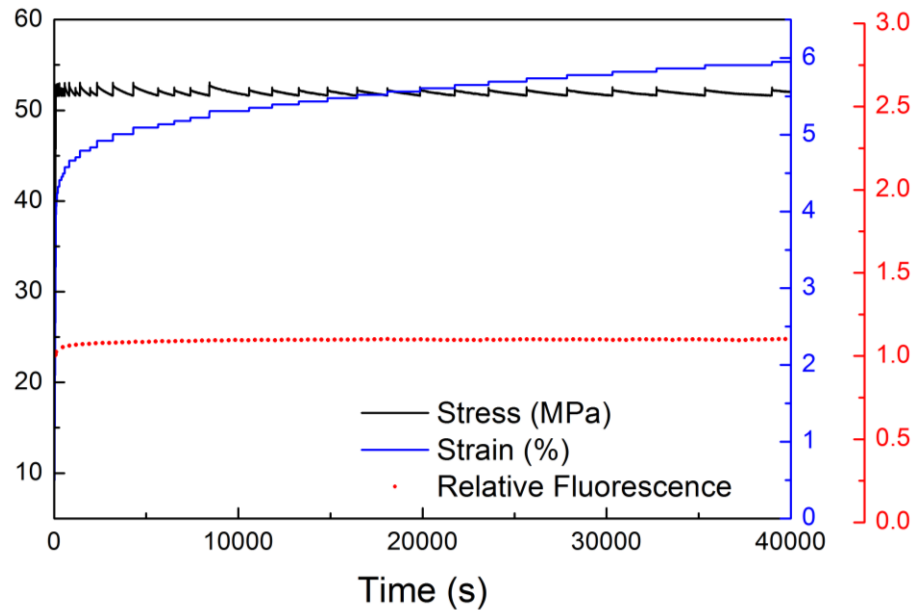


Figure 5.7. Creep behavior of active SP-Linked PMMA loaded to a stress of approximately 52 MPa.

5.4 Conclusions

SP can undergo a force driven reaction to the MC species when linked into a brittle polymer backbone, such as PMMA. Both solvent-plasticized and temperature controlled PMMA tensile testing revealed a specific range of polymer T_g and mechanical properties which promote mechanochemical activation. A similar critical range of temperatures for mechanophore activation may apply to emerging mechanophore systems in the solid state.

Activation of SP was achievable under conditions in which PMMA has sufficient mobility to yield and draw at moderate stress. No activation occurred if the polymer was too viscous and failed in a brittle manner, i.e. without a large degree of polymer flow. Relatively high stress at low strain under creep loading conditions was not sufficient to drive SP activation on a time scale greater than ten hours, further implicating the need for plastic deformation for mechanochemical conversion. For polymer T_g near the tensile testing temperature, the stresses were low and no significant activation was detectable, indicating a possible threshold of stress for SP activation in PMMA.

Plasticizing with 15-20 wt% MeOH allows drawing and activation at RT. The onset of activation was observed at strains below 10% in linear SP-linked PMMA. Dibutyl phthalate acted as a stable plasticizing agent, allowing characterization of polymer T_g and control of mechanical properties. By varying the concentration of DBP, the activation behavior of the polymer could be affected. The strain to activation in DBP plasticized polymer was tunable based on the polymer T_g , which could be controlled by the concentration of plasticizing agent. The onset of detectable activation coincided with stresses in the polymer reaching ca. 10 MPa, which agrees closely with the onset of an effect on reaction kinetics in the elastomeric polymer system described in section 3.3.6.

In comparison with other linear, moldable polymers, the onset of activation for the linear PMMA was achieved at orders of magnitude lower strain levels. A mechanochemical system acting at such low strains could be applied to structural applications as a deformation sensor. We show a range of activation onsets from strains of ca. 5% to greater than 100%, corresponding to varied T_g , indicating versatility of this system, which could be applied to a variety of different structural load bearing applications.

CHAPTER 6

FLUORESCENCE POLARIZATION MEASUREMENTS OF MECHANOPHORE ORIENTATION[§]

6.1 Introduction

The birefringence measurements presented in Chapter 3 quantify the average orientation of polymer chains under tensile deformation. A second optical technique, fluorescence polarization measurement, can be applied to quantify the orientation of the mechanophore subunits within the polymer backbone. As described in the Chapter 1, a fluorescent molecule emits photons polarized in the direction of a transition dipole. The transition dipole, (\vec{r}), of merocyanine (MC) fluorescence has directionality roughly across the long axis of the molecule (see Fig 1.2) [53, 54]. The spiropyran (SP) form has virtually no fluorescence signal and does not contribute to this measurement. MC fluorescence polarization can be analyzed by adding a linear polarizer to the mechanical/optical set-up described in Chapter 3, between the sample and the CCD detector. The modified set-up for measuring MC orientation is shown in Fig 6.1.

Degree of orientation in general terms is evaluated by an order parameter, S , based on the second order Legendre polynomial, P_2 [47]:

$$\langle P_2 \rangle = \frac{\langle 3 \cos^2(\beta) - 1 \rangle}{2} \equiv S \quad 6.1,$$

where β is the angle between a laboratory frame (the tensile direction) and a component director (the dominant MC transition dipole). Order parameter values vary between 0 (random distribution) and 1 (perfectly aligned) in this study. An order parameter can be derived from

[§] The results presented in this chapter are published in: Beiermann, B.A., et al., *Role of Mechanophore Orientation in Mechanochemical Reactions*. ACS Macro Letters, 2011.

Eq. 6.1 based on the measured fluorescence intensities with the analyzing polarizer oriented parallel and perpendicular to the tensile direction [52, 86, 87]:

$$S = \frac{(I_{\parallel} - I_{\perp})}{(I_{\parallel} + 2I_{\perp})} \quad 6.2$$

where I_{\parallel} and I_{\perp} denote the total fluorescence intensity with the polarizer parallel and perpendicular to the tensile direction, respectively. Eq. 6.2 assumes that the mechanophore is rotationally fixed during measurement. MC orientation has been correlated with mechanophore activation to provide information on the nature of orientation and force transfer at the mechanophore level.

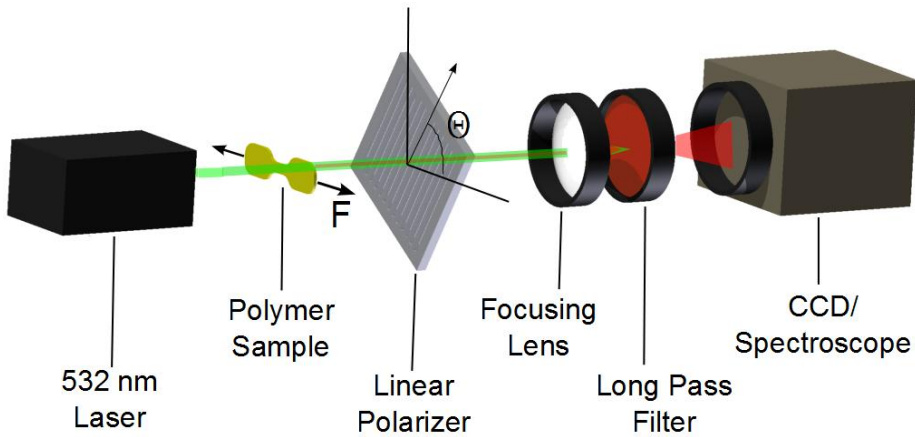


Figure 6.1. Experimental set-up for analysis of polarized fluorescence emission.

6.2 Experimental Methods

6.2.1 SP-Linked Polymer Samples

SP was linked into linear poly(methyl acrylate) (PMA) and poly(methyl methacrylate) (PMMA) backbones. Relevant details for each polymer type are listed in Table 6.1. PMMA was

either tested at elevated temperature (PMMA^a) or plasticized (PMMA^b) to allow drawing and mechanical activation of SP [88]. Samples were prepared as described in previous chapters.

Optical images of SP-linked polymer samples discussed in this Chapter are included in Fig 6.2. As-molded samples exhibited orange or pink color, indicating a combination of SP and MC forms due to thermal activation of SP to MC. The mechanophore equilibrium could be driven toward either the SP form or the MC form photochemically. SP-linked PMA was driven toward the SP form using a strong green light source ($\lambda = 532$ nm), or toward the MC form using UV light ($\lambda = 385$ nm). UV-irradiated samples will be referred to as UV-activated. Images of SP-linked PMA samples driven toward the SP and MC forms are shown in Figs 6.2a and 6.2b, respectively, before and after tensile testing. SP-linked PMMA could not be driven toward the MC form using UV light, but was effectively driven toward the SP form with 532 nm light. Images of SP-linked PMMA samples as molded and driven toward the SP form before and after tensile testing are included in Figs 6.2c and 6.2d, respectively. After mechanical testing of polymer samples driven toward the SP forms (Figs 6.2a and 6.2d), mechanical activation of SP to MC was present in the gauge sections indicated by the emergence of a purple color.

Table 6.1. Properties of SP-Linked Polymers

Polymer	PMA	PMMA^a	PMMA^b
M _N (kDa)	230	180	180
PDI	1.1	1.8	1.8
T _g (°C)	12	128	-
ε _{ult} (%)	~1500	35-70	65
σ _{ult} , Engr. (MPa)	4	20	15

^a Tested at 90 °C, unplasticized.

^b Plasticized with 17 wt% methanol (MeOH), tested at room temperature.

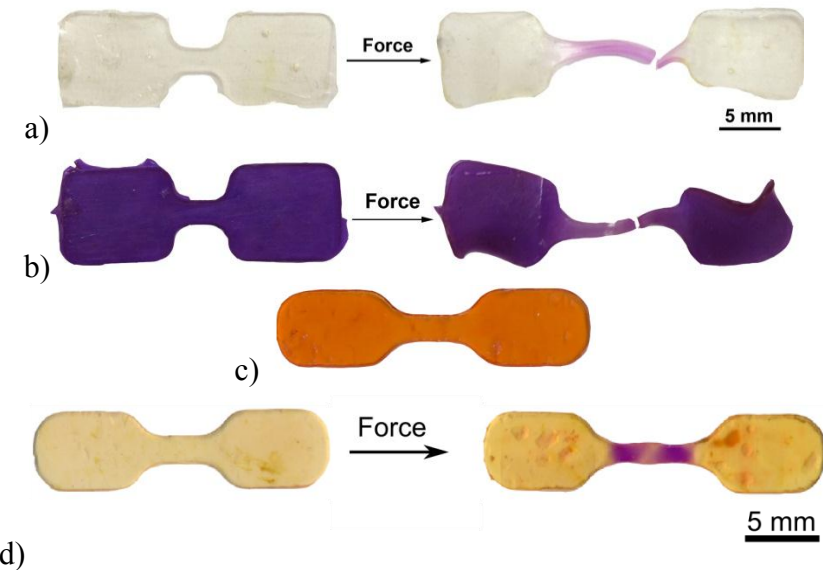


Figure 6.2. SP-linked polymer specimens studied. a) SP-linked PMA driven toward the SP form and tested in tension. b) UV-activated SP-linked PMA before and after mechanical testing. c) Thermally-activated (as molded) SP-linked PMMA. d) SP-linked PMMA driven toward the SP form and tested in tension.

6.2.2 Mechanical Testing

A SP-linked PMMA^a sample, driven toward the SP form was deformed at 90 °C in order to achieve mechanical activation. The sample was strained 35% in tension (see Chapter 4 for mechanical testing parameters) and demonstrated a purple color (MC) in the gauge section. The sample was then brought to room temperature, effectively quenching the polymer and the activation of the SP. The purple color from the MC form was relatively stable and was visible on the order of months. This sample was examined *ex situ* (section 6.3.1) to examine the effect of varying polarizer orientation, Θ , with respect to the sample, on fluorescence intensity.

Other polymer samples (PMA and PMMA^b) were tested in tension at room temperature and studied *in situ* using the experimental set-up described in Chapter 3, modified as shown in Fig 6.1. A tensile deformation was applied incrementally, with fluorescence polarization images taken between each deformation step. The deformation steps corresponded to a change in stretch

ratio of $\Delta\lambda = 2$ for PMA and change in strain of $\Delta\varepsilon = 5\%$ for PMMA^b. The loading rate was 0.10 s^{-1} for PMA and 0.001 s^{-1} for PMMA^b, in accordance with the rates for Chapters 3 and 4. Fluorescence polarization images were taken with the polarizer parallel and perpendicular to the direction of applied force, such that the frame of reference for the order parameter in Eq. 6.2 was the loading direction. Due to the incremental nature of the deformation, some relaxation occurred during image acquisition, but the stresses reached during incremental testing were nearly the same as those in monotonic tensile loading.

6.3 Results and Discussion

6.3.1 Alignment of Mechanophores with the Tensile Direction

The effect of varying polarizer angle, Θ , with respect to the tensile direction, on the fluorescence signal of SP-linked PMMA samples was first investigated to establish whether the mechanophore orientation was measurable. Relative fluorescence intensity is plotted as a function of polarizer orientation in Fig 6.3 for two samples: mechanically activated and thermally activated SP-linked PMMA. The mechanically activated sample was driven toward the SP form with green light, then drawn to $\varepsilon = 35\%$ at 90°C , resulting in a strong purple color in the gauge section. The fluorescence signal was anisotropic with a maximum intensity when the polarizer was oriented parallel to the tensile direction, indicating that the transition dipole of MC was oriented predominately in the direction of applied force. The data closely fits the expected $\cos^2\Theta$ relationship for a preferred orientation of the fluorescent molecule [47]. In contrast, undeformed SP-linked PMMA, thermally activated at 170°C during molding, showed no preferential orientation.

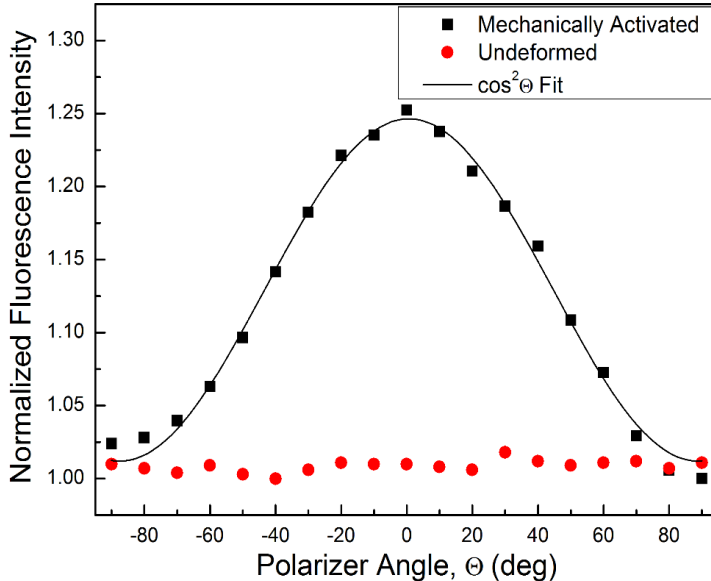


Figure 6.3. Fluorescence intensity vs. polarizer orientation for mechanically activated ($\varepsilon = 35\%$) and un-deformed (thermally-activated) SP-linked PMMA.

6.3.2 Role of Mechanophore Orientation in a SP-Linked Elastomer

The order parameter calculated from Eq. 6.2 was used to determine the average orientation of the MC form within SP-linked PMA. Fluorescence images or spectra were taken at increments of odd integer values for the stretch ratio, λ , defined as the instantaneous sample gauge length divided by the initial length. The order parameter was averaged over the gauge section for a number of samples (minimum 3 per data point). A plot of order parameter as a function of stretch ratio is shown in Fig 6.4 for UV-activated and mechanically-activated SP-linked PMA.

Activation by UV light drove virtually all SP subspecies to the fluorescent MC form. The order parameter for unstrained material was nearly 0, indicating a randomly oriented sample. The small degree of orientation present was due to a pre-stress on the sample before testing. With increasing stretch ratio, the UV-activated MC subspecies became increasingly oriented in the tensile direction, reaching a maximum order parameter of *ca.* 0.5.

Prior to testing, mechanically activated samples were irradiated with visible light to drive any MC form to the closed SP form. Because the SP form has virtually no fluorescence signal, the order parameter remained undefined until the samples began to exhibit a detectable fluorescence (i.e. activation). The onset of mechanical activation occurred well before polymer failure. The order parameter for mechanically activated samples was significantly higher than in the UV-activated case, indicating that SP subspecies which were more aligned with the tensile force activated preferentially.

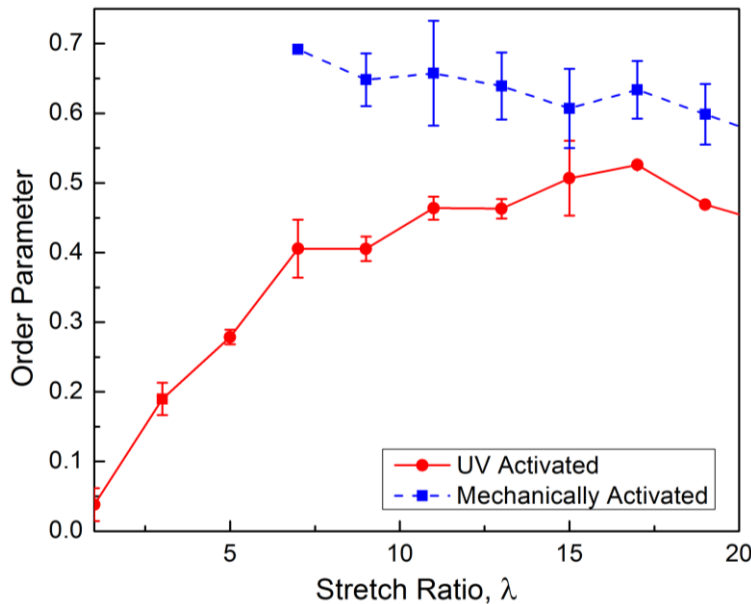


Figure 6.4. Average MC order parameter as a function of stretch ratio, λ , for UV activated and mechanically activated SP-linked PMA. Error bars represent the standard deviation between 3 samples of each type.

6.3.3 Orientation in a Mechanically-Activated Glassy Polymer

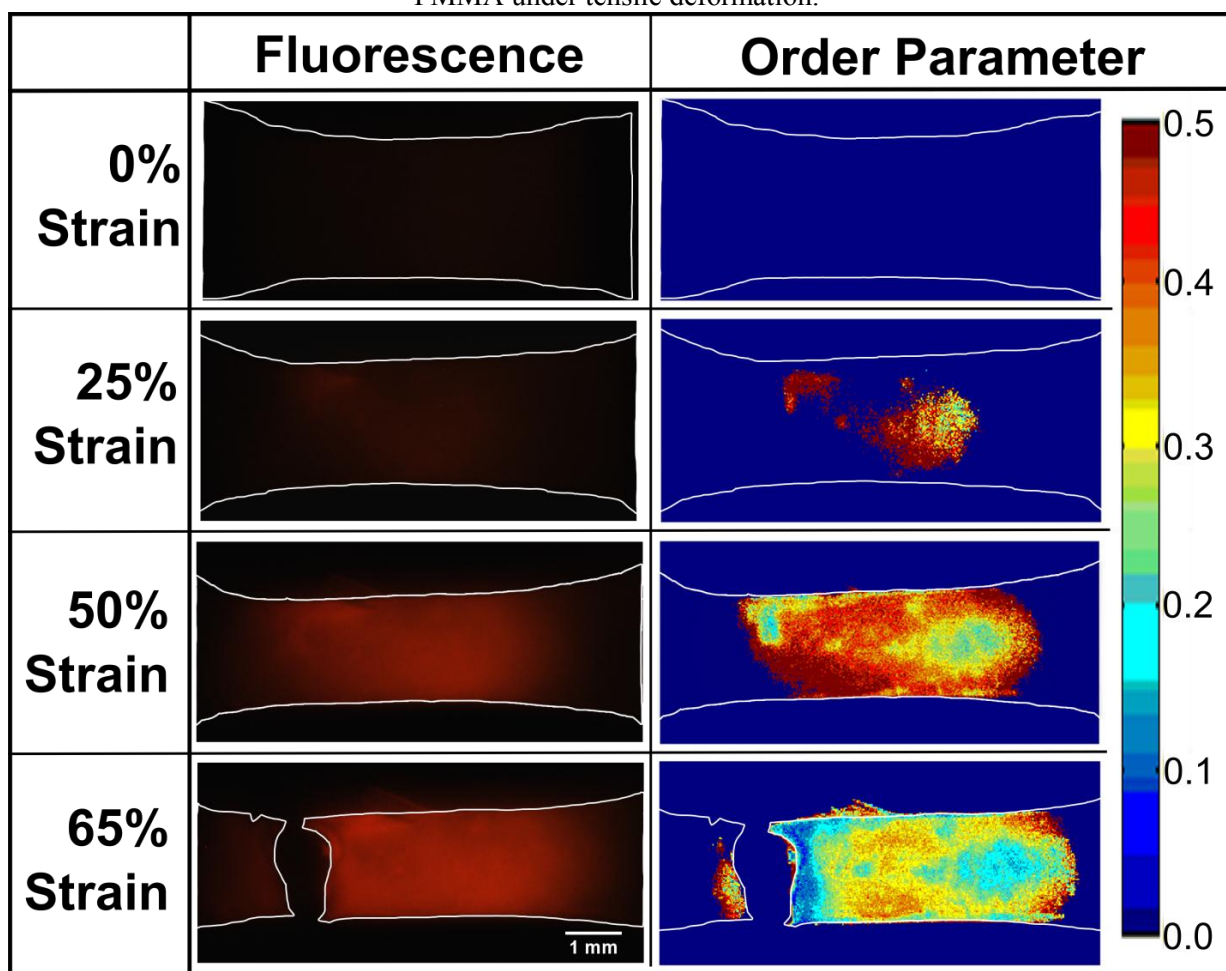
While SP-linked PMA exhibited a relatively consistent degree of fluorescence anisotropy throughout the gauge section, activation and degree of orientation were highly localized in SP-linked PMMA. SP-linked PMMA was plasticized with MeOH (17 wt% uptake). A region of

interest (ROI) was monitored for MeOH-plasticized SP-linked PMMA, which was driven to the SP form using visible light prior to testing. The sample was tested in tension with increments of 5% strain between fluorescence measurements (Table 6.2). After the polymer yielded and began to draw, the fluorescence increased with increasing strain. When the fluorescence signal was sufficient to define an order parameter, the order parameter initially demonstrated relatively high values (0.4-0.5), again indicating that the mechanophores oriented in the direction of force are preferentially reacting. Both fluorescence and order parameter were spatially heterogeneous and localized across the ROI. After failure, the order parameter dropped to levels below 0.1 near the failure surface. The same trend was evident in unplasticized SP-linked PMMA samples tested at elevated temperature (90 °C), and examined *ex situ*. The authors hypothesize that this decrease in order parameter at failure, particularly near the failure surface, indicates significant polymer recoil and relaxation.

6.4 Summary and Conclusions

Fluorescence anisotropy of MC enabled measurement of the orientation of subspecies covalently bonded into bulk polymers under tensile load. *In situ* testing of mechanophore-linked PMA revealed increasing overall mechanophore orientation with increasing strain. Mechanophores aligned along the tensile direction were shown to be preferentially activated by force. We provide evidence suggesting substantial relaxation of polymer chains at failure in SP-linked PMMA. Results indicate that MC fluorescence polarization may provide an effective molecular probe to study the full-field orientation of polymer chains during deformation and failure.

Table 6.2. Fluorescence images and calculated order parameter in the gauge section of SP-Linked PMMA under tensile deformation.^a



^a Fluorescence images taken with polarizer oriented parallel to tensile force. Approximate sample edges have been artificially outlined in white.

CHAPTER 7

MECHANOPHORE ACTIVATION IN POLYSTYRENE THIN FILMS

7.1 Introduction

Mechanophore activation was investigated for thin films on a rigid substrate using a high strain rate loading criteria. Thin films exhibit different mechanical behavior when compared to bulk polymers. Glassy polymers in thin films such as polystyrene can deform plastically, while large-scale plastic deformation in bulk glassy polymers is typically preceded by brittle failure [89].

Mechanochemically active polymer thin film behavior was probed using a laser-induced stress wave technique first introduced by Stephens and Vossen [90], and further developed by Gupta *et al.* [91] and Wang *et al.*[92]. In this method a high energy laser pulse is incident on an absorbing surface, which converts laser energy into a high amplitude compressive stress pulse, and is ultimately transferred to a tensile stress pulse on a film at a free surface (see Fig 7.1a). Strain rates measured by this test method are typically on the order of 10^7 - 10^8 s⁻¹ [91, 93-95]. This test method provides a means to probe mechanophore behavior at large applied stresses over very high strain rates, and can be applied toward ballistic or shockwave damage-responsive materials.

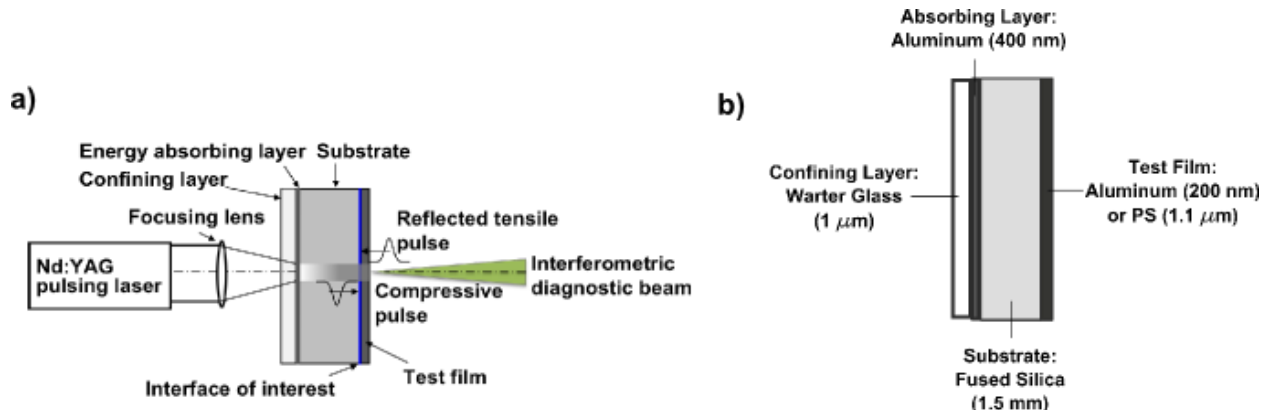


Figure 7.1. High strain rate shockwave loading of mechanophore-linked polymer films. a) Experimental set-up for laser spallation technique. b) Schematic of samples tested with layer thicknesses labeled.

7.2 Experimental Methods

7.2.1 SP-Linked Polystyrene

Active SP-linked polystyrene (PS) was synthesized by an ATRP polymerization as described in Chapter 2. Difunctional control SP-linked PS and plain PS were synthesized by the same method, and all molecular weights were approximately 200 kDa. After synthesis, the polymer was dried at 60 °C for 24 hours, then redissolved into tetrahydrofuran (THF) for thin film preparation by spin coating. Polymer concentration in THF was 50 mg/mL for all samples.

7.2.2 Nd:YAG Shockwave Sample Preparation

Substrates for Nd:YAG laser-induced shockwave loading consisted of a fused silica wafer (1" diameter, 1.5 mm thick) with an aluminum layer (400 nm thick) deposited on one side *via* electron beam deposition, and a 1 μm sodium silicate (water glass, spin coated at 3000 rpm) layer deposited by spin coating from solution on top of the aluminum. Finally a test film was formed on the opposite side of the substrate. Mechanochemically active polymer films were deposited by spin coating the polymer/THF solution with a 5 s ramp to 1500 rpm for 60 s. After

film deposition the sample was held under vacuum for 30 minutes to remove residual solvent. Polymer film thickness was on average 1.1 μm thick as determined by stylus profilometry. Additional calibration samples were produced with aluminum (200 nm thick) instead of polymer as the test film. Sample geometry is diagrammed in Fig 7.1b.

7.2.3 Mechanical Loading and Analysis

A neodymium doped yttrium aluminum garnet (Nd:YAG) laser pulse (New Wave Tempest) was incident on substrates as described in the previous section. The substrate converted the laser pulse to a mechanical pulse in the fused silica and ultimately in the sample film. Fig 7.1a schematically shows the laser incident on the water glass/aluminum side of the substrate, wherein aluminum acts as the energy absorbing layer to convert the laser energy to a mechanical pulse, and the water glass served as a confining layer to prevent rapid expansion of the aluminum layer. The relatively thick fused silica layer (1.5 mm) separated the test film from thermal effects of the laser impact.

Interferometric analysis was used to measure the displacement and calculate the stress state in the substrate and film. Because polymer films of interest were not highly reflective (i.e. not suited for interferometry), stress profiles were measured using reflective calibration samples. A thin aluminum layer (200 nm) served as the calibration test film. Displacement of the test film was monitored using the interferometric fringe pattern of a 532 nm laser incident on the surface using the following relationship [92, 93]:

$$u(t) = \frac{\lambda_0 n(t)}{2} \quad 7.1$$

where u is the displacement, λ_0 is the wavelength of the laser used for interferometry ($\lambda_0 = 532$ nm), and n is the number of fringes. Figs 7.2a and 7.2b demonstrate representative fringe patterns and the resultant displacements of calibration samples at three laser fluences.

The stresses in the substrate, σ_{sub} , and applied stress at the interface between the substrate and a thin film, σ_{int} , were calculated based on the displacement, u , of the free surface [92]:

$$\sigma_{sub} = -\frac{1}{2}(\rho c)_{sub} \frac{\partial u}{\partial t} \quad 7.2a$$

$$\sigma_{int} = -(\rho h)_{film} \frac{\partial^2 u}{\partial t^2} \quad 7.2b$$

where ρ is the density of the substrate or film, c is the wave speed for acoustic propagation in fused silica, and h is the thickness of the film.

Stresses in the substrate and at the substrate-film interface were measured at different levels of laser fluence (energy per area), varied by incrementally adjusting the energy of the Nd:YAG laser while keeping the spot size constant. Typical stress profiles of calibration samples as a function of time at three laser fluences are included in Fig 7.2c-d. The duration of each pulse was on the order of 10 ns. The difference in thickness and stiffness between the aluminum calibration films and the mechanochemically active polymer films was accounted for in the calculation of stress in the polymer films [92]. Aluminum calibration films and polymer films were tested over the same range of laser fluences at a number of sites along the same film and the film was rastered between laser pulses and one measurement was taken at each laser fluence studied. Separation between impact sites along the sample was greater than 3x the radius of the laser beam.

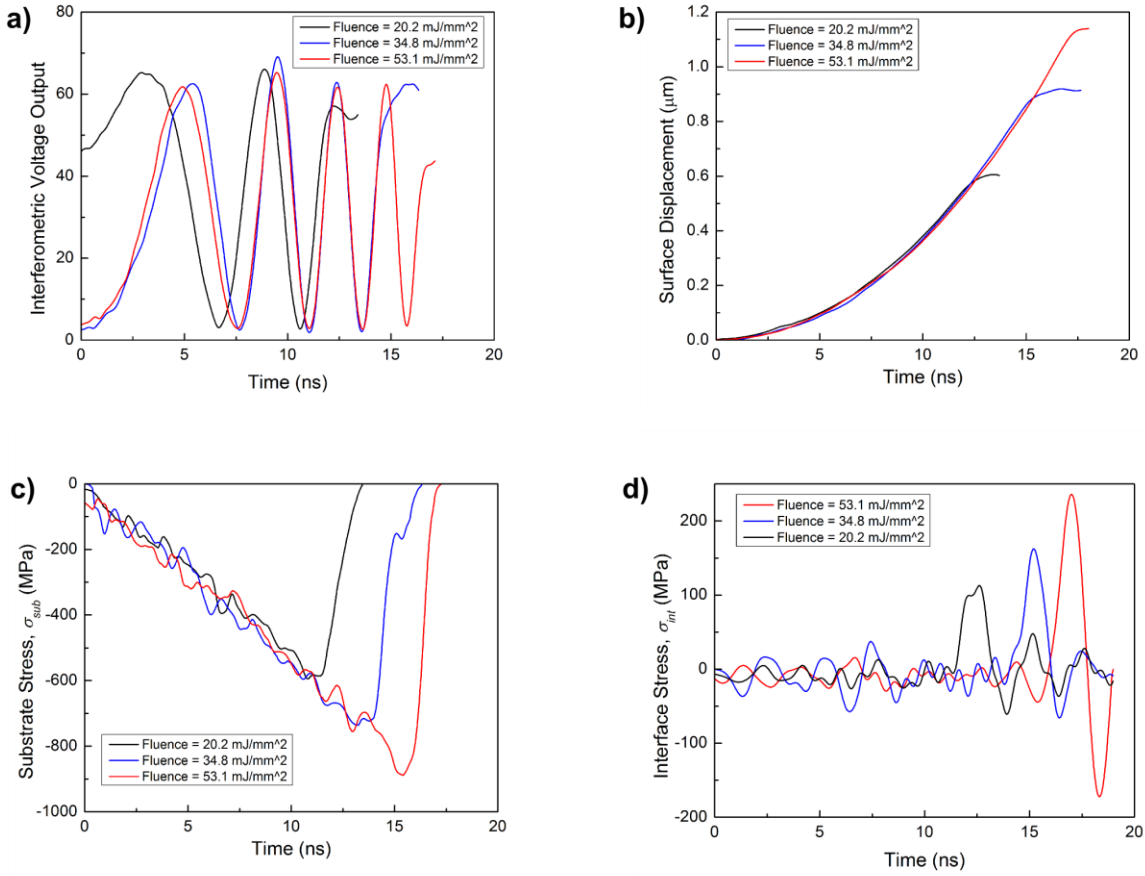


Figure 7.2. Experimental data and stress analysis as a function of time for calibration samples tested at laser fluences of 20.2 mJ/mm^2 , 34.8 mJ/mm^2 , and 53.1 mJ/mm^2 . a) Interferometric fringe pattern for calibration samples. b) Displacement as a function of time at the calibration test film's free surface. c) Stress in the fused silica substrate. d) Tensile stress applied at the interface between the substrate and the aluminum calibration test film.

Tested polymer films were imaged *ex situ* at various stress levels and analyzed optically and under fluorescence microscopy with 532 nm excitation light and collection at $\lambda > 575 \text{ nm}$. The field of view, incident light intensity, and fluorescence exposure were kept constant for all imaging. Average fluorescence intensity of each data point – a measure of SP activation [40, 88] – was quantified by the average red pixel intensity over the entire image field of view. The field of view was of the same size for each impact site and fluorescence measurement.

7.3 Results and Discussion

Bulk SP-linked PS was molded into dog-bone specimens (ca. 0.6 mm thick) and tested in tension. The samples deformed elastically at room temperature and failed at stress of *ca.* 60 MPa. Failure proceeded in a brittle manner, similar to room temperature failure of PMMA described in Chapter 4. Brittle failure does not typically promote conversion of SP to its activated MC form [15, 40, 88]. Previous success activating mechanochemical species in glassy polymers required plasticizing the polymer or changing the test temperature to allow plastic deformation [88]. This study instead utilized thin films of mechanochemically active polymer (as opposed to bulk material) and a novel shockwave loading method as a means for inducing large stresses and deformation in a glassy polymer system.

7.3.1 Shockwave Loading of Thin Films

Calibration samples with reflective aluminum as the test film were used to measure the stress of the shockwave through the substrate, following from Wang *et al.* [93]. The stress pulse induced by the Nd:YAG laser through the substrate (Fig 7.2c) was compressive, lasting approximately 10-20 ns. The intensity and duration of the laser pulse increased with increasing input laser power. Substrate stresses in this work reached values of nearly 1 GPa. The stress applied at the substrate-film interface (Fig 7.2d) was calculated based on the substrate stress and material properties as described in by Eq. 7.2a-b. Stresses on the films were greater than 200 MPa using this technique, applied at strain rates on the order of 10^8 s^{-1} .

Thin films of polystyrene were subjected to mechanical loading in the same manner as the calibration samples. Calculated stresses were adjusted to account for differing material

properties between aluminum and polymer test films. Three sample types were investigated: plain polystyrene without SP linked into the backbone, difunctional SP-linked control, and mechanochemically active SP-linked PS. All sample films were spin-coated under the same conditions, and average film thicknesses were 1.1 μm , 1.0 μm and 1.1 μm , respectively. Mechanical behavior of the three materials was virtually identical.

Representative optical, profilometry and fluorescence images for films loaded at interfacial stresses of 166 MPa, 186 MPa, and 216 MPa are shown in Fig 7.3. In the optical images, dark coloring of the background occurred where the laser was incident on the aluminum film. Light areas and coloration indicated polymer film delamination from the surface and deformation out of the plane of the image. The zone of deformation is roughly circular, in accordance with the laser beam shape.

At loading of approximately 160 MPa, the polymer film began to delaminate and deform off of the silica substrate (Fig 7.3a). Figures 7.3b-c show the increasing delamination zone with increasing interfacial stress (186 MPa and 216 MPa, respectively). The color present in the optical images owes to elevation variation of the film off of the substrate and resultant interference of visible light.

The film elevation was characterized by optical profilometry (Figs 7.3d-f) after loading at varied stresses. Elevation changes in the film (10-100 nm) were measured at an interfacial stress above approximately 160 MPa, indicating delamination of the film off of the substrate. Below this stress level ($\sigma_{\text{int}} < 160$ MPa) the film height was effectively uniform. At higher stresses, fold-like features with elevation on the order of microns were present, as well as film cracking due to bulging strain of the film.

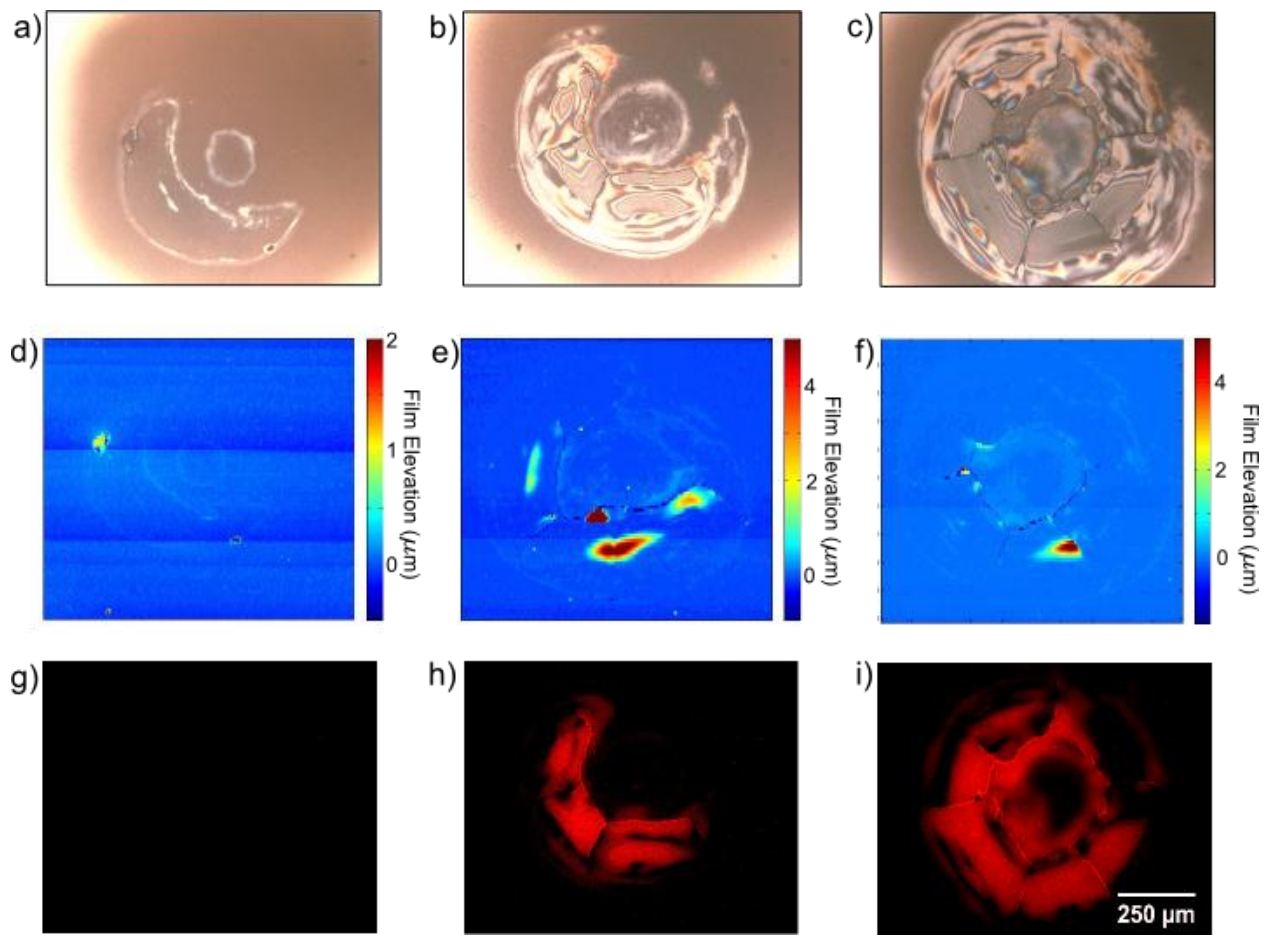


Figure 7.3. Images of active SP-linked PS films under Nd:YAG-induced shockwave loading at interfacial tensile stress levels of 166 MPa, 186 MPa, and 216 MPa, from left to right. a-c) Optical images of polymer films. d-f) Corresponding profilometry. g-i) Fluorescence images indicating SP activation.

Activation of SP was indicated by fluorescence signal from the MC form. Fluorescence signal was not detectable in the polymer films prior to testing, implying that the mechanophore was predominantly in the SP form. SP activation was evident at applied stress greater than 180 MPa (Figs 7.3h-i) in which film deformation and delamination was observed. Film delamination without detectable SP activation occurred at a range of interfacial stresses between $\sigma_{int} \approx 160$ MPa and $\sigma_{int} \approx 175$ MPa. The delamination area, maximum film elevation and amount of activation increased with increasing stress. SP activation was quantified by analyzing the

average red pixel intensity, corresponding to the MC fluorescence emission range [88], of the fluorescence images at varied applied stresses. Fluorescence intensity (averaged over the all pixels within a uniform sized field of view) was compared in active, difunctional control, and plain polystyrene, plotted in Fig 7.4. The relative amount of fluorescence (activation) increased with increasing applied load in active SP-linked PS. At stresses greater than 200 MPa the activation was relatively consistent, reaching a level of saturation.

Fluorescence could be detected at stresses greater than approximately 180 MPa. Assuming a typical Young's modulus for polystyrene of 3 GPa and purely elastic deformation (expected for polymer deformation at very high strain rates), the strain in the polymer would be approximately 6%, in agreement with the minimum required strain to activation reported in Chapter 5 for SP-linked PMMA, coinciding with yield and polymer flow.

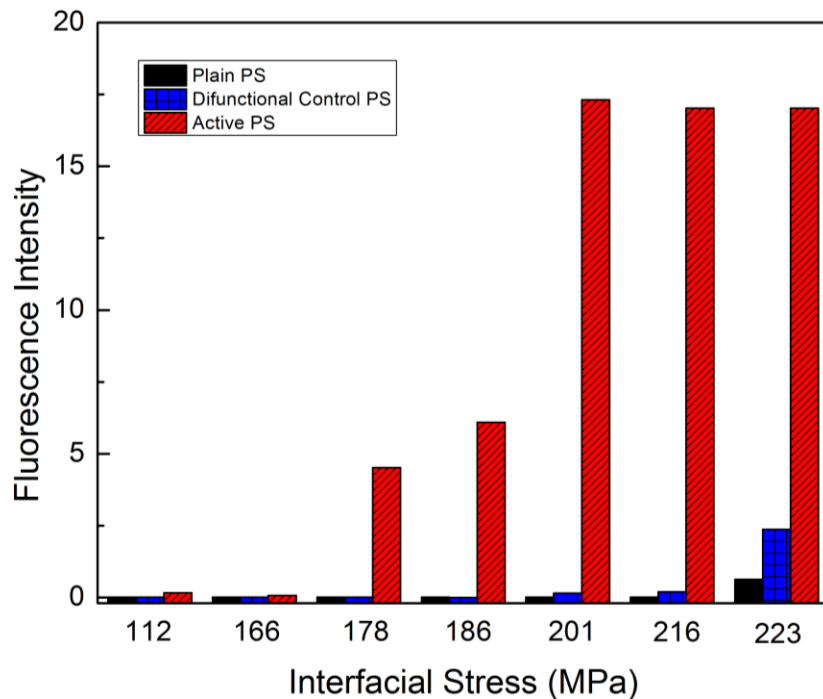


Figure 7.4. Fluorescence intensity (average red pixel intensity), indicating SP activation in plain (without SP), difunctional control and active SP-linked PS films at varying interfacial stress, σ_{int} . Measurements were taken for varied laser fluences at multiple sites. One measurement was taken at each interfacial stress.

Plain PS, without SP incorporated into the polymer backbone, demonstrated no detectable fluorescence. The fluorescence signal of difunctional control SP-linked PS was also negligible when compared with the active polymer. Films of active SP-linked poly(methyl acrylate), an elastomeric polymer, were tested at the same laser fluences, and showed no detectable fluorescence signal *ex situ*, indicating that a glassy polymer is more effective than an elastomer at converting SP to MC under this loading condition.

7.4 Conclusions

Mechanochemical activation has been demonstrated in SP-linked polystyrene thin films. SP activation was detectable via a fluorescence signal in the polymer film. Mechanochemically active polymer films have potential as coatings to structural, load bearing applications, in which the film can indicate a level of deformation or yielding of the structure.

The mechanochemical activation presented in this work elucidates a fundamental difference in mechanical behavior of polymer thin films *vs.* bulk material. Namely the reduced bending moment and lower flaw sensitivity allow for plastic deformation and subsequent activation of the film, while bulk samples exhibited brittle failure and no mechanophore conversion. The thin film plastic deformation allows mechanophore activation in glassy thin films even under high loading rates ($d\varepsilon/dt = 10^8 \text{ s}^{-1}$).

A novel experimental test protocol has been implemented to impart force on a polymer film sample and achieve a chemical response. The shock wave loading experiment subjects the film to high stresses (100s of MPa) over very short duration (~10 ns), leading to a particularly high deformation rate - on the order of 10^8 s^{-1} . Such an approach can be applied to emerging

mechanochemical systems requiring large stresses which cannot be achieved by conventional loading methods.

CHAPTER 8

SUMMARY AND FUTURE WORK

8.1 Summary of Thesis Research

SP was covalently bonded into both glassy and elastomeric linear polymer backbones. Mechanochemical conversion of SP to MC was studied under tensile loading using a novel combined mechanical and optical test system. The thermomechanical dependence of SP activation was investigated using a variety of loading conditions and polymer properties. Experimental results indicate two requirements prior to detectable SP activation: 1) Yielding and plastic deformation, i.e. polymer flow, and 2) a threshold of macroscopic stress.

The onset of SP activation in an elastomeric polymer, SP-linked PMA, was observed at deformation greater than 100% (stretch ratios greater than 2), and the onset and degree of activation were strongly deformation rate dependent. Faster deformation rate led to higher macroscopic stress, which in turn caused greater activation at lower stretch ratios.

SP activation in glassy polymers (PMMA and PS) occurred only for a range of mechanical properties corresponding to a ductile response at significant stress. The mechanical response of SP-linked PMMA was altered through both temperature control and polymer plasticizing. Activation trends were similar for both methods. The strain at which SP activation was detectable in PMMA could be controlled by the plasticizer content, and a minimum strain to activation was approximately 5%, coinciding with the onset of yielding.

Activation of glassy SP-linked PS was demonstrated in thin film coatings on substrates. A thin film testing protocol applied stresses with magnitude on the order of hundreds of MPa by

an acoustic mechanical pulse. Such stress levels are not attainable under quasi-static polymer tensile testing methods, and apply to ballistic and/or shockwave loading conditions.

The optical and mechanical techniques developed for this work provide insight on the nature of polymer deformation and force on a polymer chain. Birefringence and fluorescence polarization measurements presented in Chapters 3 and 6, respectively, quantify the orientation of polymer chains and mechanophores in the direction of applied force. At large deformations in an elastomeric polymer, rapid activation of the mechanophore occurs when alignment reaches a maximum level, implying large force across the polymer backbones at maximum alignment. Collaborative computational work is currently under way to model the force on polymer chains and compare with the experimental results in Chapter 3, thereby further defining the force experienced by polymer chains at the molecular level [96]. Fluorescence polarization studies of glassy polymer failure demonstrated a region of polymer relaxation and recoil within approximately 500 μm of the failure surface. The combined optical and mechanical techniques can be applied to various polymer systems and loading conditions to further explore the mechanics of polymer deformation.

8.2 Future Work

8.2.1 Solid State Activation of New Mechanophores

The fundamental trends for mechanophore activation have been explored in virtually all relevant polymer systems using a single mechanophore (SP). SP activation in amorphous linear polymers has been thoroughly characterized in this dissertation. Cross-linked polymer systems, using SP as a cross-linking unit, were investigated by Kingsbury *et al.* [15, 40]. Semi-crystalline

polymers are currently being explored by coworkers at UIUC. The question remains whether these trends translate to other mechanophores.

An appealing mechanophore system has been developed by Professor Stephen Craig's group at Duke University [17]. The mechanophore can be easily synthesized by functionalizing a double bond in a polymer backbone with bromoform to create a strained 3-member ring referred to as a gem-dibromocyclopropane (g-DBC, Fig 8.1a). Sonication of polybutadiene functionalized with g-DBC results in the rearrangement product [17] in Fig 8.1a. Lenhardt *et al.* reported solid state g-DBC ring-opening and rearrangement under pressure applied in a confined environment via a pellet press. Activation was seen at pressures as low as 36 MPa [16].

Polybutadiene was functionalized with the mechanophore (45 mole% conversion of double bonds by $^1\text{H-NMR}$) in house to reproduce the results of the Craig group and attempt to apply SP activation trends to g-DBC. At an applied pressure of 120 MPa via a pellet press, mechanophore activation was confirmed by the emergence of peaks in the $^1\text{H-NMR}$ at 4.6 ppm and 6.1 ppm, corresponding to the rearrangement product of g-DBC. An NMR spectrum for pressure-activated product is included in Fig 8.1b. In contrast, no activation was detected in solvent-cast g-DBC linked polymer after tensile testing. Room temperature testing led to stresses lower than 1 MPa at failure. In order to increase stress in the polymer, the test temperature was controlled using an environmental chamber, following from the results in Chapter 5. The glass transition temperature of the in-house synthesized polymer was measured (by dynamic mechanical analysis) to be approximately -10 °C. Samples were tested in tension at temperatures of 30 °C to 40 °C below the T_g (-40 °C to -50 °C). These temperatures maximized stress while still promoting yield and draw of the polymer. Stress-strain curves in Fig 8.1c show that the macroscopic stress reached levels greater than 45 MPa during tensile testing at -50 °C.

NMR of this sample after tensile testing, included in Fig 8.1b, demonstrated no detectable activation of the mechanophore.

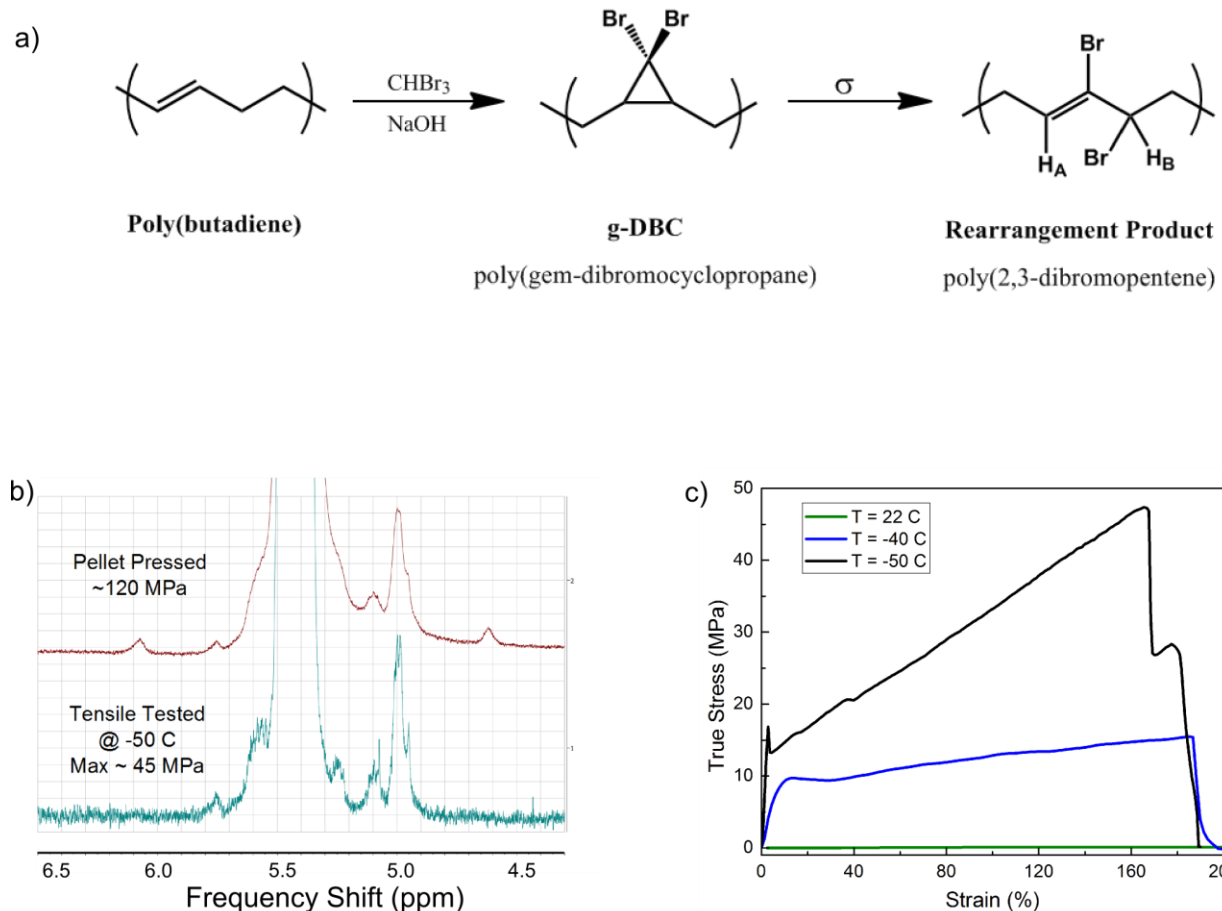


Figure 8.1 Mechanical testing of g-DBC-linked polybutadiene. a) Chemical synthesis and ring-opening rearrangement of the g-DBC mechanophore. b) Region of interest of mechanophore-linked polymer ^1H -NMR spectrum after compression with a pellet press and tensile testing. g-DBC rearrangement product peaks are expected at 6.1 and 4.6 ppm. c) Stress-strain curves for tensile testing at varied temperatures.

The stresses reached during tensile testing of g-DBC-linked polybutadiene at $-50\text{ }^\circ\text{C}$ were higher than the analogous pressures required to detect activation of g-DBC in a pellet press ($\sim 36\text{ MPa}$). Applied stresses were far higher than an apparent threshold of ring opening in SP-linked polymers ($\sim 10\text{ MPa}$). The lack of g-DBC activation at $-50\text{ }^\circ\text{C}$ may be due to low temperature testing, since reaction rate follows an Arrhenius agreement and can be drastically reduced at low temperatures. A future avenue for exploration of this system would involve

incorporation of g-DBC into polymer with higher stiffness backbones containing double bonds and achieving comparable stresses in tension at room temperature. This work is currently under way in collaboration with Duke University.

A similar mechanophore developed by Diesendruck *et al.* undergoes a 3-member ring opening reaction, but promotes a pathway for acid generation. This mechanophore has also shown activation in the solid state by application of large pressures. The polymer was brittle at room temperature, and required plasticizing with MeOH before activation was detectable [18]. Plasticizer-mediated activation of this mechanophore system provides supporting evidence of a requirement of polymer yield and flow for force-induced chemical reactions in mechanophore systems other than SP. Proposed future work for this mechanophore system involves synthesis of tensile specimens with varying mechanical properties, controlled by plasticizer content.

Various mechanophores, described in Chapter 1, have demonstrated mechanochemical activation in solution but have not been explored in solid state. For example, the Sijbesma [23] and Bielawski [25] research groups have demonstrated mechanically-triggered release of coordination catalysts which can initiate polymerization reactions. A hybrid system could be developed based on the self-healing concepts of the Autonomic Materials Systems research group (UIUC), utilizing either a microcapsule or microvascular system embedded in a catalyst-releasing mechanophore-linked polymer [97]. Mechanical stimuli could release liquid monomer from a microcapsule or microvascular network and simultaneously mechanochemically release catalyst to cure the monomer, heal cracking and/or stiffen the polymer.

Another exciting mechanophore developed by Bielawski *et al.* demonstrated a force-driven retro Diels-Alder reaction, cleaving a 6-member ring to release a diene and an olefin dienophile [20]. Wudl and colleagues reported a similar self-healing chemistry in which 6-

member rings - products of a forward Diels-Alder reaction - were incorporated into a polymer as cross-linking units. The Diels-Alder products could be cleaved at 120 °C, and cross-links were re-formed at new sites by simply cooling to room temperature [98]. The Bielawski system forms similar “living” functional groups (Diels-Alder reactants), available as new cross-linking units, simply under mechanical force. A self-healing system utilizing this chemistry would not require incorporation of additional phases (microcapsules or microchannels) and could autonomically rebond cross-links without intervention of temperature or other stimuli. With a variety of current and emerging mechanophore chemistries demonstrating activation in the solution state, implementation to solid state remains an active area of research.

8.2.2 A Bio-Inspired Mechanochemical System: Synthetic Mechanotransductive Channels

The foundations for a novel mechanically-stimulated, chemically active system have been developed with inspiration from mechanotransductive channels in biological systems. Mechanotransductive channels provide a mechanism for release of ions across cell membranes, and control processes such as maintaining cell pressure and transduction of sound waves for hearing [2-4, 99]. Fig 8.2 shows two mechanisms which are proposed for mechanically-induced opening of mechanotransductive channels in cell membranes. The first mechanism (Fig 8.2a) is a simple stretch-induced opening, which can be triggered by high internal cell pressure. The second mechanism (Fig 8.2b) is a tethered approach in which deflection of the cell relative to other attached (tethered) cells triggers opening of a channel and release of ions. An interesting application of this latter mechanism is mammalian hearing, in which hair cells in the ear are

tethered to each other and deflection in response to sound waves, triggering release of calcium ions which are interpreted by the brain as sound [100].

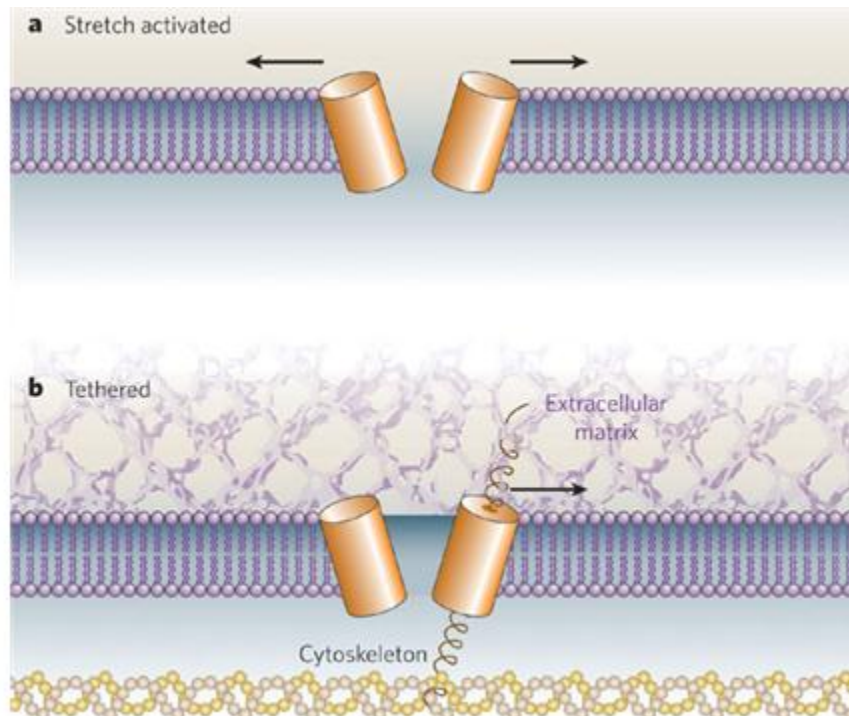


Figure 8.2. Mechanisms for mechanotransductive channel opening. a) Stretch active cell membrane. b) Spring-like tether model. Image reproduced from Lumpkin *et al.* [2].

A proposed synthetic approach to mechanotransductive channels is depicted schematically in Fig 8.3. Channels of an active liquid phase are separated from a solid polymer matrix by a synthetic membrane. The strain to failure of the membrane is selected to be lower than the strain to failure of the matrix, such that the membrane ruptures and releases active liquid into the matrix prior to ultimate failure of the system. The active liquid, when diffused into the matrix, could trigger functionality similar to mechanophores under development, e.g. color change for mechanical sensors or cross-linking for reinforcement of the polymer. To achieve a color change, a solvent and dye can serve as the active liquid. Cross-linking for reinforcement of the polymer could be achieved using pendant epoxide groups on a linear polymer backbone, such

as poly(glycidyl methacrylate), for the matrix phase and an acid or an amine as the active liquid phase to initiate cross-linking.

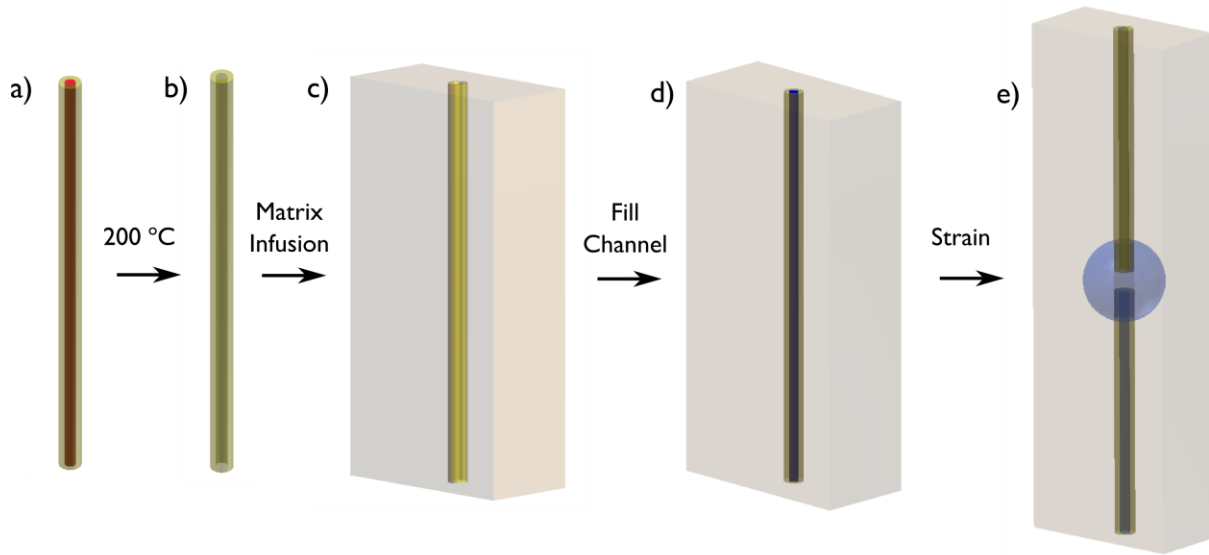


Figure 8.3. Synthesis and activation of mechanotransductive channels. a) Poly(lactide) fiber (red) coated in PDMS (yellow). b) Hollow PDMS membrane after evacuation of fiber. c) Membrane incorporated into a polymer matrix. d) *In situ* sample; channels filled with active liquid (blue). e) Strain-induced membrane opening and diffusion of active liquid into the matrix.

A model system was developed as a proof of concept for synthetic mechanotransductive channels. The synthetic membrane was formed by evacuating a poly(lactide) fiber with a poly(dimethyl siloxane) (PDMS) coating at 200 °C under vacuum (Fig 8.3a-b). The hollow PDMS membrane was then embedded in a polymer matrix (8.3c) by curing liquid components around the membrane. Both epoxy and polyurethane matrices were studied. The failure strain of PDMS (Sylgard 184) was approximately 50%. Flexibilized epoxy (Epon 815C resin and Epikure 3164 hardener) and polyurethane (hexamethylene diisocyanate and poly(tetramethylene glycol)) chemistries were selected such that their strains to failure were greater than 100%, i.e. more deformable than PDMS. The hollow channel was then filled with a solvent and dye

combination (dimethyl sulfoxide and bromophenol blue) which diffuses into both epoxy and polyurethane matrices (8.3d).

Tensile testing resulted in PDMS membrane rupture at strains as low as 50% in both polymer matrices. Subsequent diffusion of the dye and solvent into the matrix was visually detectable. A representative sample with an epoxy matrix is shown before and after tensile testing in Fig 8.4. The sample was held at a constant strain of 180% for 4 hours after testing, and diffusion of the active liquid continued over time (Fig 8.4d).

The synthetic mechanotransductive channels studied so far have potential in quasi-static loading conditions as strain or damage indicators. New active liquid and matrix chemistries could lead to materials which adapt their mechanical properties in response to deformation. An ideal system would provide flexibility at small deformations, but cross-link and stiffen prior to failure and maintain mechanical integrity of the system at large applied loads. Although this mechanism for mechanically-triggered chemical response differs from the mechanophore approach discussed throughout this thesis dissertation, synthetic mechanotransductive channels offer a novel bio-inspired approach toward similar advantageous material response.

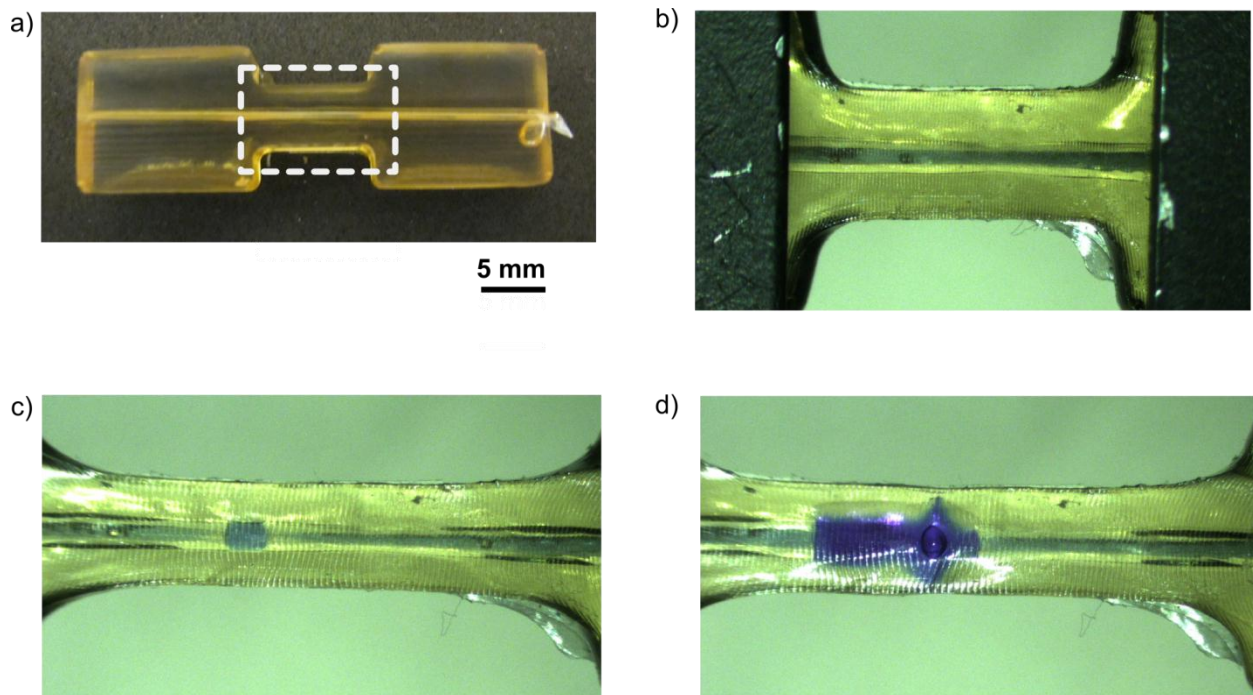


Figure 8.4. Tensile testing of mechanotransductive channels, filled with bromophenol blue and dimethyl sulfoxide solution, embedded in a flexibilized epoxy matrix. a) Image of a polymer sample with the region of interest for test images outlined. b) Region of interest for the sample prior to testing, with blue color indicating the active liquid. c) Sample at a strain of 180% with ruptured membranes immediately after tensile testing. d) Four hours after testing at constant strain of 180%, demonstrating diffusion of the active liquid into the polymer matrix.

REFERENCES

1. Norman, J.J., et al., *Microsystems for biomechanical measurements*. Pediatric Research, 2008. **63**(5): p. 576-583.
2. Lumpkin, E.A. and M.J. Caterina, *Mechanisms of sensory transduction in the skin*. Nature, 2007. **445**(7130): p. 858-865.
3. Kung, C., *A possible unifying principle for mechanosensation*. Nature, 2005. **436**(7051): p. 647-654.
4. Phillips, K.R., A. Biswas, and J.L. Cyr, *How hair cells hear: the molecular basis of hair-cell mechanotransduction*. Current Opinion in Otolaryngology & Head and Neck Surgery, 2008. **16**(5): p. 445-451.
5. Kauzmann, W. and H. Eyring, *The Viscous Flow of Large Molecules*. Journal of the American Chemical Society, 1940. **62**(11): p. 3113-3125.
6. Staudinger, H., *Über Isopren und Kautschuk, 20. Mitteil.: Über die Kolloidnatur von Kautschuk, Guttapercha und Balata*. Berichte der deutschen chemischen Gesellschaft (A and B Series), 1930. **63**(4): p. 921-934.
7. Zhurkov, S.N., et al., *Polymer Bonds Under Mechanical Stress Investigated By Infrared Spectroscopy*. Doklady Akademii Nauk Sssr, 1967. **176**(3): p. 623-&.
8. Zhurkov, S.N., E.E. Tomashevskii, and A.Y. Savostin, *Mechanism Behind Breakdown of Polymers Investigated by Means of Electron Spin Resonance*. Doklady Akademii Nauk Sssr, 1964. **159**(2): p. 303-&.
9. Zhurkov, S.N. and V.E. Korsukov, *Atomic Mechanism of Fracture of Solid Polymers*. Journal of Polymer Science Part B-Polymer Physics, 1974. **12**(2): p. 385-398.
10. Kaupp, G., *Mechanochemistry: the varied applications of mechanical bond-breaking*. Crystengcomm, 2009. **11**(3): p. 388-403.
11. Zhang, Q. and F. Saito, *A review on mechanochemical syntheses of functional materials*. Advanced Powder Technology, 2012. **23**(5): p. 523-531.
12. Molchanov, V.V. and R.A. Buyanov, *Mechanochemistry of catalysts*. Russian Chemical Reviews, 2000. **69**(5): p. 435-450.
13. Hickenboth, C.R., et al., *Biasing reaction pathways with mechanical force*. Nature, 2007. **446**(7134): p. 423-427.
14. Potisek, S.L., et al., *Mechanophore-linked addition polymers*. Journal of the American Chemical Society, 2007. **129**(45): p. 13808-+.
15. Davis, D.A., et al., *Force-induced activation of covalent bonds in mechanoresponsive polymeric materials*. Nature, 2009. **459**(7243): p. 68-72.
16. Lenhardt, J.M., et al., *Characterizing the mechanochemically active domains in gem-dihalocyclopropanated polybutadiene under compression and tension*. Journal of Materials Chemistry, 2011. **21**: p. 8454-8459.
17. Lenhardt, J.M., A.L. Black, and S.L. Craig, *gem-Dichlorocyclopropanes as Abundant and Efficient Mechanophores in Polybutadiene Copolymers under Mechanical Stress*. Journal of the American Chemical Society, 2009. **131**(31): p. 10818-+.
18. Diesendruck, C.E., et al., *Proton-Coupled Mechanochemical Transduction: A Mechanogenerated Acid*. Journal of the American Chemical Society, 2012. **134**(30): p. 12446-12449.
19. Kryger, M.J., et al., *Masked Cyanoacrylates Unveiled by Mechanical Force*. Journal of the American Chemical Society, 2010. **132**(13): p. 4558-+.

20. Wiggins, K.M., et al., *Mechanically Facilitated Retro 4+2 Cycloadditions*. Journal of the American Chemical Society, 2011. **133**(18): p. 7180-7189.
21. Brantley, J.N., K.M. Wiggins, and C.W. Bielawski, *Unclicking the Click: Mechanically Facilitated 1,3-Dipolar Cycloreversions*. Science, 2011. **333**(6049): p. 1606-1609.
22. Paulusse, J.M.J. and R.P. Sijbesma, *Selectivity of mechanochemical chain scission in mixed palladium(II) and platinum(II) coordination polymers*. Chemical Communications, 2008(37): p. 4416-4418.
23. Piermattei, A., S. Karthikeyan, and R.P. Sijbesma, *Activating catalysts with mechanical force*. Nature Chemistry, 2009. **1**(2): p. 133-137.
24. Wiggins, K.M., et al., *Mechanical Reconfiguration of Stereoisomers*. Journal of the American Chemical Society, 2010. **132**(10): p. 3256-+.
25. Tennyson, A.G., K.M. Wiggins, and C.W. Bielawski, *Mechanical Activation of Catalysts for C-C Bond Forming and Anionic Polymerization Reactions from a Single Macromolecular Reagent*. Journal of the American Chemical Society, 2010. **132**(46): p. 16631-16636.
26. Haward, R.N. and G. Thackray, *The Use of a Mathematical Model to Describe Isothermal Stress-Strain Curves in Glassy Thermoplastics*. Proceedings of the Royal Society of London. Series A. Mathematical and Physical Sciences, 1968. **302**(1471): p. 453-472.
27. Kontou, E. and G. Spathis, *Structural rearrangements during yielding of glassy polymers*. Polymer Engineering and Science, 1998. **38**(9): p. 1443-1449.
28. Beyer, M.K. and H. Clausen-Schaumann, *Mechanochemistry: The mechanical activation of covalent bonds*. Chemical Reviews, 2005. **105**(8): p. 2921-2948.
29. Nallicheri, R.A. and M.F. Rubner, *Investigations of the mechanochromic behavior of poly(urethane diacetylene) segmented copolymers*. Macromolecules, 1991. **24**(2): p. 517-525.
30. Weder, C., *Mechanoresponsive Materials*. Journal of Materials Chemistry, 2011. **21**(23): p. 8235-8236.
31. Crenshaw, B.R., et al., *Deformation-induced color changes in mechanochromic polyethylene blends*. Macromolecules, 2007. **40**(7): p. 2400-2408.
32. Azzaroni, O., et al., *Mechanically induced generation of counterions inside surface-grafted charged macromolecular films: Towards enhanced mechanotransduction in artificial systems*. Angewandte Chemie-International Edition, 2006. **45**(44): p. 7440-7443.
33. Hirshberg, Y., *Reversible Formation and Eradication of Colors by Irradiation at Low Temperatures. A Photochemical Memory Model*. Journal of the American Chemical Society, 1956. **78**(10): p. 2304-2312.
34. Hirshberg, Y., E.B. Knott, and E. Fischer, *Environmental Influences and the Colour of Some Merocyanines*. Journal of the Chemical Society, 1955: p. 3313-3321.
35. Zhang, S., et al., *Photochromism of Spiropyran in Ionic Liquids: Enhanced Fluorescence and Delayed Thermal Reversion*. The Journal of Physical Chemistry B, 2009. **113**(17): p. 6012-6019.
36. Reichardt, C., *Solvatochromic Dyes as Solvent Polarity Indicators*. Chemical Reviews, 1994. **94**(8): p. 2319-2358.

37. Tyer, N.W. and R.S. Becker, *Photochromic spiropyrans. I. Absorption spectra and evaluation of the π -electron orthogonality of the constituent halves*. Journal of the American Chemical Society, 1970. **92**(5): p. 1289-1294.
38. Lee, C.K., et al., *Force-Induced Redistribution of a Chemical Equilibrium*. Journal of the American Chemical Society, 2010. **132**(45): p. 16107-16111.
39. O'Bryan, G., B.M. Wong, and J.R. McElhanon, *Stress Sensing in Polycaprolactone Films via an Embedded Photochromic Compound*. ACS Applied Materials & Interfaces, 2010. **2**(6): p. 1594-1600.
40. Kingsbury, C.M., et al., *Shear activation of mechanophore-crosslinked polymers*. Journal of Materials Chemistry, 2011. **21**: p. 8381-8388.
41. Tobolsky, A.V., *Stress Relaxation Studies of the Viscoelastic Properties of Polymers*. Journal of Applied Physics, 1956. **27**(7): p. 673-685.
42. Williams, M., R. Landel, and J. Ferry, *The Temperature Dependence of Relaxation Mechanisms in Amorphous Polymers and Other Glass-forming Liquids*. Journal of the American Chemical Society, 1955. **77**(14): p. 3701-3707.
43. Ward, I.M., *Mechanical Properties of Solid State Polymers*. 2nd ed, ed. J.W. Sons. 1971, Great Britain: John Wiley and Sons Ltd.
44. Brazel, C.S., et al., *Plasticizing effects of imidazolium salts in PMMA: High and low temperature stable flexible engineering materials*. Abstracts of Papers of the American Chemical Society, 2002. **224**: p. 074-IEC.
45. Konczol, L., et al., *Interference Microscopic Studies on Welded PMMA Samples*. Kunststoffe-German Plastics, 1982. **72**(1): p. 46-51.
46. Retting, W., *Generation and Relaxation of the Molecular-Orientation during Hot-Stretching of Amorphous Thermoplastics*. Colloid and Polymer Science, 1979. **257**(7): p. 689-710.
47. Vangurp, M., *The Use of Rotation Matrices in the Mathematical Description of Molecular Orientations in Polymers*. Colloid and Polymer Science, 1995. **273**(7): p. 607-625.
48. Arruda, E.M. and P.A. Przybylo, *AN INVESTIGATION INTO THE 3-DIMENSIONAL STRESS-BIREFRINGENCE-STRAIN RELATIONSHIP IN ELASTOMERS*. Polymer Engineering and Science, 1995. **35**(5): p. 395-402.
49. Patterson, E.A. and Z.F. Wang, *Simultaneous observation of phase-stepped images for automated photoelasticity*. Journal of Strain Analysis for Engineering Design, 1998. **33**(1): p. 1-15.
50. Hermans, P.H. and J. Booys, *Beiträge zur Kenntnis des Deformationsmechanismus und der Feinstruktur der Hydratzellulose*. Kolloid-Zeitschrift, 1939. **88**(1): p. 73-78.
51. White, D.L. and G.N. Taylor, *New Absorptive Mode Reflective Liquid-Crystal Display Device*. Journal of Applied Physics, 1974. **45**(11): p. 4718-4723.
52. Grabchev, I. and J.M. Chovelon, *Photophysical and photochemical properties of green fluorescent liquid crystalline systems*. Zeitschrift Fur Naturforschung Section a-a Journal of Physical Sciences, 2003. **58**(1): p. 45-50.
53. Unuma, Y. and A. Miyata, *Light-Induced Molecular Orientation in Langmuir-Blodgett Films of Spiropyran*. Thin Solid Films, 1989. **179**: p. 497-502.
54. Bletz, M., et al., *Ground- and first-excited-singlet-state electric dipole moments of some photochromic spirobenzopyrans in their spiropyran and merocyanine form*. Journal of Physical Chemistry A, 2002. **106**(10): p. 2232-2236.

55. Bauman, D., H. Moryson, and E. Wolarz, *Study of Nematic Order in Guest-Host Mixtures by Polarized Optical Spectroscopy*. Journal of Molecular Structure, 1994. **325**: p. 169-175.
56. Lukyanov, B.S. and M.B. Lukyanova, *Spiropyrans: Synthesis, Properties, and Application. (Review)*. Chemistry of Heterocyclic Compounds, 2005. **41**(3): p. 281-311.
57. Tipikin, D.S., *Mechanochromism of organic compounds by the example of spiropyran*. Zhurnal Fizicheskoy Khimii, 2001. **75**(10): p. 1876-1880.
58. Lligadas, G. and V. Percec, *Synthesis of perfectly bifunctional polyacrylates by single-electron-transfer living radical polymerization*. Journal of Polymer Science Part a-Polymer Chemistry, 2007. **45**(20): p. 4684-4695.
59. Matyjaszewski, K., et al., *Controlled/"living" atom transfer radical polymerization of methyl methacrylate using various initiation systems*. Macromolecules, 1998. **31**(5): p. 1527-1534.
60. Percec, V., et al., *Ultrafast synthesis of ultrahigh molar mass polymers by metal-catalyzed living radical polymerization of acrylates, methacrylates, and vinyl chloride mediated by SET at 25 degrees C*. Journal of the American Chemical Society, 2006. **128**(43): p. 14156-14165.
61. Matyjaszewski, K., T.E. Patten, and J. Xia, *Controlled/"Living" Radical Polymerization. Kinetics of the Homogeneous Atom Transfer Radical Polymerization of Styrene*. Journal of the American Chemical Society, 1997. **119**(4): p. 674-680.
62. Wang, T.L., et al., *The effect of initiators and reaction conditions on the polymer syntheses by atom transfer radical polymerization*. Journal of Polymer Research, 2005. **12**(2): p. 67-75.
63. Stafforst, T. and D. Hilvert, *Kinetic characterization of spiropyrans in aqueous media*. Chemical Communications, 2009(3): p. 287-288.
64. May, P., *Architechture dependent force-driven chemical reactions in solution and in bulk*. Journal of the American Chemical Society, 2013. In Preparation.
65. Ihre, H., O.L. Padilla De Jesús, and J.M.J. Fréchet, *Fast and Convenient Divergent Synthesis of Aliphatic Ester Dendrimers by Anhydride Coupling*. Journal of the American Chemical Society, 2001. **123**(25): p. 5908-5917.
66. Barone, S., G. Burriesci, and G. Petrucci, *Computer aided photoelasticity by an optimum phase stepping method*. Experimental Mechanics, 2002. **42**(2): p. 132-139.
67. Kramer, S., et al., *Simultaneous Observation of Phase-Stepped Images for Photoelasticity Using Diffraction Gratings*. Experimental Mechanics, 2013: p. 327-332.
68. Saiz, E., E. Riande, and J.E. Mark, *Birefringence in poly(methyl acrylate) networks in elongation*. Macromolecules, 1984. **17**(4): p. 899-902.
69. Rouse, J.P.E., *A Theory of the Linear Viscoelastic Properties of Dilute Solutions of Coiling Polymers*. The Journal of Chemical Physics, 1953. **21**(7): p. 1272-1280.
70. Zimm, B.H., *Dynamics of Polymer Molecules in Dilute Solution - Viscoelasticity, Flow Birefringence and Dielectric Loss*. Journal of Chemical Physics, 1956. **24**(2): p. 269-278.
71. Soranno, A., et al., *Quantifying internal friction in unfolded and intrinsically disordered proteins with single-molecule spectroscopy*. Proceedings of the National Academy of Sciences, 2012. **109**(44): p. 17800-17806.
72. Hagen, S.J., *Solvent Viscosity and Friction in Protein Folding Dynamics*. Current Protein & Peptide Science, 2010. **11**(5): p. 385-395.

73. Ong, M.T., et al., *First Principles Dynamics and Minimum Energy Pathways for Mechanochemical Ring Opening of Cyclobutene*. Journal of the American Chemical Society, 2009. **131**(18): p. 6377-+.
74. Haring, M.M., *The Theory of Rate Processes* (Glasstone, Samuel; Laidler, Keith J.; Eyring, Henry). Journal of Chemical Education, 1942. **19**(5): p. 249.
75. Evans, M.G. and M. Polanyi, *Some applications of the transition state method to the calculation of reaction velocities, especially in solution*. Transactions of the Faraday Society, 1935. **31**(0): p. 875-894.
76. Eyring, H.P., M., *Über Einfache Gasreaktionen*. Zeitschrift fur Physikalische Chemie B, 1931(12): p. 298-311.
77. Li, J., *The mechanics and physics of defect nucleation*. Mrs Bulletin, 2007. **32**(2): p. 151-159.
78. Bell, G., *Models for the specific adhesion of cells to cells*. Science, 1978. **200**(4342): p. 618-627.
79. Hoffman, J.D., G. Williams, and E. Passaglia, *Analysis of the α , β , and γ relaxations in polychlorotrifluoroethylene and polyethylene: Dielectric and mechanical properties*. Journal of Polymer Science Part C: Polymer Symposia, 1966. **14**(1): p. 173-235.
80. Merkel, R., et al., *Energy landscapes of receptor-ligand bonds explored with dynamic force spectroscopy*. Nature, 1999. **397**(6714): p. 50-3.
81. Pope, L.H., et al., *Force-induced melting of a short DNA double helix*. European Biophysics Journal with Biophysics Letters, 2001. **30**(1): p. 53-62.
82. Cremar, L., *Insights for Designing Mechanochromic Spiropyrans from First Principles Dynamics and Minimum Energy Pathways*, in Department of Chemistry2012, Stanford University: Palo Alto, CA.
83. Davis, D.A., et al., Nature, 2009. **459**: p. 68.
84. Bauwens,C, J.C. Bauwens, and G. Homes, *Tensile Yield-Stress Behavior of Glassy Polymers*. Journal of Polymer Science Part A-2-Polymer Physics, 1969. **7**(4): p. 735-742.
85. Hsieh, H.C., T.J. Yang, and S. Lee, *Crack healing in poly(methyl methacrylate) induced by co-solvent of methanol and ethanol*. Polymer, 2001. **42**(3): p. 1227-1241.
86. Baur, G., A. Stieb, and G. Meier, *Polarized Fluorescence of Dyes Oriented in Room-Temperature Nematic Liquid-Crystals*. Molecular Crystals and Liquid Crystals, 1973. **22**(3-4): p. 261-269.
87. Damerau, T. and M. Hennecke, *Determination of Orientational Order Parameters of Uniaxial Films with a Commercial 90-Degrees-Angle Fluorescence Spectrometer*. Journal of Chemical Physics, 1995. **103**(14): p. 6232-6240.
88. Beiermann, B.A., et al., *Environmental effects on mechanochemical activation of spiropyran in linear PMMA*. Journal of Materials Chemistry, 2011. **21**: p. 8443-8447.
89. Brady, T.E. and G.S.Y. Yeh, *Yielding Behavior of Glassy Amorphous Polymers*. Journal of Applied Physics, 1971. **42**(12): p. 4622-4630.
90. Stephens, A.W. and J.L. Vossen, *Measurement of Interfacial Bond Strength by Laser Spallation*. Journal of Vacuum Science & Technology, 1976. **13**(1): p. 38-39.
91. Pronin, A.N. and V. Gupta, *Measurement of thin film interface toughness by using laser-generated stress pulses*. Journal of the Mechanics and Physics of Solids, 1998. **46**(3): p. 389-410.
92. Wang, J.L., R.L. Weaver, and N.R. Sottos, *A parametric study of laser induced thin film spallation*. Experimental Mechanics, 2002. **42**(1): p. 74-83.

93. Wang, J.L., N.R. Sottos, and R.L. Weaver, *Tensile and mixed-mode strength of a thin film-substrate interface under laser induced pulse loading*. Journal of the Mechanics and Physics of Solids, 2004. **52**(5): p. 999-1022.
94. Kandula, S.S.V., et al., *Dynamic delamination of patterned thin films*. Applied Physics Letters, 2008. **93**(26).
95. Tran, P., et al., *Dynamic delamination of patterned thin films: a numerical study*. International Journal of Fracture, 2010. **162**(1-2): p. 77-90.
96. Silberstein, M., *Modeling Mechanophore Activation within a Viscous Rubbery Network*. Journal of the Mechanics and Physics of Solids, 2013. **Submitted**.
97. Caruso, M.M., et al., *Mechanically-Induced Chemical Changes in Polymeric Materials*. Chemical Reviews, 2009. **109**(11): p. 5755-5798.
98. Chen, X., et al., *A Thermally Re-mendable Cross-Linked Polymeric Material*. Science, 2002. **295**(5560): p. 1698-1702.
99. Gillespie, P.G. and R.G. Walker, *Molecular basis of mechanosensory transduction*. Nature, 2001. **413**(6852): p. 194-202.
100. Breneman, K.D., W.E. Brownell, and R.D. Rabbitt, *Hair Cell Bundles: Flexoelectric Motors of the Inner Ear*. Plos One, 2009. **4**(4).

APPENDIX A

BULK SAMPLE DIMENSIONS

Polymer samples were molded in closed molds with dimensions shown in Fig A1. Two parallel plates heated to the temperature above the polymer T_g applied a pressure to the closed mold. Poly(methyl acrylate) ($T_g = 12^\circ\text{C}$) was molded at 71°C (160°F) for ten minutes at applied pressure of approximately 0.4 MPa (60 psi). Samples were then allowed to cool at room temperature for one hour before removing from the mold. Poly(methyl methacrylate) ($T_g = 127^\circ\text{C}$) was molded at temperature of 140°C (285°F) for 20 minutes at a pressure of 1.4 MPa (200 psi).

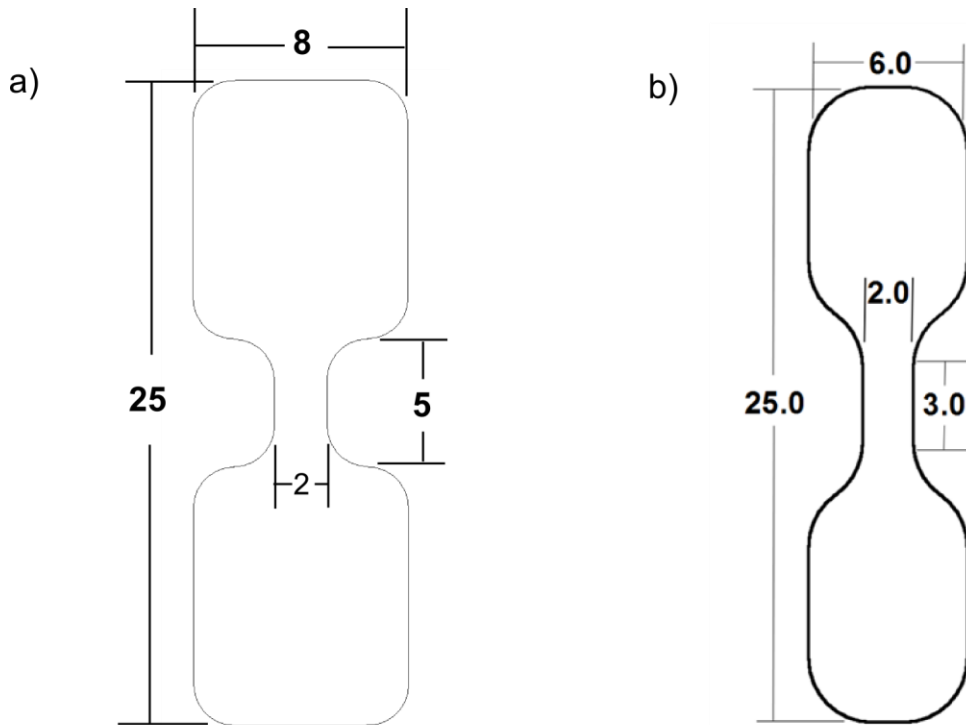


Figure A1. Sample dimensions for a) SP-linked PMA and b) SP-linked PMMA. All dimensions are in mm.

APPENDIX B

EMPIRICALLY DERIVED SP-LINKED PMA FLUORESCENCE KINETICS

Kinetics Modeling Code

The reaction kinetics for SP-MC equilibrium was monitored based on the fluorescence signal as described in Chapter 4 and described by the following equation:

$$\frac{d(I_{fl} / I_{fl,max})}{dt} = k_f(1 - \frac{I_{fl}}{I_{fl,max}}) - k_r \frac{I_{fl}}{I_{fl,max}} \quad B1.$$

The data collected for kinetics measurement was I_{fl} , and time, t . Additionally the stress, σ , was measured at each fluorescence measurement based on the applied load and thickness of the sample. The kinetics of the fluorescence was predicted using the following relationships, with forms corresponding to the argument in the previous section:

$$\begin{aligned} k_f &= k_{f,\sigma=0} && \text{for } \sigma \leq \sigma_{f,lim} \\ k_f &= k_{f,\sigma=0} + C_f(\sigma - \sigma_{f,lim}) && \text{for } \sigma > \sigma_{f,lim} \end{aligned} \quad B2$$

and

$$\begin{aligned} k_r &= k_{r,\sigma=0} && \text{for } \sigma \leq \sigma_{r,lim} \\ k_r &= k_{r,\sigma=0} - C_r(\sigma - \sigma_{r,lim}) && \text{for } \sigma > \sigma_{r,lim} \end{aligned} \quad B3.$$

The only measured input in the prediction of fluorescence change was the stress on the polymer sample. Boundary conditions, $k_{f,\sigma=0}$ and $k_{r,\sigma=0}$, were determined as described in Chapter 4. The Matlab code determined best fit values for C_f , C_r , $\sigma_{f,lim}$ and $\sigma_{r,lim}$. The fluorescence for each predicted combination of values was compared with the experimental data. Variable values giving the lowest standard error between experimental and calculated fluorescence were selected as the best fit and defined the empirically derived shape of rate constants k_f and k_r . Activation energies were calculated from the best fit rate constants, following Eq. 4.1.

The Matlab code contained two fundamental components: a loop to cycle through attempts at values for variables C_f , C_r , $\sigma_{f,lim}$ and $\sigma_{r,lim}$ (Fig B1), and loops to calculate the fluorescence intensity at each data point for every sample (using the values C_f , C_r , $\sigma_{f,lim}$ and $\sigma_{r,lim}$) and compare the prediction with experimental data (Fig B1). The latter loops for each sample were nested within the loop cycling through variable values. A standard error was averaged over each data point for each combination of attempted variable values. The values for C_f , C_r , $\sigma_{f,lim}$ and $\sigma_{r,lim}$ corresponding to minimum error were inserted into Eqs. B2 and B3, predicting the response of the SP-MC kinetics to applied stress (Fig 4.4).

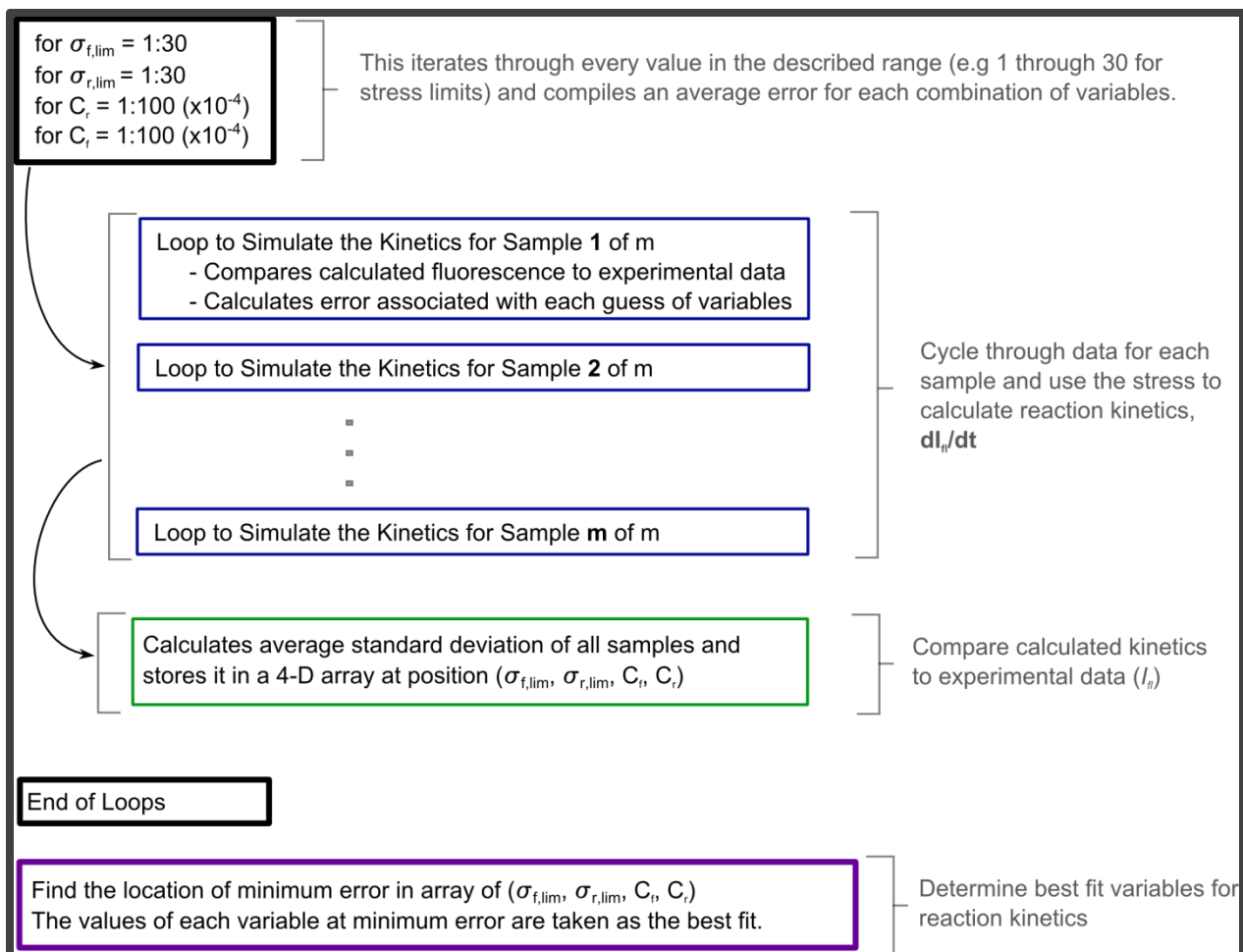


Figure B1. Schematic of logic for cycling through values C_f , C_r , $\sigma_{f,lim}$ and $\sigma_{r,lim}$ to predict the kinetics of I_f (see Fig. B2 for details) for each sample and determining best fit variable values.

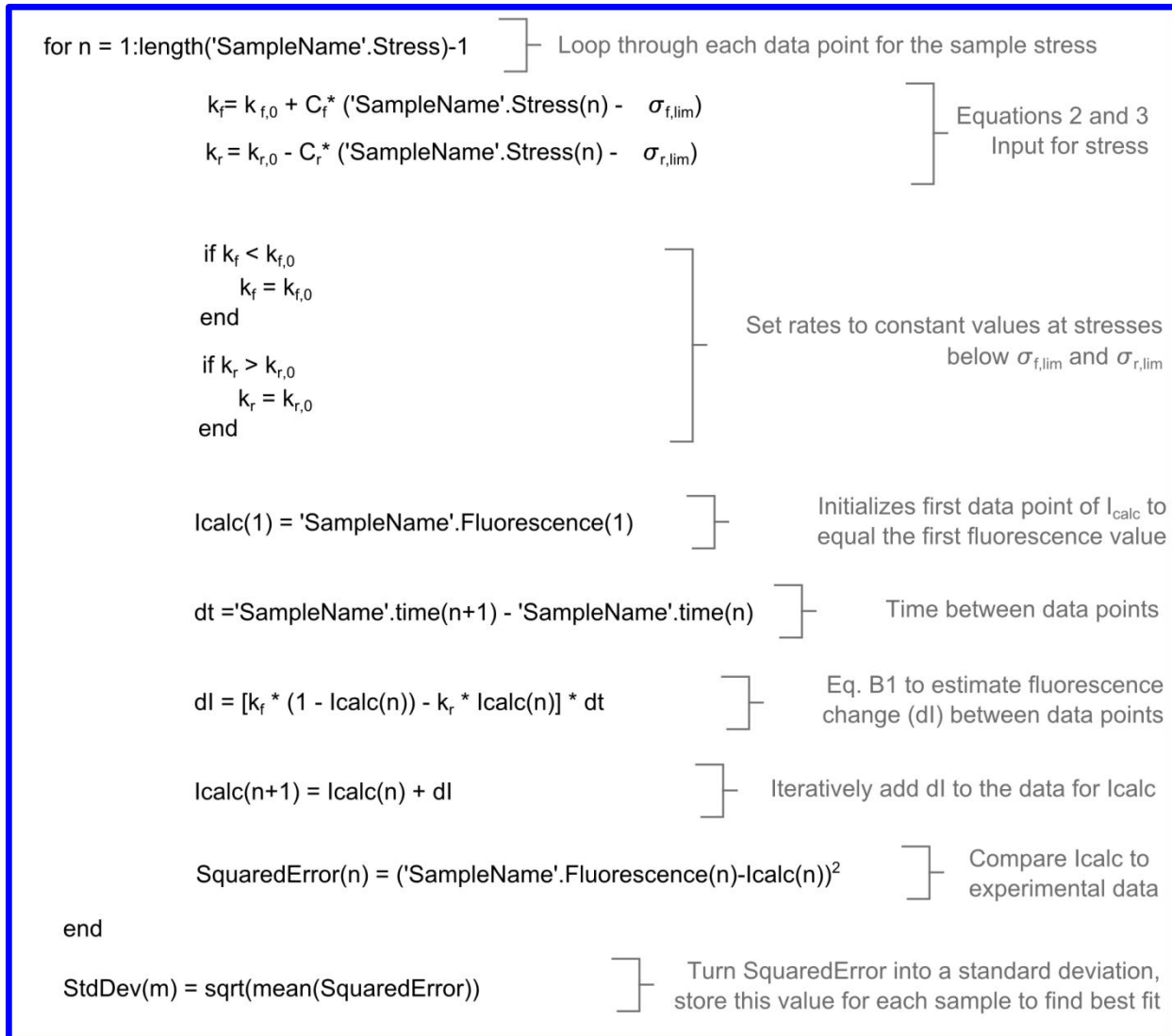


Figure B2. Schematic logic to compute a predicted I_{fl} over time (kinetics) based on the stress in the sample for each attempted value of C_f , C_r , $\sigma_{f,lim}$ and $\sigma_{r,lim}$. The fluorescence intensity was compared to the experimental values to calculate a standard deviation for each data point.

Effect of Varying I_{max}

Eq. B1 includes a normalization constant, $I_{fl,max}$, which corresponds to the theoretical intensity of the sample if all mechanophores were in the fluorescent MC form. This constant was not been determined experimentally and was assumed to be twice the average value of the UV-irradiated sample fluorescence intensity, I_{UV} . A parametric study was carried out using a

variety of values of $I_{fl,max}$. Varying the normalization constant did not have a significant effect on the average error of the empirically fit kinetics data, but it did have an effect on calculated rate constants and activation energies. Fig B3 demonstrates the influence of varying $I_{fl,max}$ with respect to I_{UV} on the behavior of the SP-to-MC conversion. Ultimately, the change in activation energy for SP-to-MC conversion due to applied stress, $\Delta E_{f,mech}$ remained constant regardless of $I_{fl,max}$.

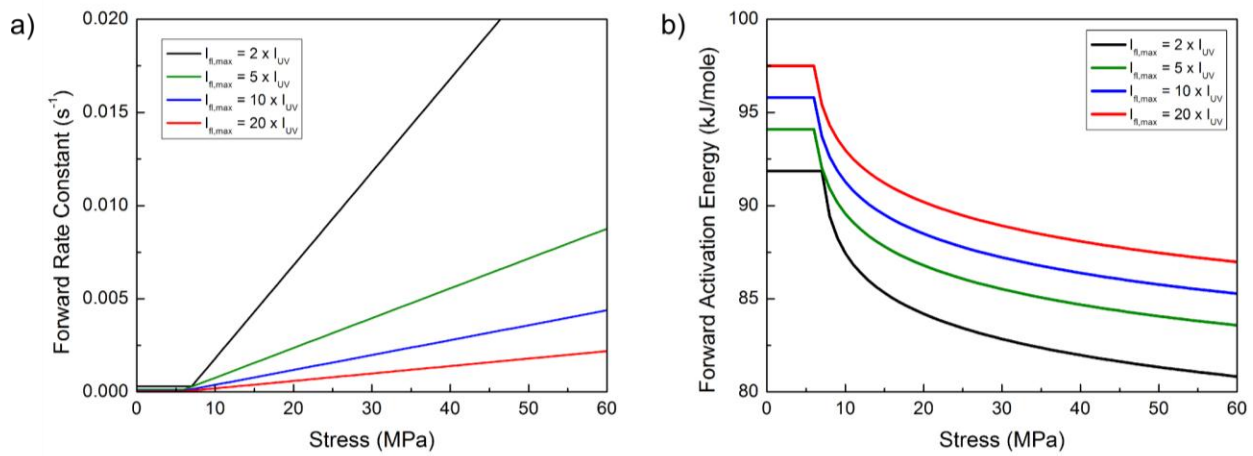


Figure B3. Effect of varying $I_{fl,max}$. a) Forward rate constant. b) Activation energy for the forward reaction, $\Delta E_{a,f}$.